

GW astrophysics with LIGO/VIRGO data

March 2021

Matias Zaldarriaga

GW @ IAS



**Barak
Zackay**



**Tejaswi
Venumadhav**



**Javier
Roulet**



**Liang
Dai**



**Horng-Sheng
Chia**



**Seth
Olsen**

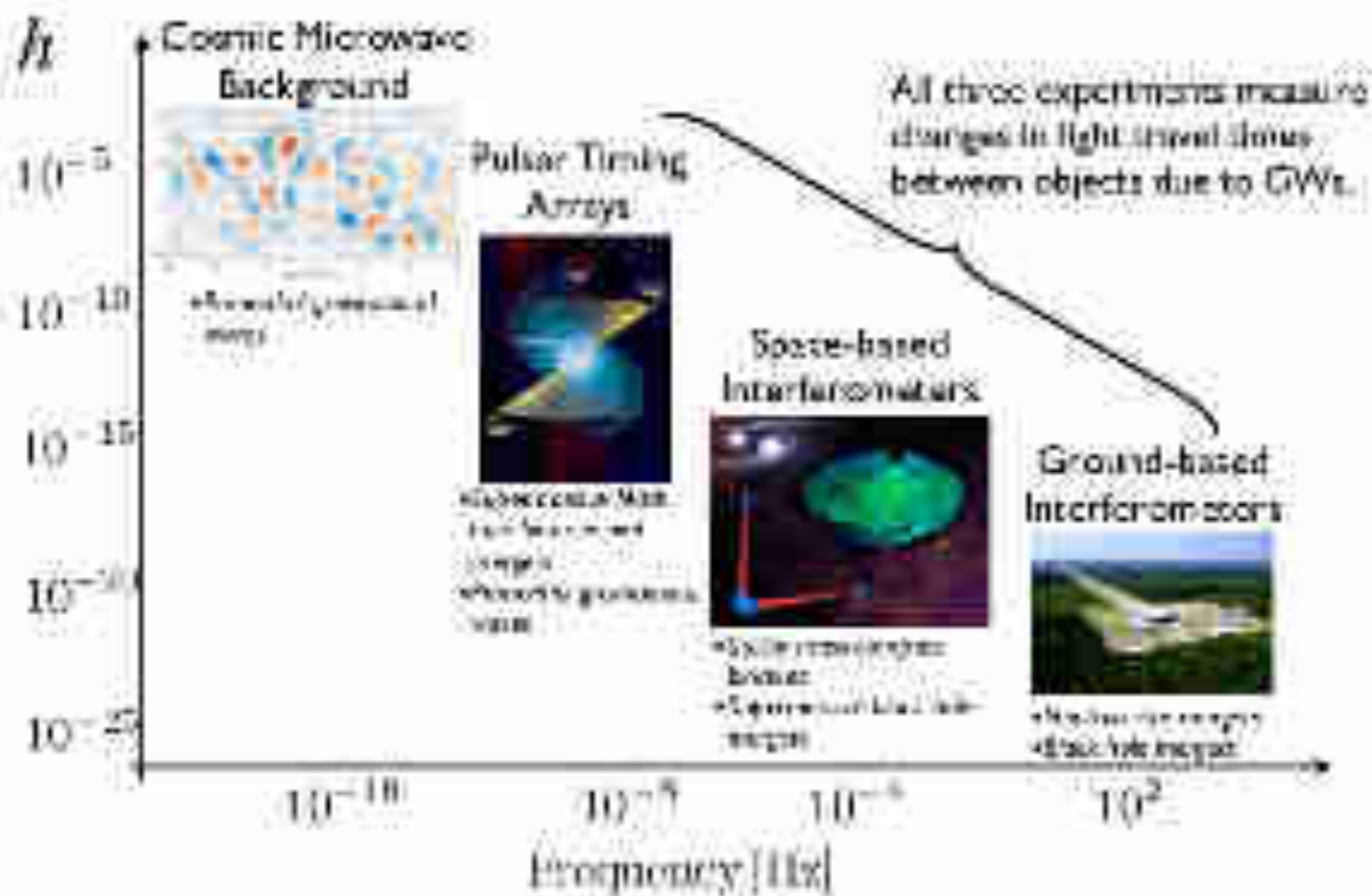


**Matias
Zaldarriaga**

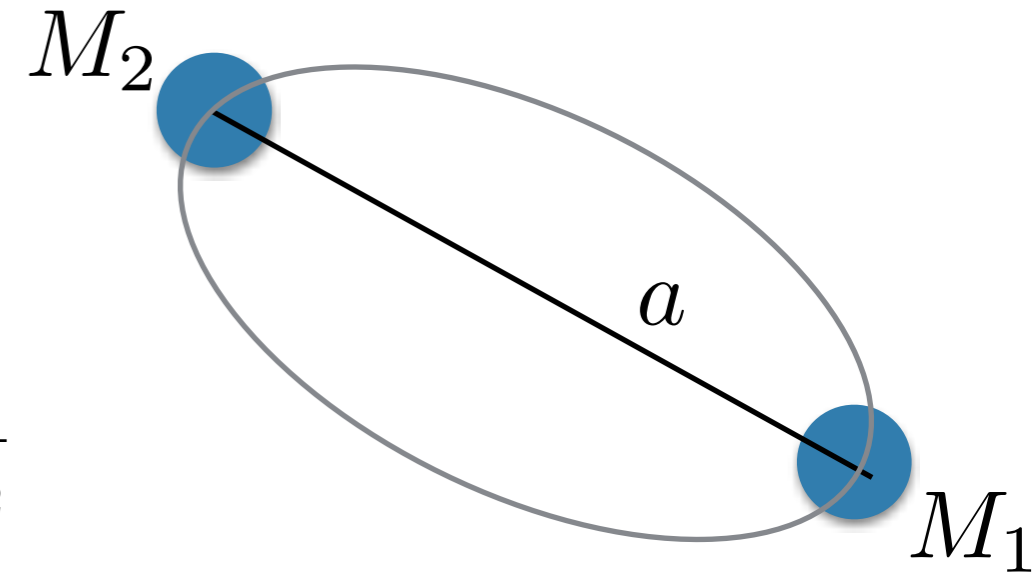
Outline

- Introduction
- Status of observations and outstanding questions
- The IAS O2 search

The spectrum of gravitational wave astronomy



Binary system

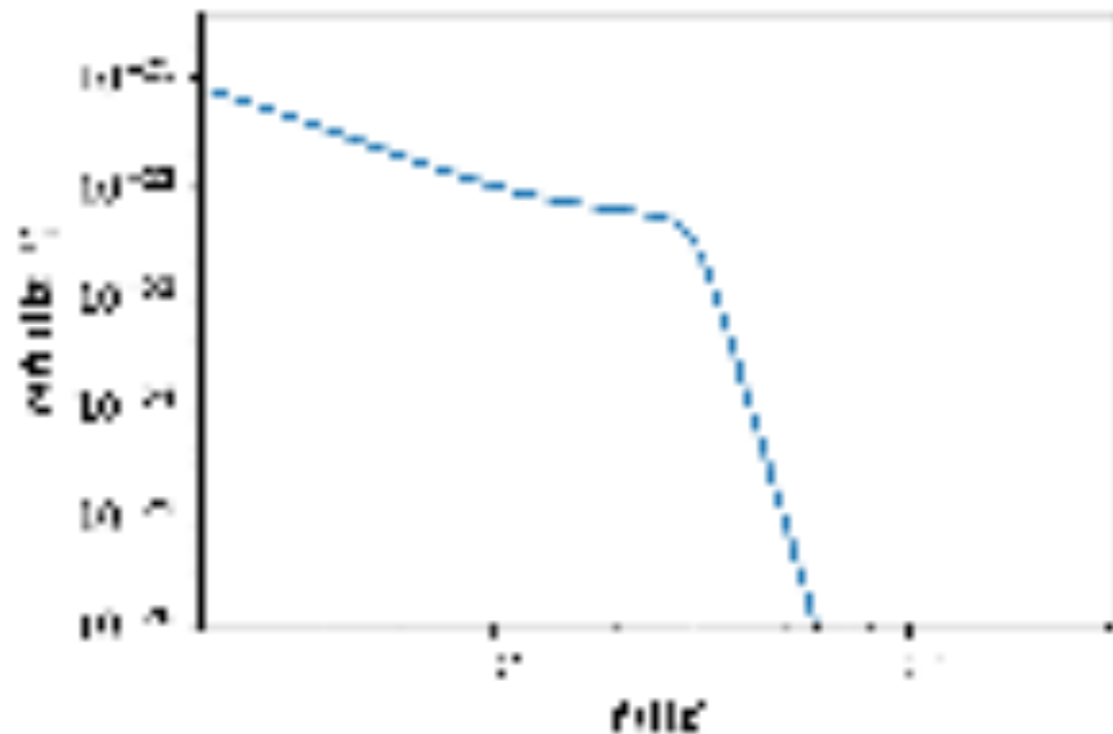
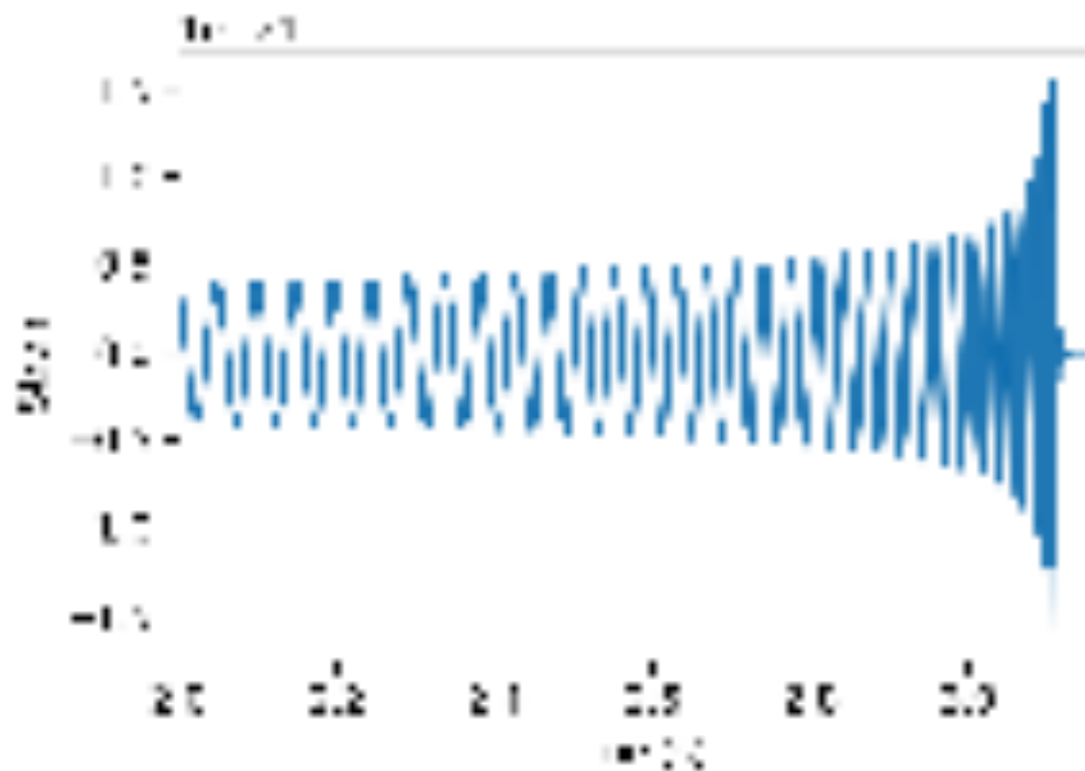


$$M = m_1 + m_2 \quad \eta = \frac{m_1 m_2}{(m_1 + m_2)^2} \quad q = \frac{m_1}{m_2}$$

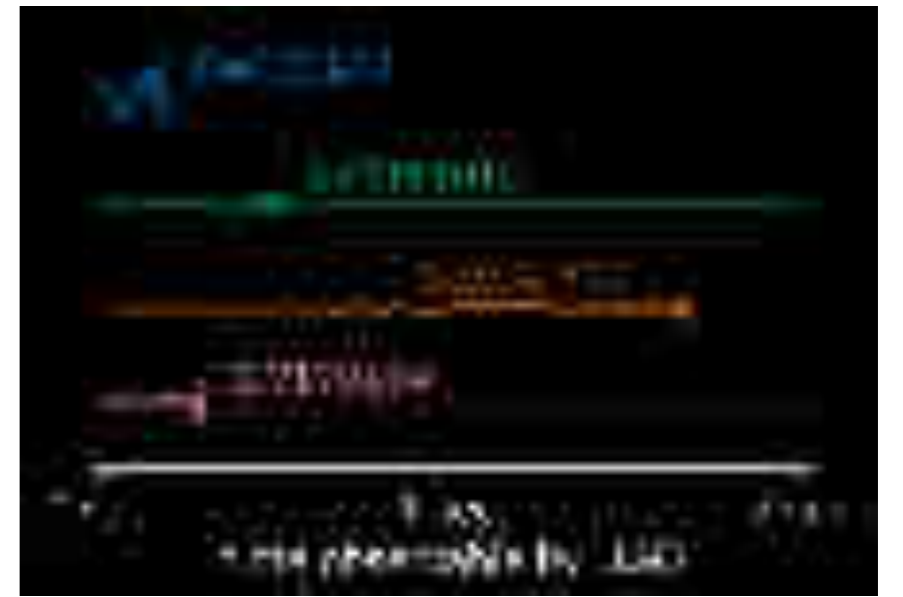
$$M_c = M \eta^{3/5} \quad \omega_{\text{GW}}(t) \sim M_c^{-5/8} (t_0 - t)^{-3/8} \quad \text{"Chirping"}$$

$$h(\omega_0) \propto M_c^{5/6} D^{-1} \omega_0^{-7/6} e^{i\phi(\omega_0)}$$

$$\phi(\omega_0) \propto (M_c \omega_0)^{-5/3} \quad \omega_{\text{max}} \sim 100 \text{ Hz} \left(\frac{50 M_\odot}{M} \right)$$



Post Newtonian wave-forms



$$x = f/f_0$$

$$\eta = \frac{m_1 m_2}{(m_1 + m_2)^2}$$

$$\tilde{h}(f) = A(f; \theta_x) e^{i\Psi(f; \lambda_i)}$$

$$\Psi = 2\pi f_0 x t_c - \phi_c + \lambda_0 x^{-5/3} + \lambda_2 x^{-1} + \lambda_3 x^{-2/3} + \lambda_4 x^{-1/3} + \lambda_{5L} \log(x) + \lambda_6 x^{1/3} + \lambda_{6L} \log(x) x^{1/3} + \lambda_7 x^{2/3},$$

$$\lambda_0 = \frac{3}{128} (\pi \mathcal{M} f_0)^{-5/3},$$

$$\lambda_2 = \frac{5}{96 \eta^{2/5}} \left(\frac{743}{336} + \frac{11}{4} \eta \right) (\pi \mathcal{M} f_0)^{-1},$$

$$\lambda_3 = -\frac{3\pi}{8 \eta^{3/5}} \left(1 - \frac{1}{4\pi} \beta \right) (\pi \mathcal{M} f_0)^{-2/3},$$

$$\lambda_4 = \frac{15}{64 \eta^{4/5}} \left(\frac{3058673}{1016064} + \frac{5429}{1008} \eta + \frac{617}{144} \eta^2 - \sigma \right) (\pi \mathcal{M} f_0)^{-1/3}$$

$$\beta = \frac{1}{12} \sum_{i=1}^2 \left[113 \left(\frac{m_i}{m_1 + m_2} \right)^2 + 75 \eta \right] \hat{\mathbf{L}} \cdot \boldsymbol{\chi}_i$$

$$\sigma = \frac{\eta}{48} \left(-247 \boldsymbol{\chi}_1 \cdot \boldsymbol{\chi}_2 + 721 \hat{\mathbf{L}} \cdot \boldsymbol{\chi}_1 \hat{\mathbf{L}} \cdot \boldsymbol{\chi}_2 \right).$$

Dependence approximated by two parameter model:

$$\chi_{\text{eff}} = \frac{m_1 \chi_{1,z} + m_2 \chi_{2,z}}{m_1 + m_2} = \frac{q \chi_{1,z} + \chi_{2,z}}{q + 1},$$

$$\chi_{\text{p}} = \frac{1}{A_1 m_1^2} \max(A_1 S_{1,\perp}, A_2 S_{2,\perp}) = \max \left(\chi_{1,\perp}, \frac{A_2}{A_1 q^2} \chi_{2,\perp} \right)$$

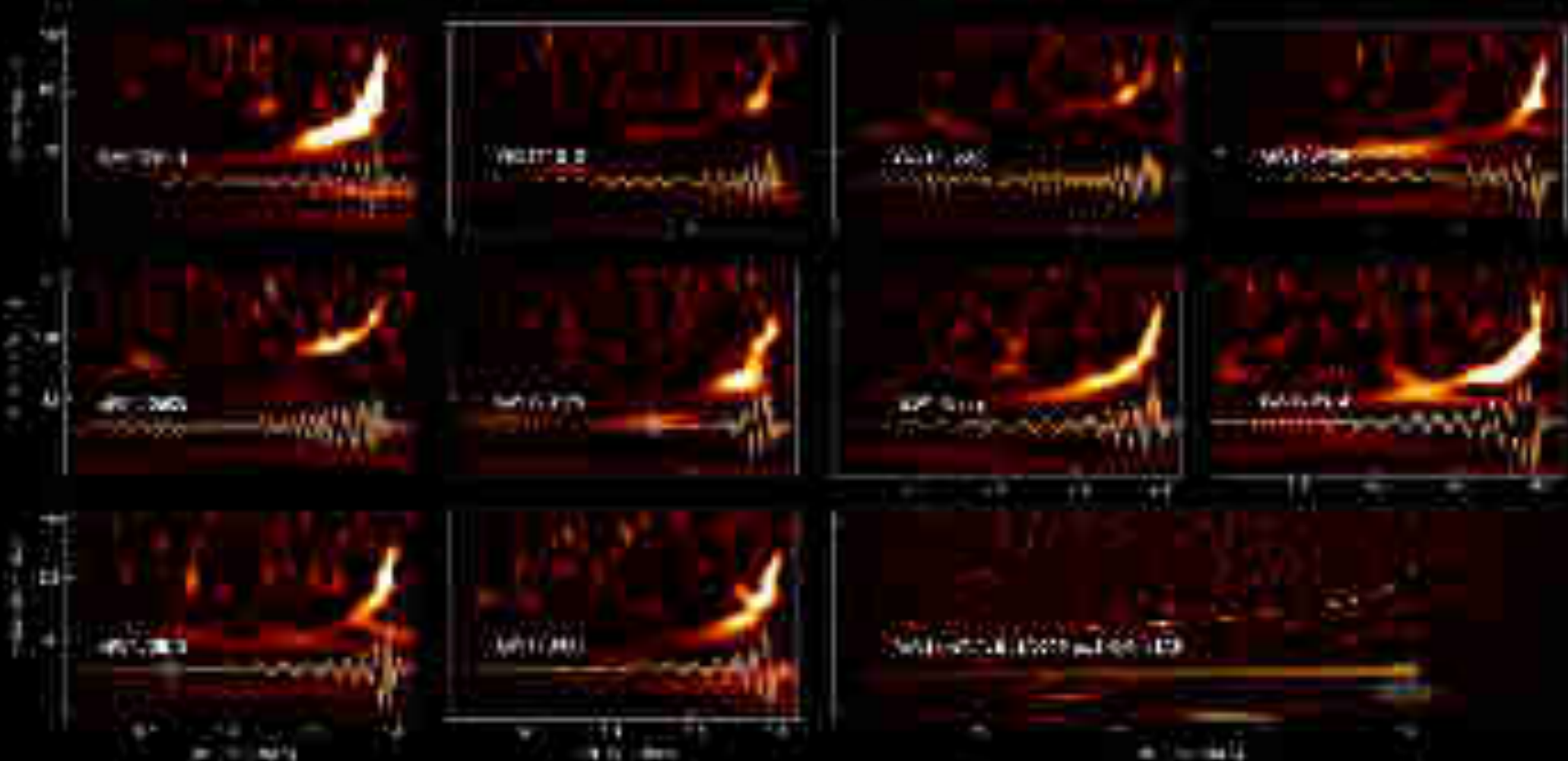
So far only the chirp mass, mass ratio and spin-orbit phase have been detected in an event.

In addition there can be precession in the orbit.

GRAVITATIONAL-WAVE TRANSIENT CATALOG-1


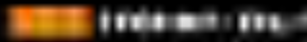










 High SNR (50 or more)  Evidence of merger

 Evidence of merger  High SNR (50 or more)

What can we learn

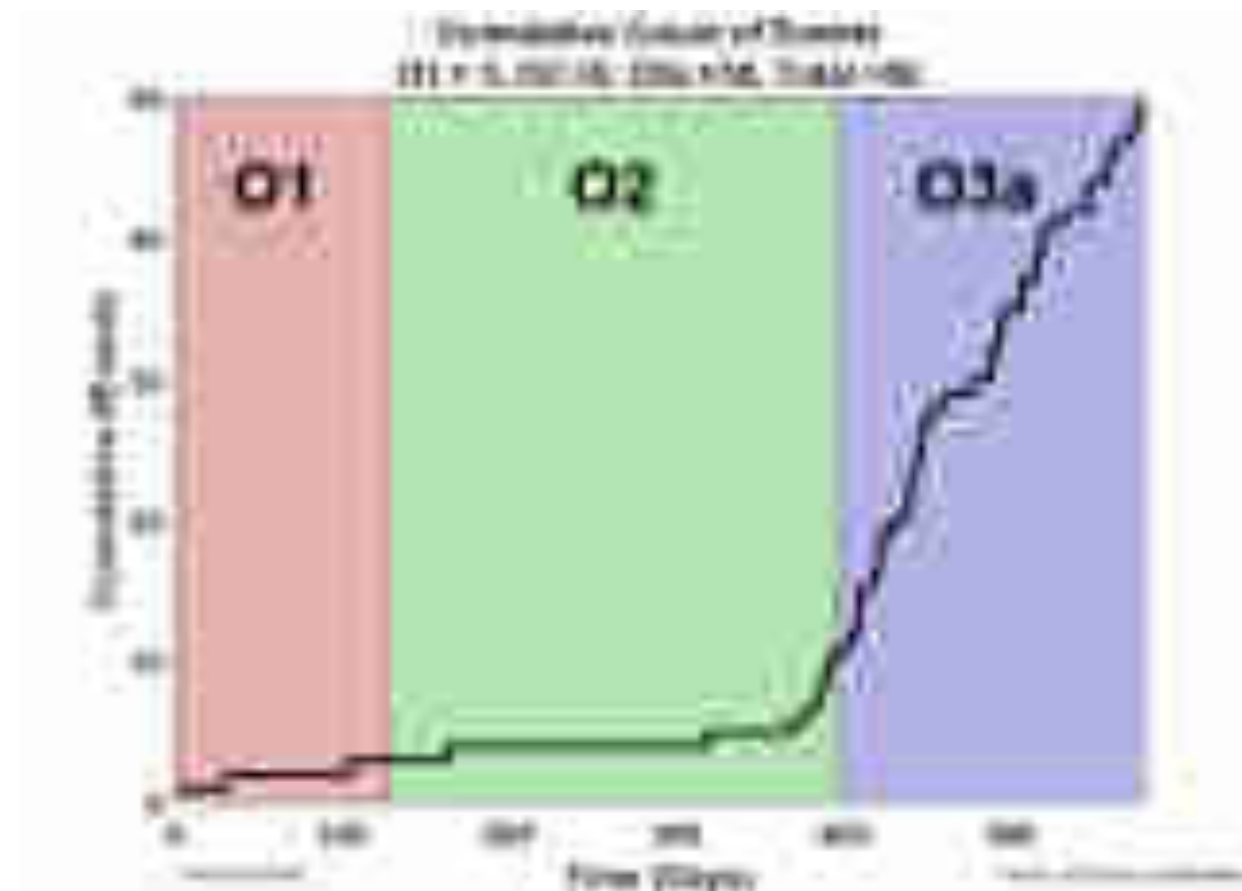
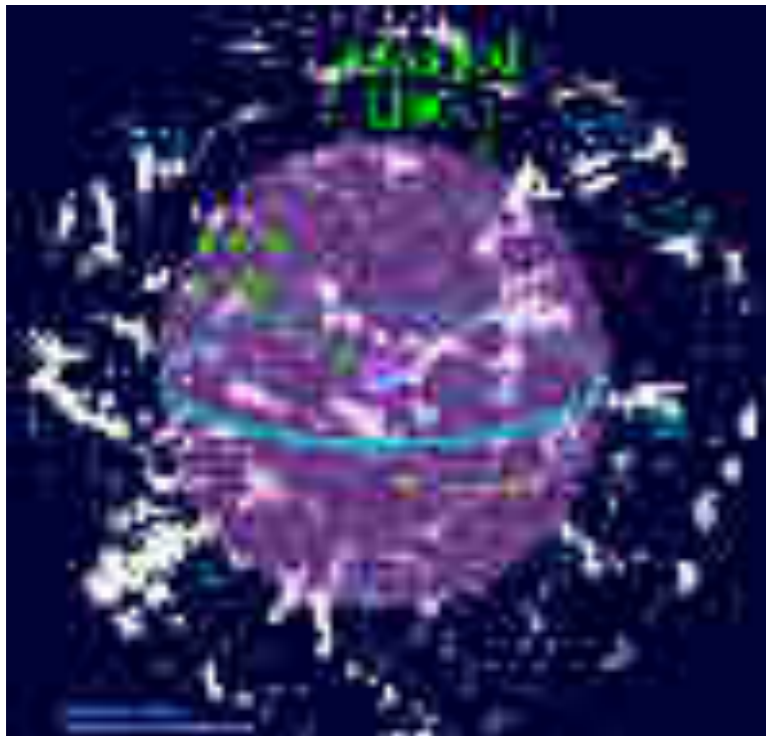
- Properties of Black Holes and Neutron Stars.
- Test the laws of gravity in a regime we have never done so before.
- Processes that result in Black Hole and Black Hole binary systems.

Status of Observations

LIGO Observing Runs

In the volume from where binary black holes are visible by LIGO in O3 there are roughly 10 million Milky Way size galaxies.

In these volume there were forty black hole mergers in six months.



Highlight 01

III Möglichkeiten der Immunität

Frank Krumm

Die Immunität ist ein zentraler Bestandteil des Strafrechts. Sie schützt den Staat vor einer Strafverfolgung, die gegen seine Souveränität verstoßen würde. In der deutschen Rechtslehre wird die Immunität in drei Hauptkategorien unterteilt: die diplomatische Immunität, die konsularische Immunität und die Immunität der Staatsoberhäupter.

Die diplomatische Immunität ist die umfassendste Form der Immunität. Sie schützt Diplomaten vor Strafverfolgung in dem Land, in dem sie akkreditiert sind. Diese Immunität erstreckt sich auf die Person des Diplomaten, seine Familie und seine Dienstwagen. Die Immunität ist jedoch nicht absolut. Sie ist durch die Wiener Konvention über die diplomatische Immunität von 1961 geregelt. Die Immunität ist nur für die Dauer der diplomatischen Mission gültig.

Die konsularische Immunität ist eine eingeschränkte Form der Immunität. Sie schützt Konsuln vor Strafverfolgung in dem Land, in dem sie akkreditiert sind. Diese Immunität erstreckt sich auf die Person des Konsuls, seine Familie und seine Dienstwagen. Die Immunität ist jedoch nicht absolut. Sie ist durch die Wiener Konvention über die konsularischen Privilegien und Immunitäten von 1963 geregelt. Die Immunität ist nur für die Dauer der konsularischen Mission gültig.

Die Immunität der Staatsoberhäupter ist eine absolute Form der Immunität. Sie schützt die Staatsoberhäupter vor Strafverfolgung in dem Land, in dem sie sich befinden. Diese Immunität erstreckt sich auf die Person des Staatsoberhauptes und seine Familie. Die Immunität ist durch die Wiener Konvention über die Immunität der Staatsoberhäupter von 1991 geregelt.



Freizeit Camp 

Entwicklungsworkshop für Kinder & Jugendliche (7-14 Jahre) am 2.10.2020 in der Stadthalle
Anmeldung bis zum 25.09.2020
Kosten: 10,- €

U100 

#Gravitationswellen Detektiert (Teil 1)
#Eins: Elekt. via 100% aller Ereignisse:
produktion, #Eins: 91% der Fälle



Multi-messenger Observations of a Binary Neutron Star Merger

LIGO Scientific Collaboration and Virgo Collaboration, Fermi GBM, INTEGRAL, IceCube Collaboration, AstroSat Cadmium Zinc Telluride Imager Team, IPN Collaboration, The Insight-Hxmt Collaboration, ANTARES Collaboration, The Swift Collaboration, AGILE Team, The IM2H Team, The Dark Energy Camera GW-EM Collaboration and the DES Collaboration, The DLT40 Collaboration, GRAWITA: GRAVitational Wave Inaf TeAm, The Fermi Large Area Telescope Collaboration, ATCA: Australia Telescope Compact Array, ASKAP: Australian SKA Pathfinder, Las Cumbres Observatory Group, OzGrav, DWF (Deeper, Wider, Faster Program), AST3, and CAASTRO Collaborations, The VINROUGE Collaboration, MASTER Collaboration, J-GEM, GROWTH, JAGWAR, Caltech-NRAO, TTU-NRAO, and NuSTAR Collaborations, Pan-STARRS, The MAXI Team, TZAC Consortium, KU Collaboration, Nordic Optical Telescope, ePESSTO, GROND, Texas Tech University, SALT Group, TOROS: Transient Robotic Observatory of the South Collaboration, The BOOTES Collaboration, MWA: Murchison Widefield Array, The CALET Collaboration, IKI-GW Follow-up Collaboration, H.E.S.S. Collaboration, LOFAR Collaboration, LWA: Long Wavelength Array, HAWC Collaboration, The Pierre Auger Collaboration, ALMA Collaboration, Euro VLBI Team, Pi of the Sky Collaboration, The Chandra Team at McGill University, DFN: Desert Fireball Network, ATLAS, High Time Resolution Universe Survey, RIMAS and RATIR, and SKA South Africa/MeerKAT (See the end matter for the full list of authors.)

Received 2017 October 3; revised 2017 October 6; accepted 2017 October 6; published 2017 October 16

Abstract

On 2017 August 17 a binary neutron star coalescence candidate (later designated GW170817) with merger time 12:41:04 UTC was observed through gravitational waves by the Advanced LIGO and Advanced Virgo detectors. The *Fermi* Gamma-ray Burst Monitor independently detected a gamma-ray burst (GRB 170817A) with a time delay of ~ 1.7 s with respect to the merger time. From the gravitational-wave signal, the source was initially localized to a sky region of 31 deg^2 at a luminosity distance of 40^{+8}_{-8} Mpc and with component masses consistent with neutron stars. The component masses were later measured to be in the range 0.86 to $2.26 M_{\odot}$. An extensive observing campaign was launched across the electromagnetic spectrum leading to the discovery of a bright optical transient (SSS17a, now with the IAU identification of AT 2017gfo) in NGC 4993 (at ~ 40 Mpc) less than 11 hours after the merger by the One-Meter, Two Hemisphere (1M2H) team using the 1 m Swope Telescope. The optical transient was independently detected by multiple teams within an hour. Subsequent observations targeted the object and its environment. Early ultraviolet observations revealed a blue transient that faded within 48 hours. Optical and infrared observations showed a redward evolution over ~ 10 days. Following early non-detections, X-ray and radio emission were discovered at the transient's position ~ 9 and ~ 16 days, respectively, after the merger. Both the X-ray and radio emission likely arise from a physical process that is distinct from the one that generates the UV/optical/near-infrared emission. No ultra-high-energy gamma-rays and no neutrino candidates consistent with the source were found in follow-up searches. These observations support the hypothesis that GW170817 was produced by the merger of two neutron stars in NGC 4993 followed by a short gamma-ray burst (GRB 170817A) and a kilonova/macronova powered by the radioactive decay of *r*-process nuclei synthesized in the ejecta.

Key words: gravitational waves – stars: neutron



Figure 1. Localization of the gravitational-wave, gamma-ray, and optical signals. The left panel shows an orthographic projection of the 90% credible regions from LIGO (190 deg²; light green), the initial LIGO-Virgo localization (31 deg²; dark green), IPN triangulation from the time delay between *Fermi* and *INTEGRAL* (light blue), and *Fermi*-GBM (dark blue). The inset shows the location of the apparent host galaxy NGC 4993 in the Swope optical discovery image at 10.9 hr after the merger (top right) and the DLT40 pre-discovery image from 20.5 days prior to merger (bottom right). The reticle marks the position of the transient in both images.

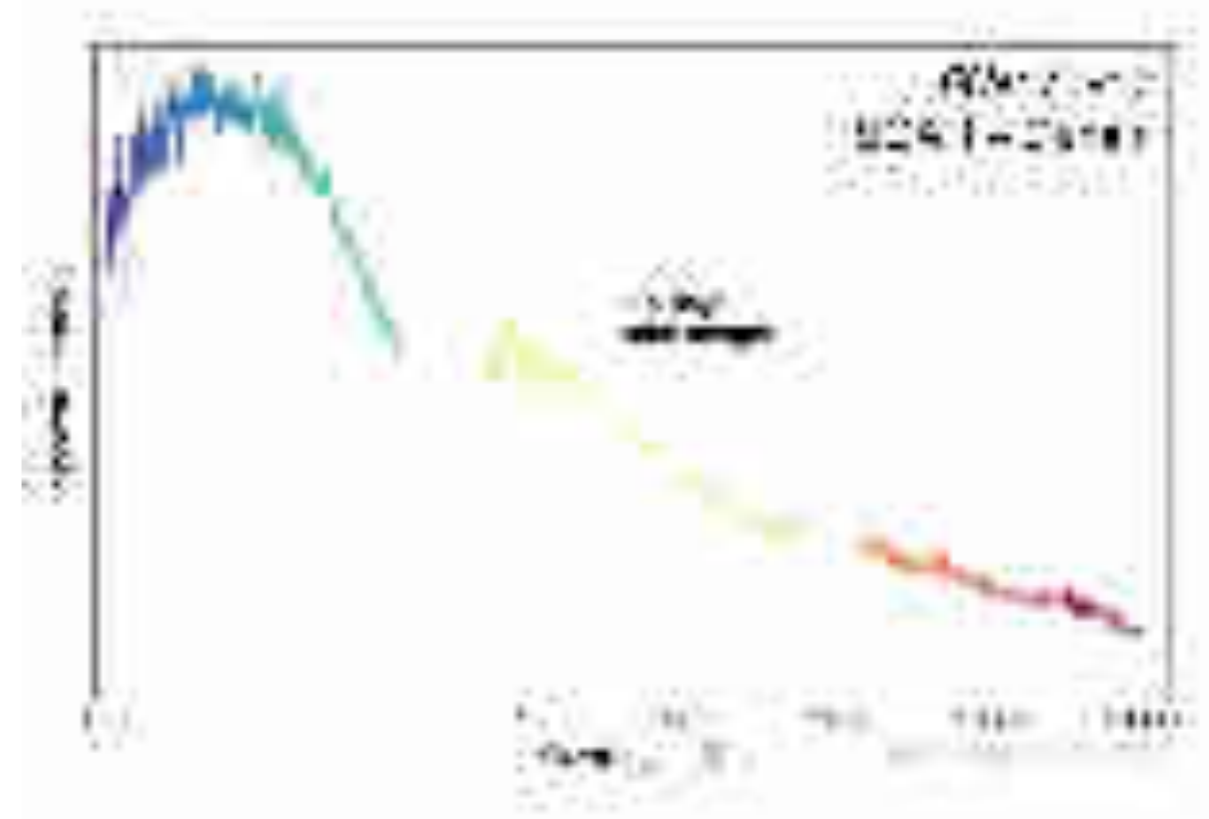
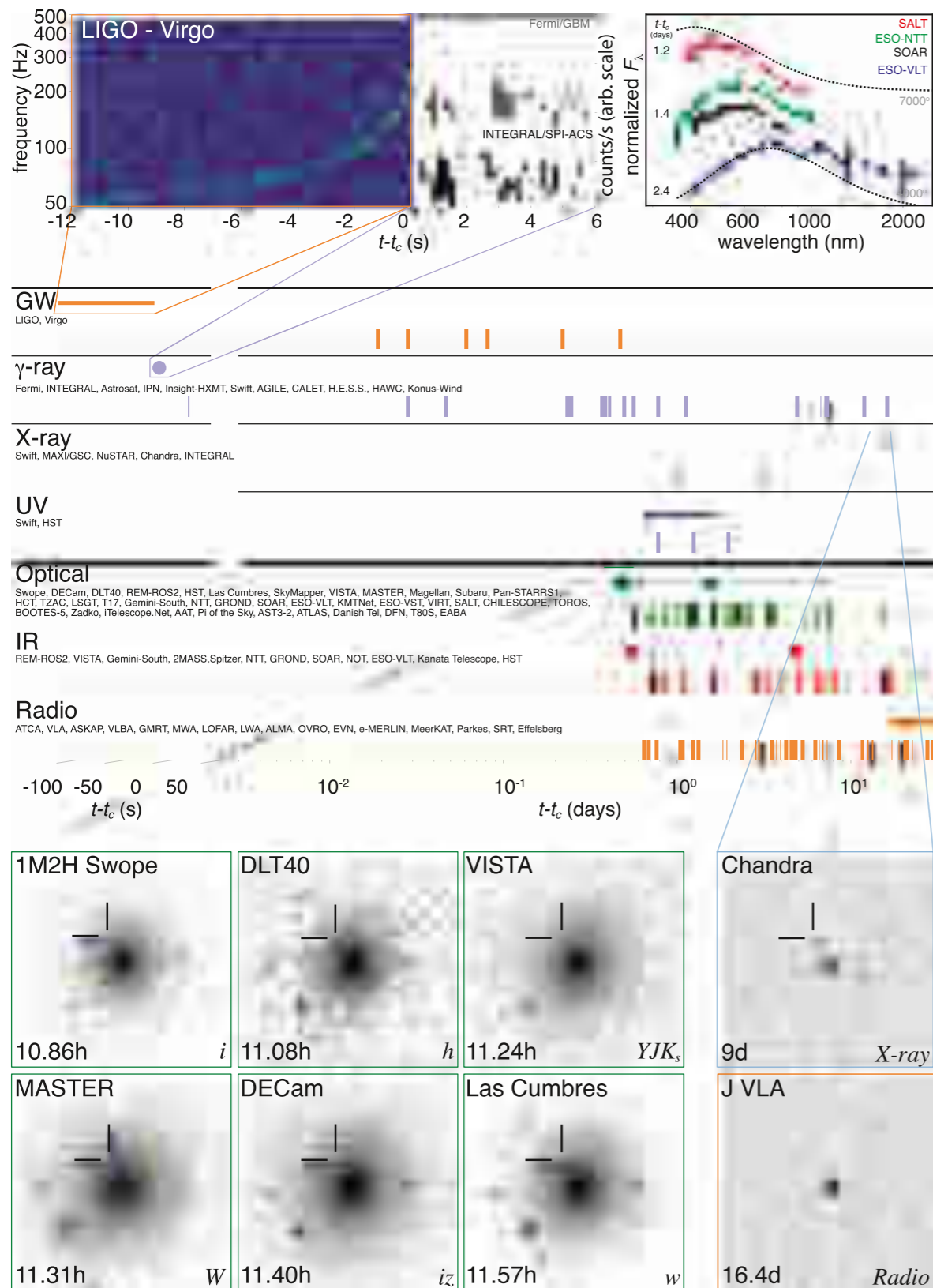


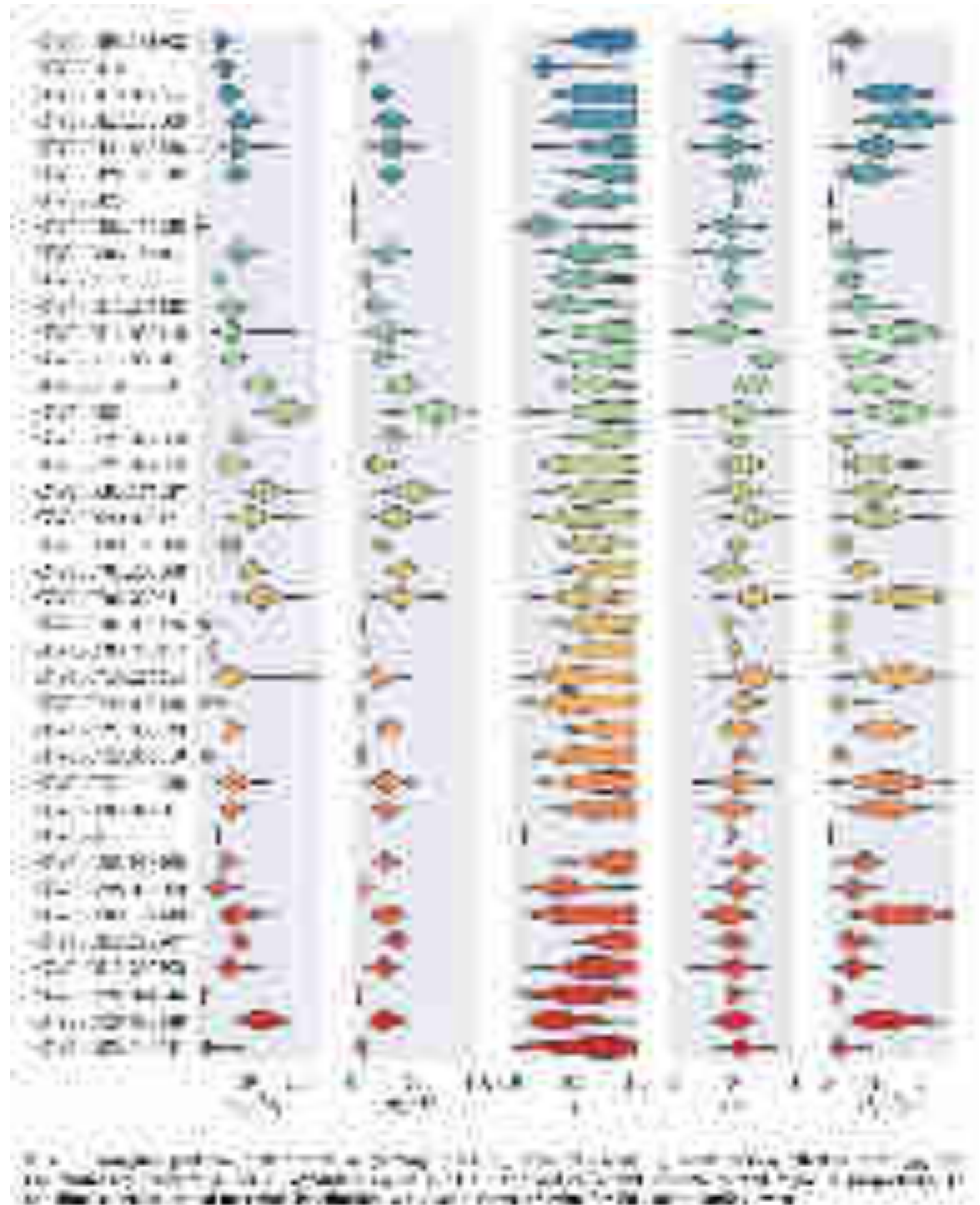
Figure 2. Timeline of the discovery of GW170817, GRB 170817A, SSS17a/AT 2017gfo, and the follow-up observations are shown by messenger and wavelength relative to the time t_c of the gravitational-wave event. Two types of information are shown for each band/messenger. First, the shaded dashes represent the times when information was reported in a GCN Circular. The names of the relevant instruments, facilities, or observing teams are collected at the beginning of the row. Second, representative observations (see Table 1) in each band are shown as solid circles with their areas approximately scaled by brightness; the solid lines indicate when the source was detectable by at least one telescope. Magnification insets give a picture of the first detections in the gravitational-wave, gamma-ray, optical, X-ray, and radio bands. They are respectively illustrated by the combined spectrogram of the signals received by LIGO-Hanford and LIGO-Livingston (see Section 2.1), the *Fermi*-GBM and *INTEGRAL*/SPI-ACS lightcurves matched in time resolution and phase (see Section 2.2), $1/5 \times 1/5$ postage stamps extracted from the initial six observations of SSS17a/AT 2017gfo and four early spectra taken with the SALT (at $t_c + 1.2$ days; Buckley et al. 2017; McCully et al. 2017b), ESO-NTT (at $t_c + 1.4$ days; Smartt et al. 2017), the SOAR 4 m telescope (at $t_c + 1.4$ days; Nicholl et al. 2017d), and ESO-VLT-XShooter (at $t_c + 2.4$ days; Smartt et al. 2017) as described in Section 2.3, and the first X-ray and radio detections of the same source by *Chandra* (see Section 3.3) and JVLA (see Section 3.4). In order to show representative spectral energy distributions, each spectrum is normalized to its maximum and shifted arbitrarily along the linear y-axis (no absolute scale). The high background in the SALT spectrum below 4500 \AA prevents the identification of spectral features in this band (for details McCully et al. 2017b).

Highlight O3

With so many events we can start to ask questions about the way these binary black hole systems formed.

There are two main puzzles:

- How come many of the Black Holes are so heavy?
- How did the pair of black holes get so close to eventually merge by emitting GW



Masses of individual Black Holes

The BHs observed by LIGO are surprisingly heavy. They are both heavier than the BH in binaries in our own galaxy and some of them seem heavier than what our theoretical calculations seem to allow.

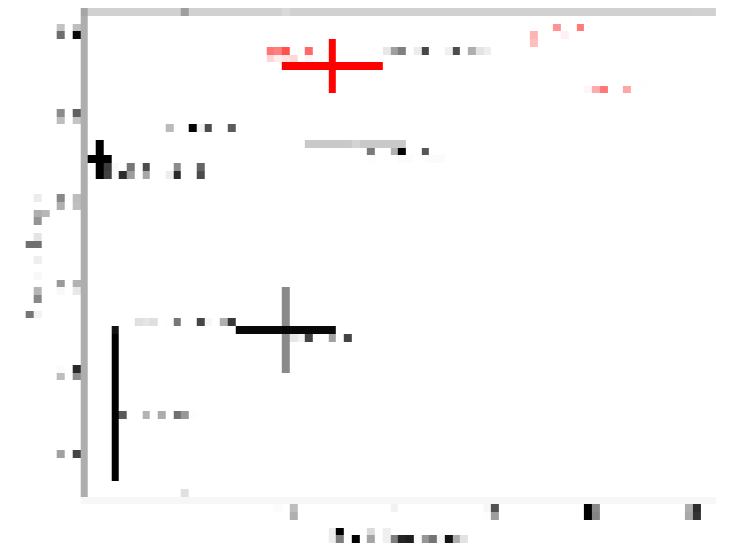
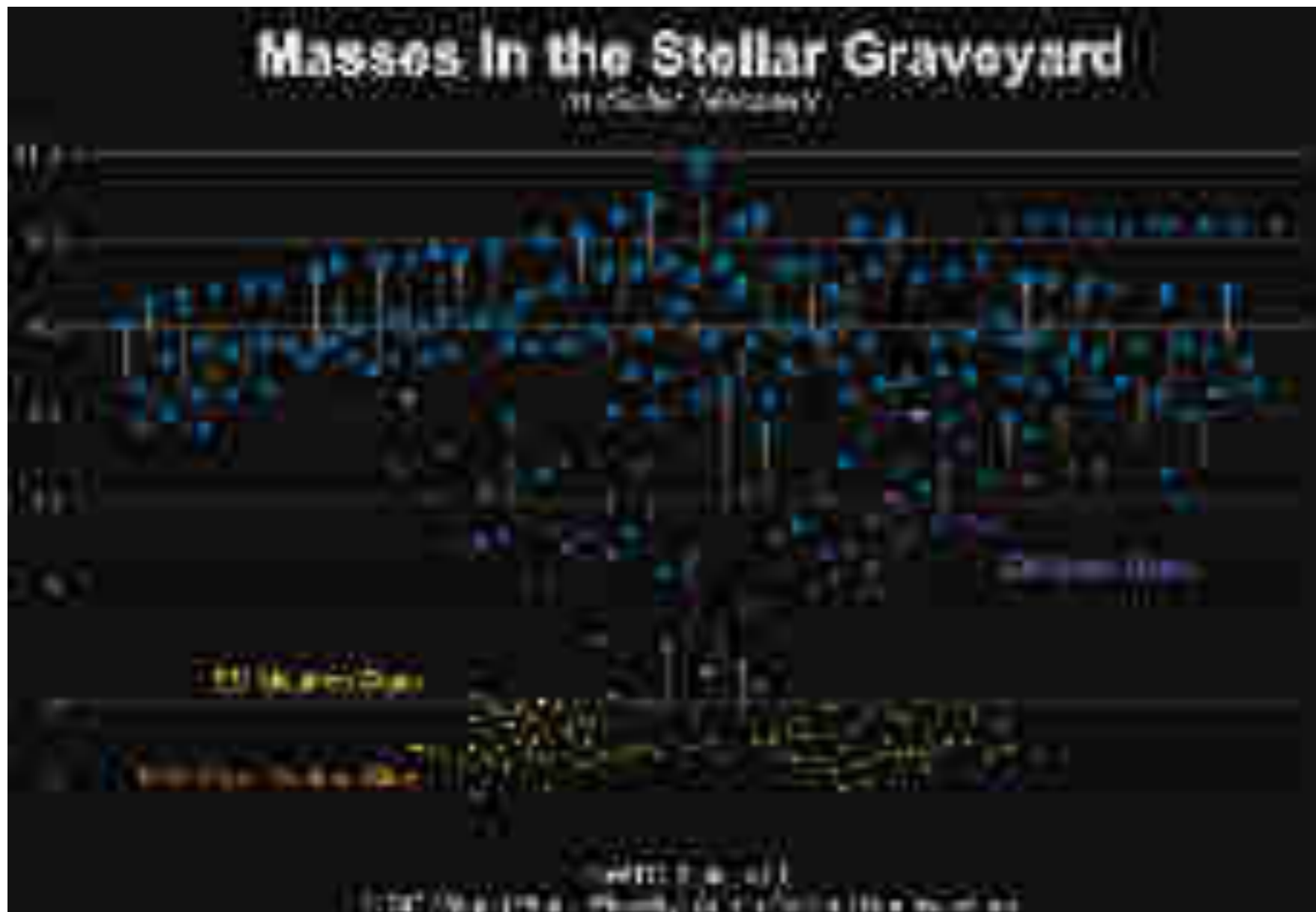


Figure 1. Masses and spins for 10 black holes with approximate error bars. The three high-mass-X-ray-binary systems, LMC X-1, Cygnus X-1 and M33 X-7 are indicated by names above the line and in red online.

Nielsen 1604.00778



High Mass End after O2

19

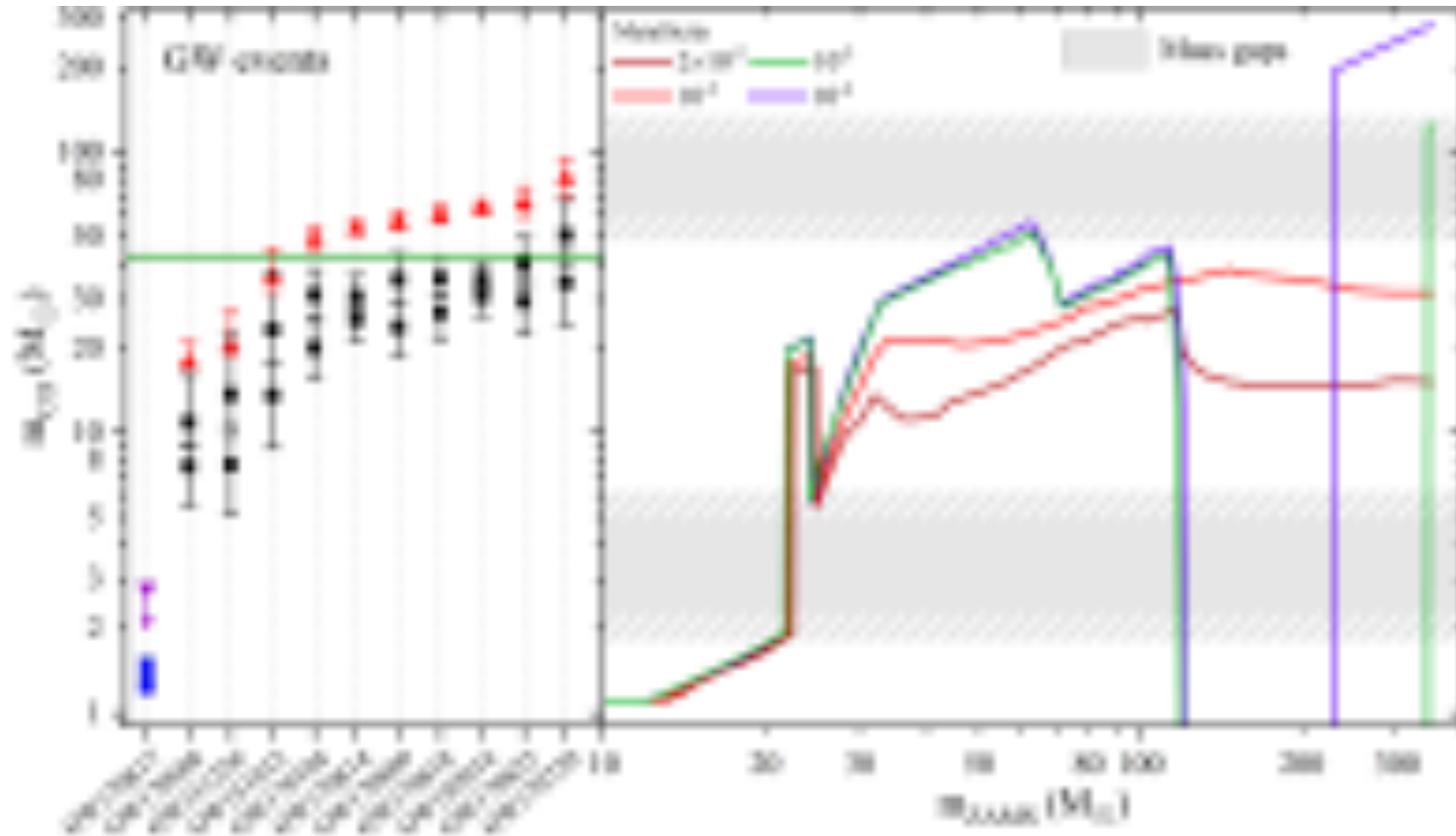
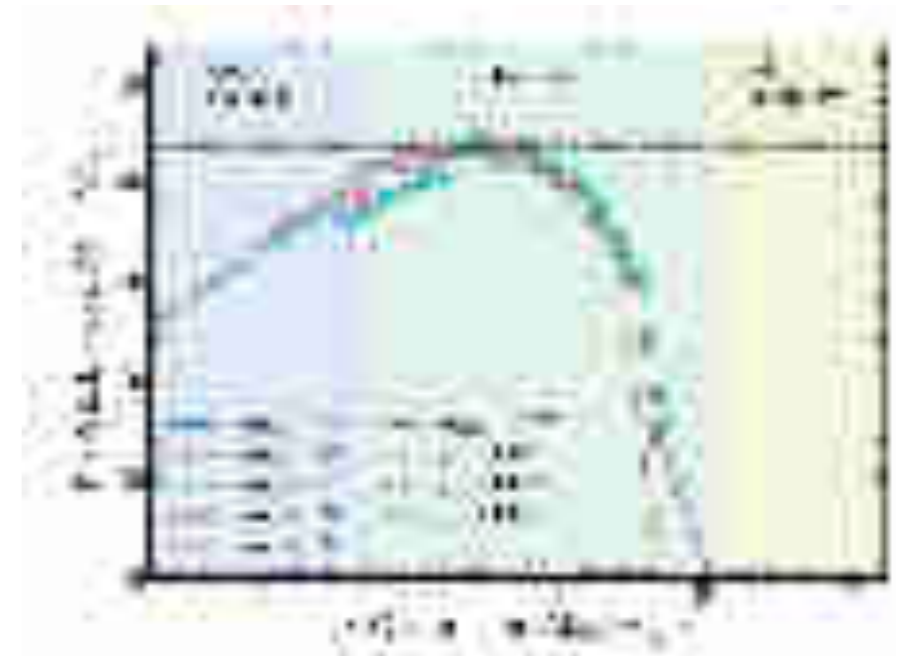


Figure 4. The left-hand panel shows compact object masses (m_{CO}) from GW detections in O1 and O2, with the black squares and error bars representing the component masses of the merging black holes and their uncertainties, and red triangles representing the mass and associated uncertainties of the merger products. The horizontal green line shows the 99th percentile of the mass distribution inferred from the Model B PPD. In the right-hand panel, the predicted compact-object mass is shown as a function of the zero-age main sequence mass of the progenitor star (m_{ZAMS}) and for four different metallicities of the progenitor star (ranging from $Z = 10^{-4}$ to $Z = 2 \times 10^{-2}$, Spera & Mapelli 2017). This model accounts for single stellar evolution from the PARSEC stellar-evolution code (Bressan et al. 2012), for core-collapse supernovae (Fryer et al. 2012), and for pulsational-pair instability and pair-instability supernovae (Woosley 2017). The shaded areas represent the lower and upper mass gaps. There is uncertainty as to the final product of GW170817. It is shown in the left-hand panel to emphasize that BNS mergers might fill the lower gap.



[arxiv:1910.12874]

High Mass End

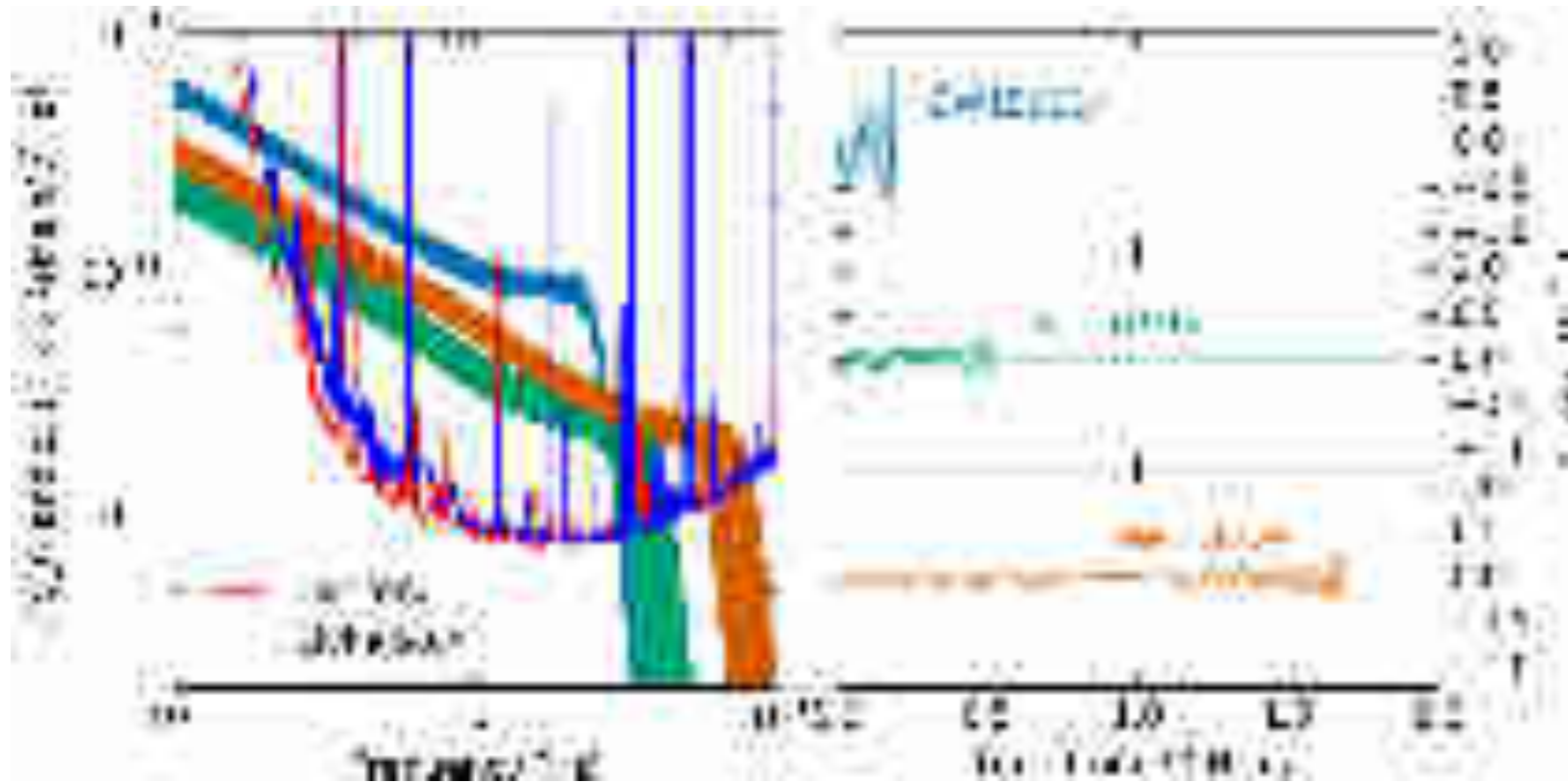


There are several examples of events with masses above the pair instability threshold.

Note that there is already one event O2 (GW170812) in the IAS sample. GW170729 was also heavy although consistent with the cut-off. It was marginal in the LIGO pipeline but was completely above the background in our search.

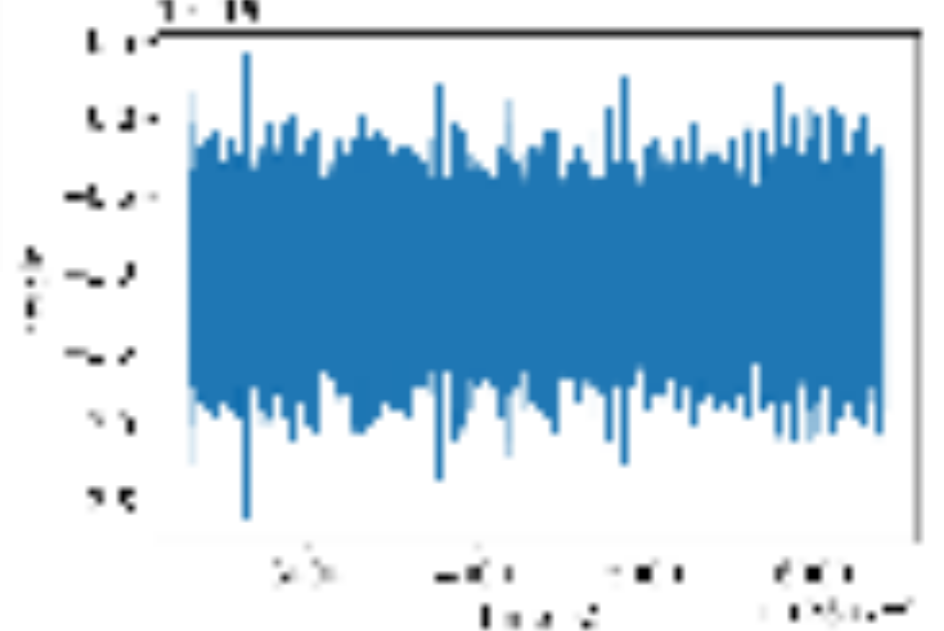
Noise PSD

Matched filtering



$h(t)$ (whitened)

$d(t)$ (whitened)



GWTC-1: A Gravitational-Wave Transient Catalog of Compact Binary Mergers Observed by LIGO and Virgo during the First and Second Observing Runs

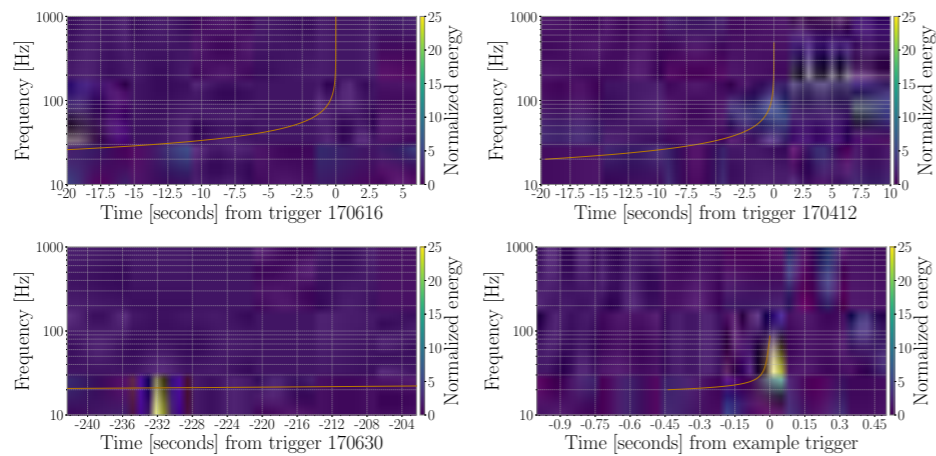
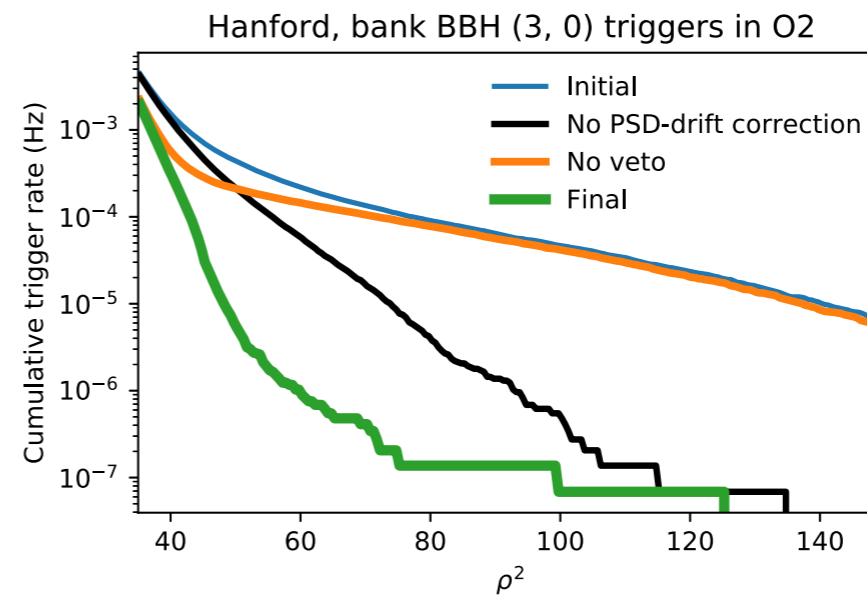
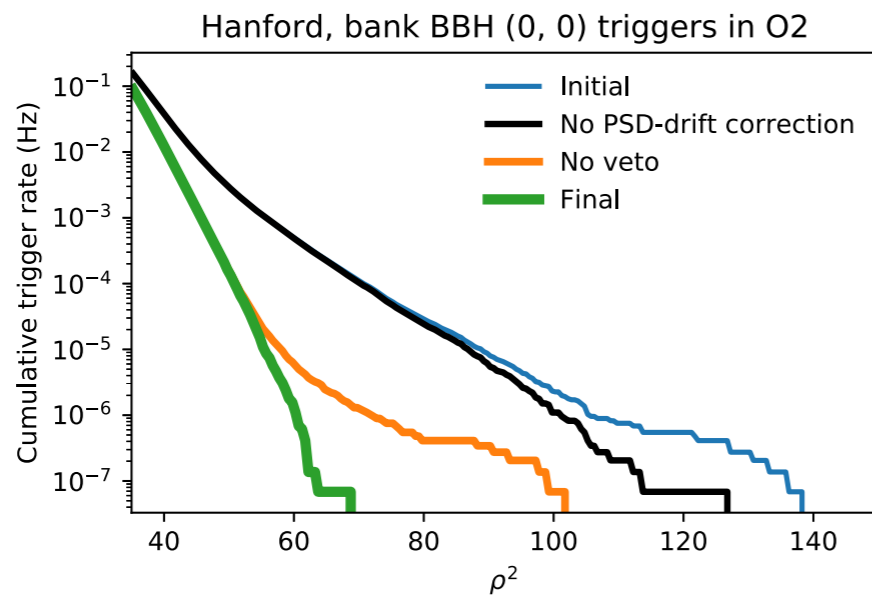
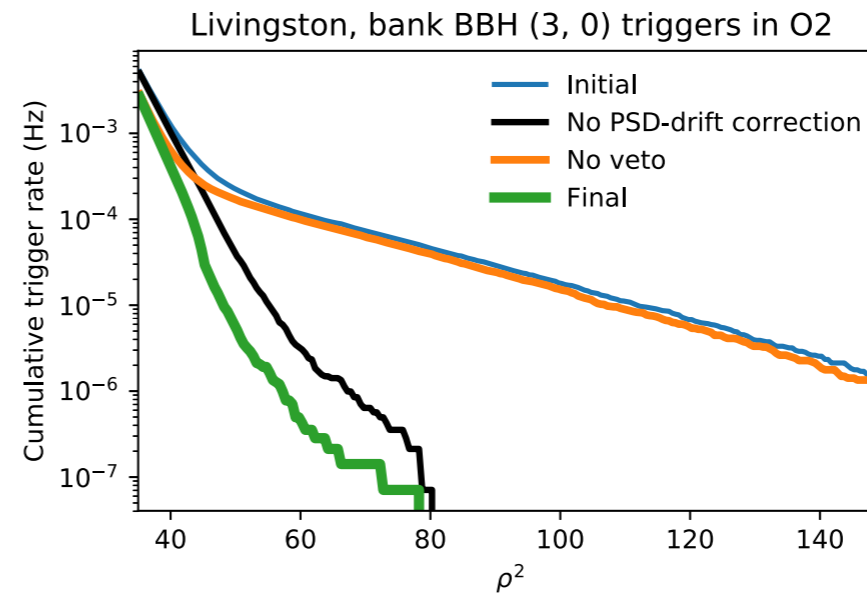
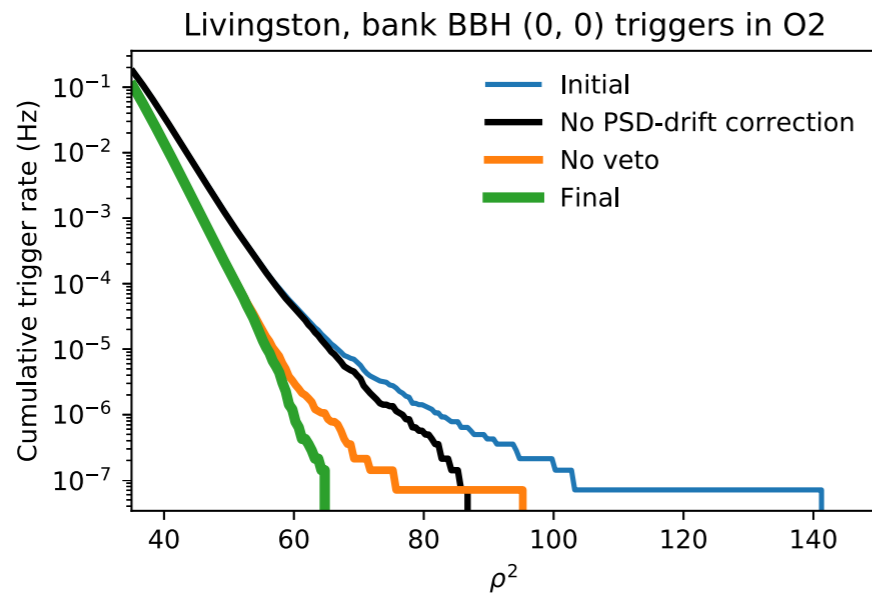


FIG. 15. Normalized spectrograms of the time around common noise artifacts with a time-frequency evolution of a related trigger template overlaid. Top Left: Scattered light artifacts at Hanford with the template of trigger 170616 overlaid. Top Right: A 60-200 Hz nonstationarity at Livingston with the template of trigger 170412 overlaid. Bottom Left: A short duration transient at Livingston with the template of trigger 170630 overlaid. Bottom Right: A blip at Hanford with the template of a sub-threshold high mass trigger overlaid.

$$\frac{Z}{\sigma_Z} = \frac{\sum_f \frac{h^*(f)d(f)}{S_n(f)}}{\sqrt{\sum_f \frac{|h(f)|^2}{S_n(f)}}} \equiv \rho$$

signal/noise

Effect of PSD drift and vetoes



Note that these plots are produced with data after masking (holes + in-painting).

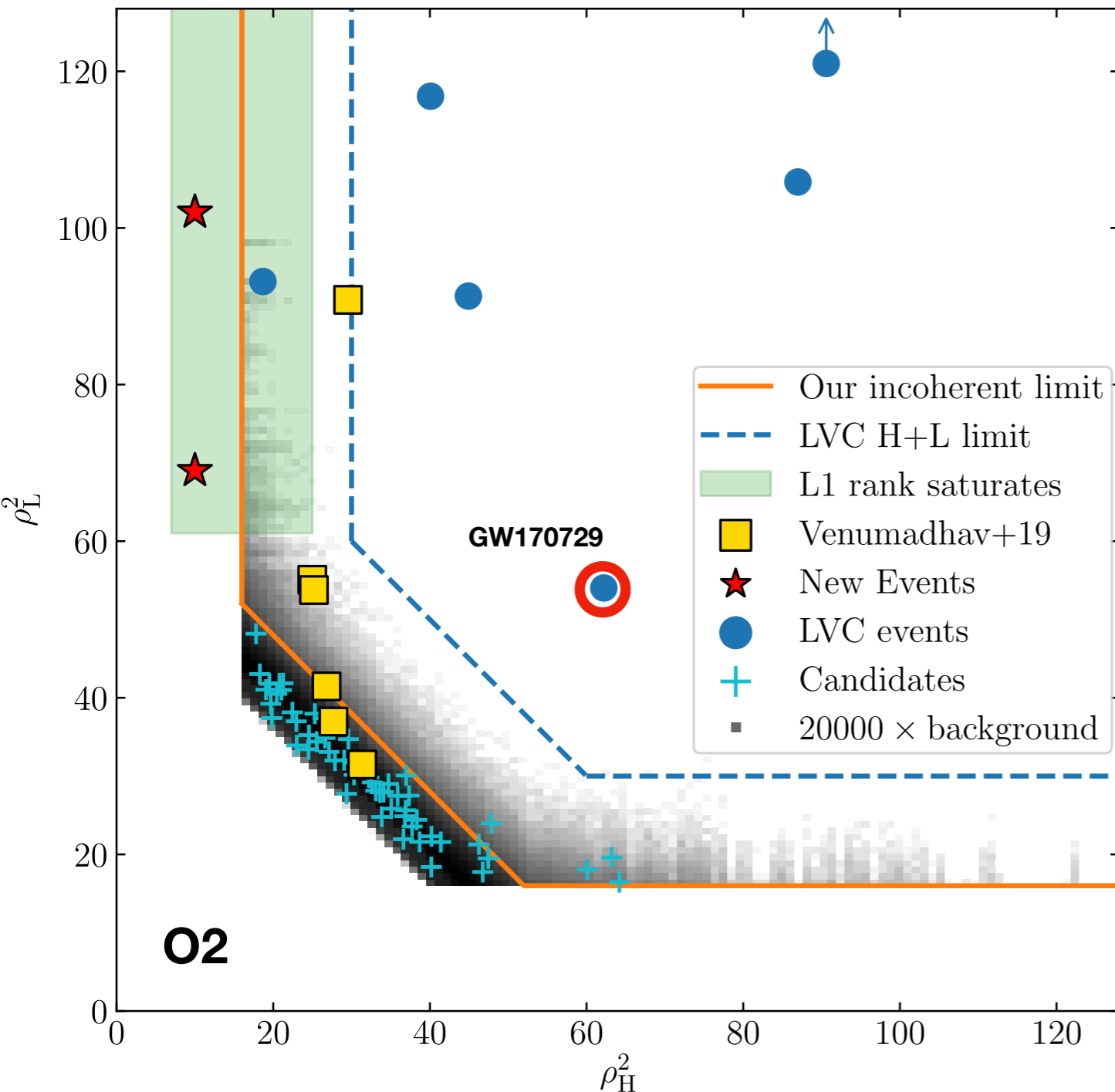
Non-G of the data results in orders of magnitude increase in the rate of triggers.

Even in this heavy BBH bank all the outliers in a single detector are real events. Light BBHs and BNS have basically no glitches after masking all the non-G is PSD drift.

Trigger rate for PyCBC above 64 approx 10^{-4} Hz.

Sensitivity Comparison

Prior to demanding consistency between detectors



GW170729

LIGO FAR = 1 in 5 yrs

IAS FAR < 1 in 20000 O2 = 1 in 6500 yrs
(saturated by the amount of background we collected)

Additional suppression approximately $\Delta \text{snr}^2 = 20$. In trigger distributions going from 40 to 60 is approximately 3 orders of magnitude in the rate.

$$(90/64)^{1/2} = 1.2 \quad \text{and} \quad (90/64)^{3/2} = 1.7$$

Equivalent to reducing the strain noise amplitude by $\sim 20\%$

Equivalent to increasing the volume by $\sim 70\%$

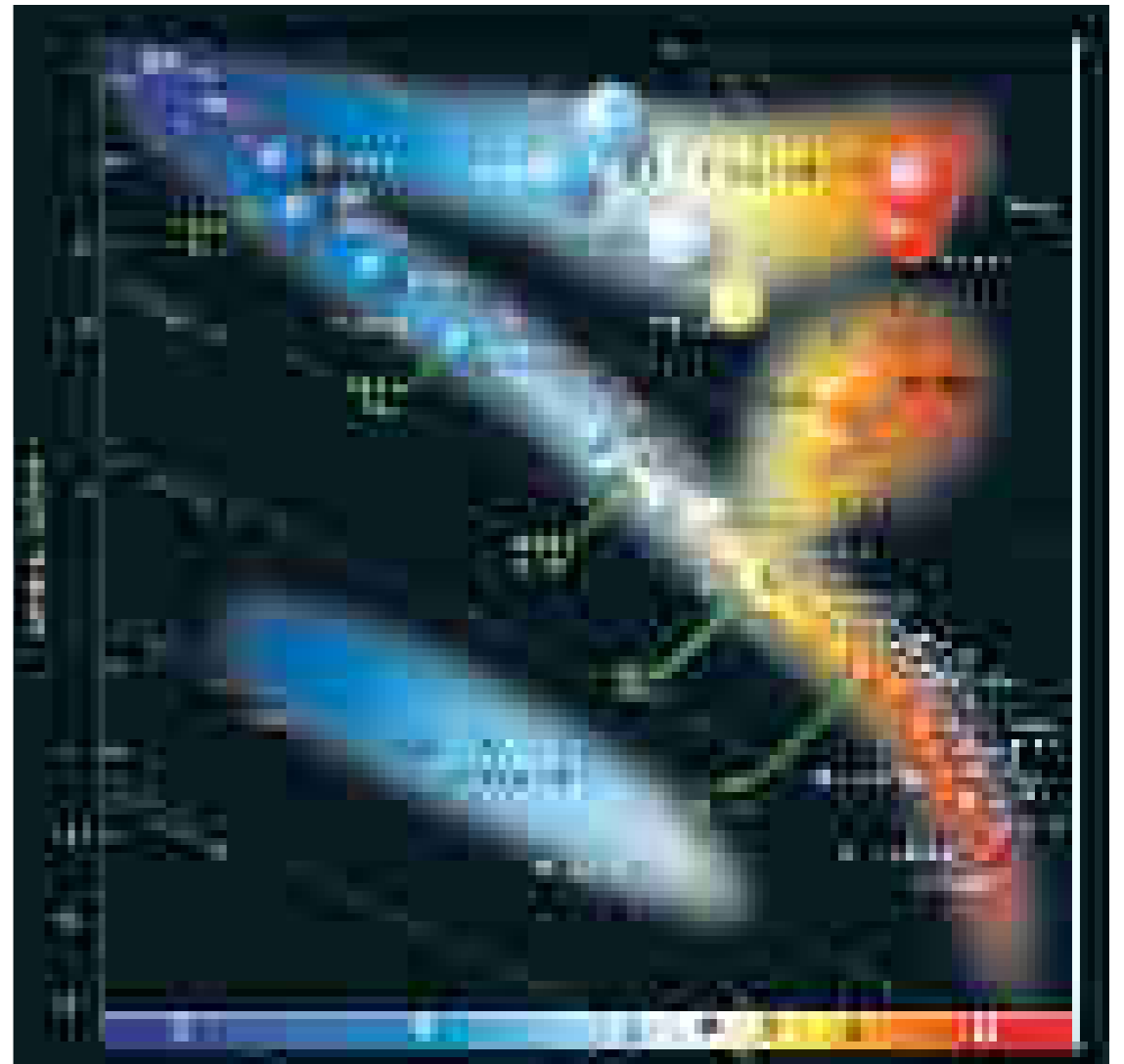
You can reach the same conclusion about LVT during O1. The plot looks very similar.

Compact binaries

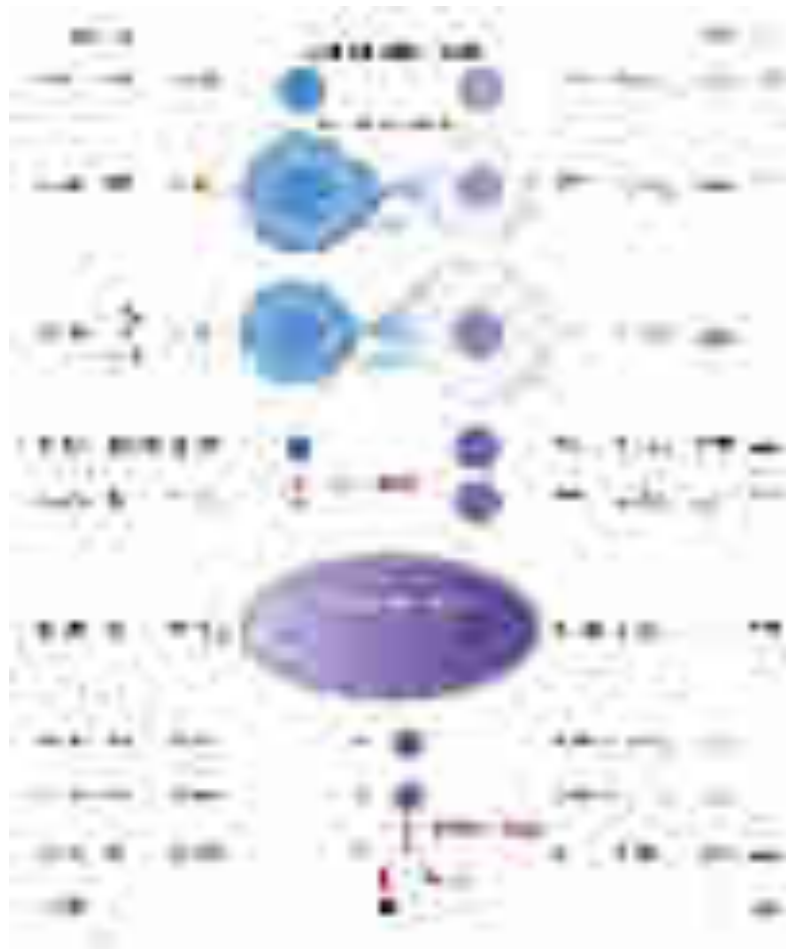
To merge due to emission of GW radiation two 20 solar mass black holes need to be closer than 30 solar radii.

The massive stars that are the progenitors of these black holes are much bigger than that during their giant phase. How did the black holes come together?

Color, luminosity and sizes of stars



Formation channels



Belczynski et al. 2016



Rodriguez et al. 1604.04254

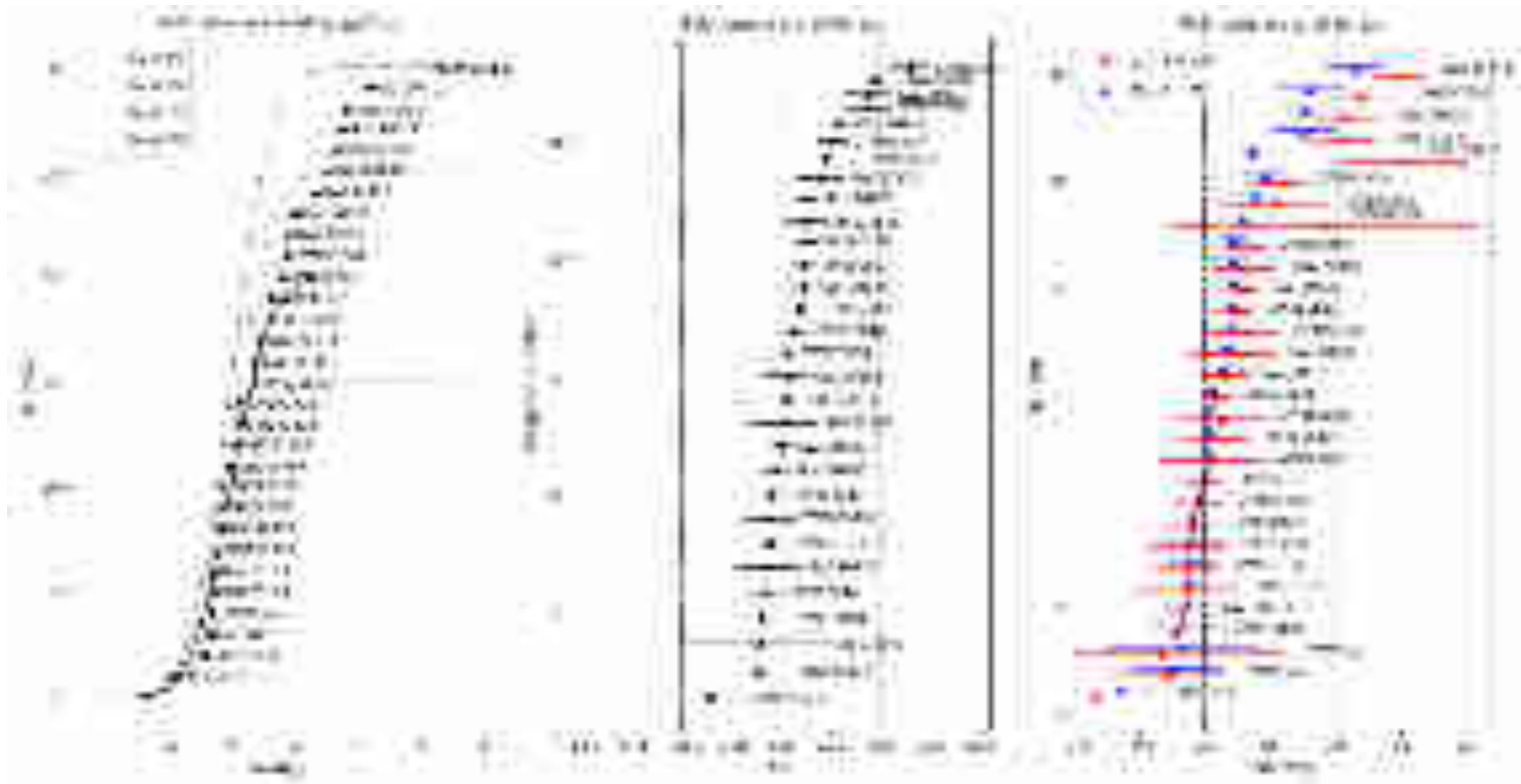


- Rate
- Masses
- Spin
- Eccentricity

There already is interesting spin information

Spin measurements

$$\chi_{\text{eff}} = (m_1 \chi_{1z} + m_2 \chi_{2z})/M$$

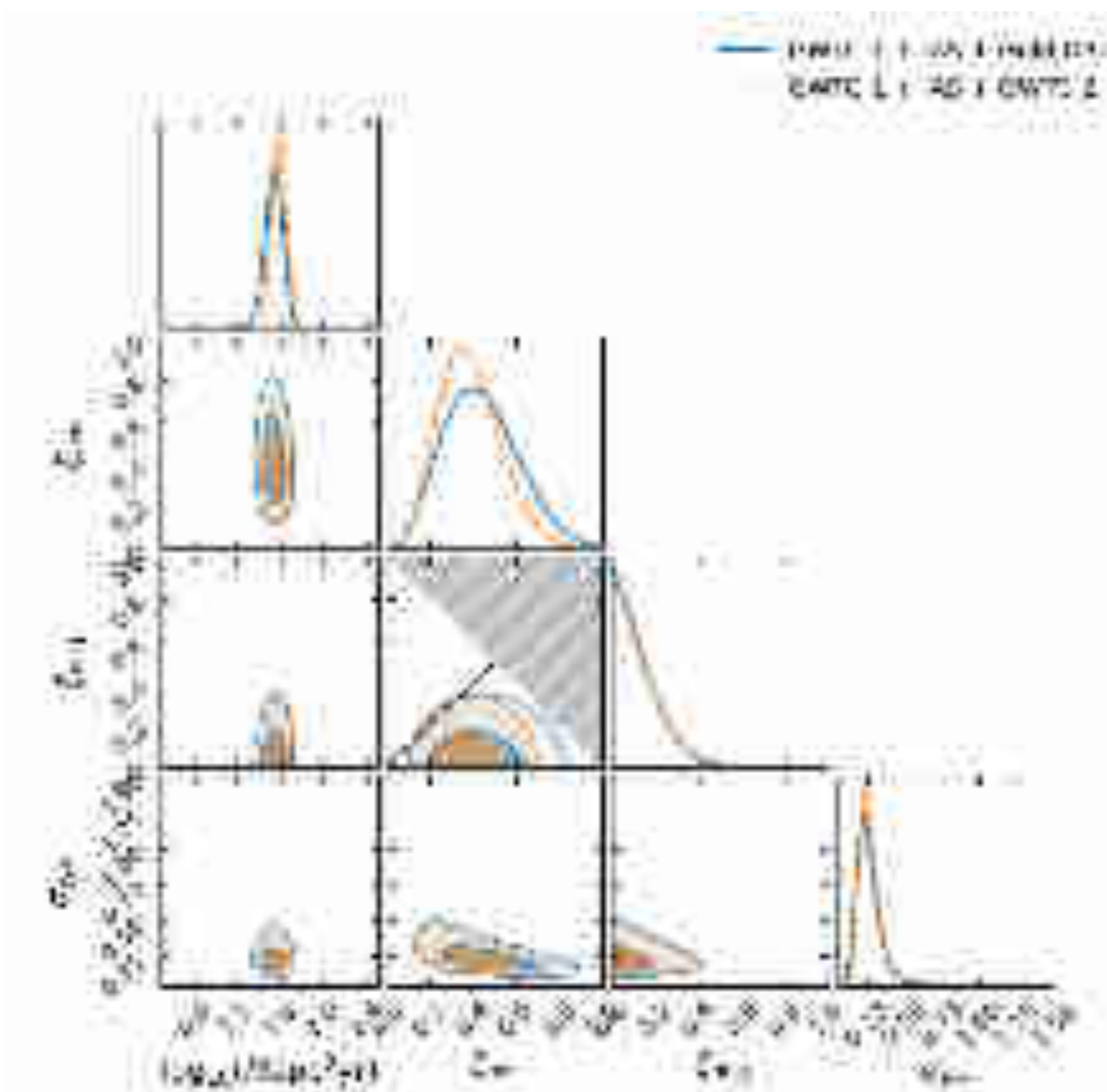


Spins are small. The distribution is not consistent with no spin. All the significant detections are on the positive spin side (small caveat, positive spin events are louder). This points to a significant contribution of the binary channel.

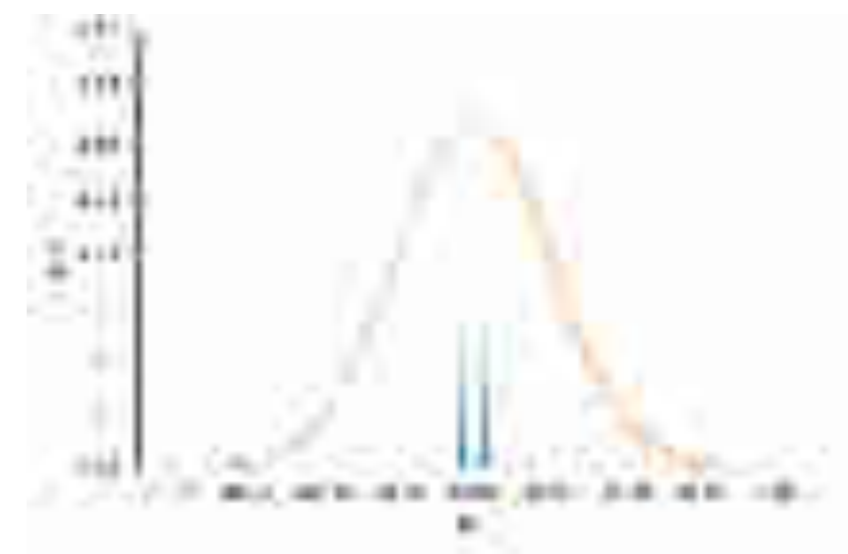
There is no evidence for negative spin.

Several of the spins that are significantly different from zero are still small. Not very consistent with the naive tide scenario.

Spin measurements



Model



The IAS independent search for events in the LIGO data



**Barak
Zackay**



**Tejaswi
Venumadhav**



**Javier
Roulet**



**Liang
Dai**



**Matias
Zaldarriaga**

Summary

O1: one new events (LIGO had 3)

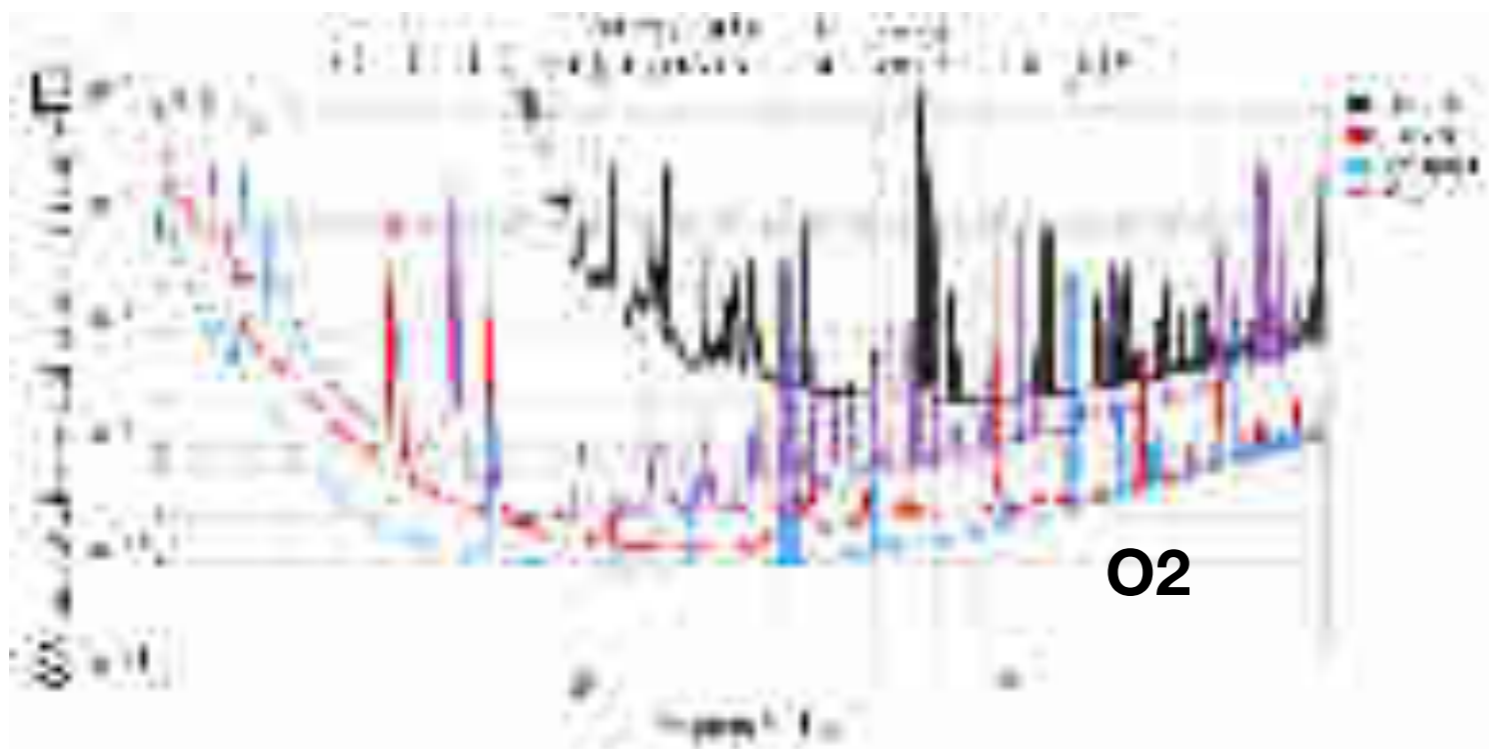
O2: six new events (LIGO had 7)

O2: 2 “detector and a half” events

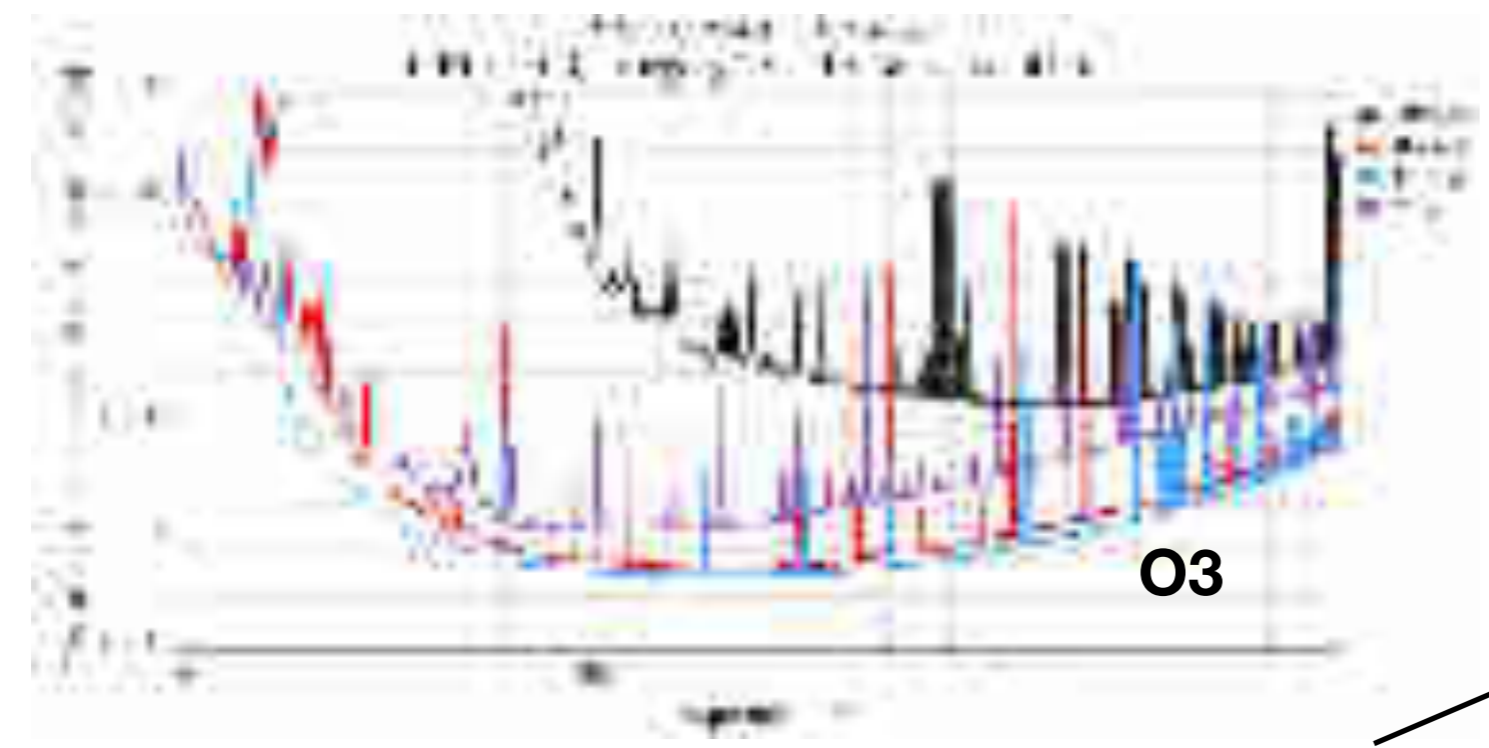
O2: One intriguing triplet of events from the same location in the sky and the same parameters

Approximately double the volume where events can be found. **The criteria to declare an event is the same.**

Noise PSD



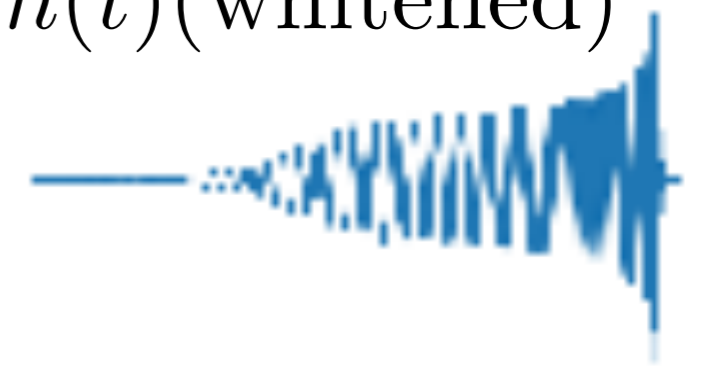
O2



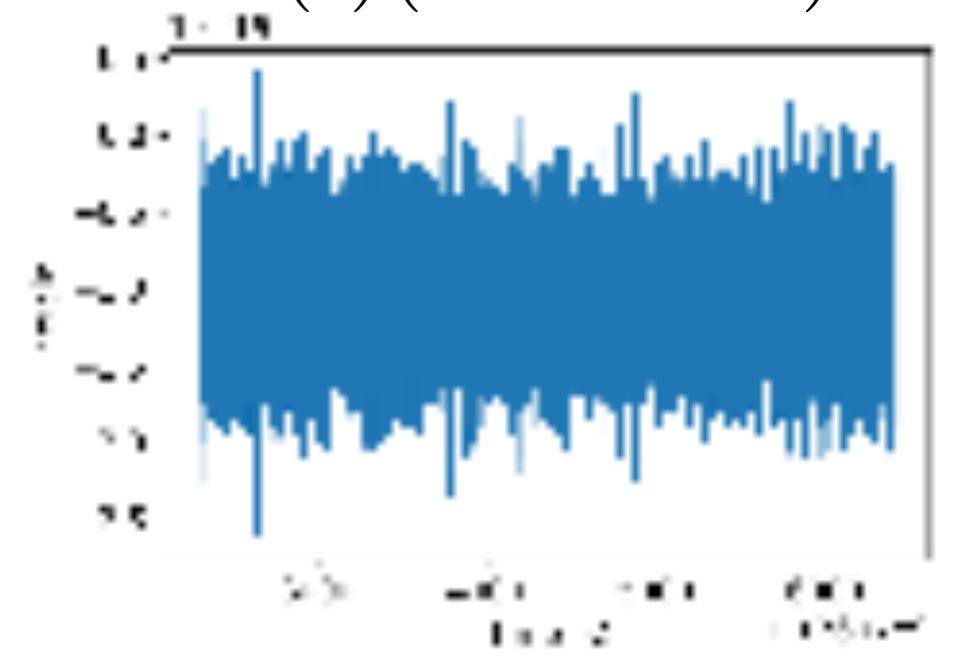
O3

Matched filtering

$h(t)$ (whitened)



$d(t)$ (whitened)

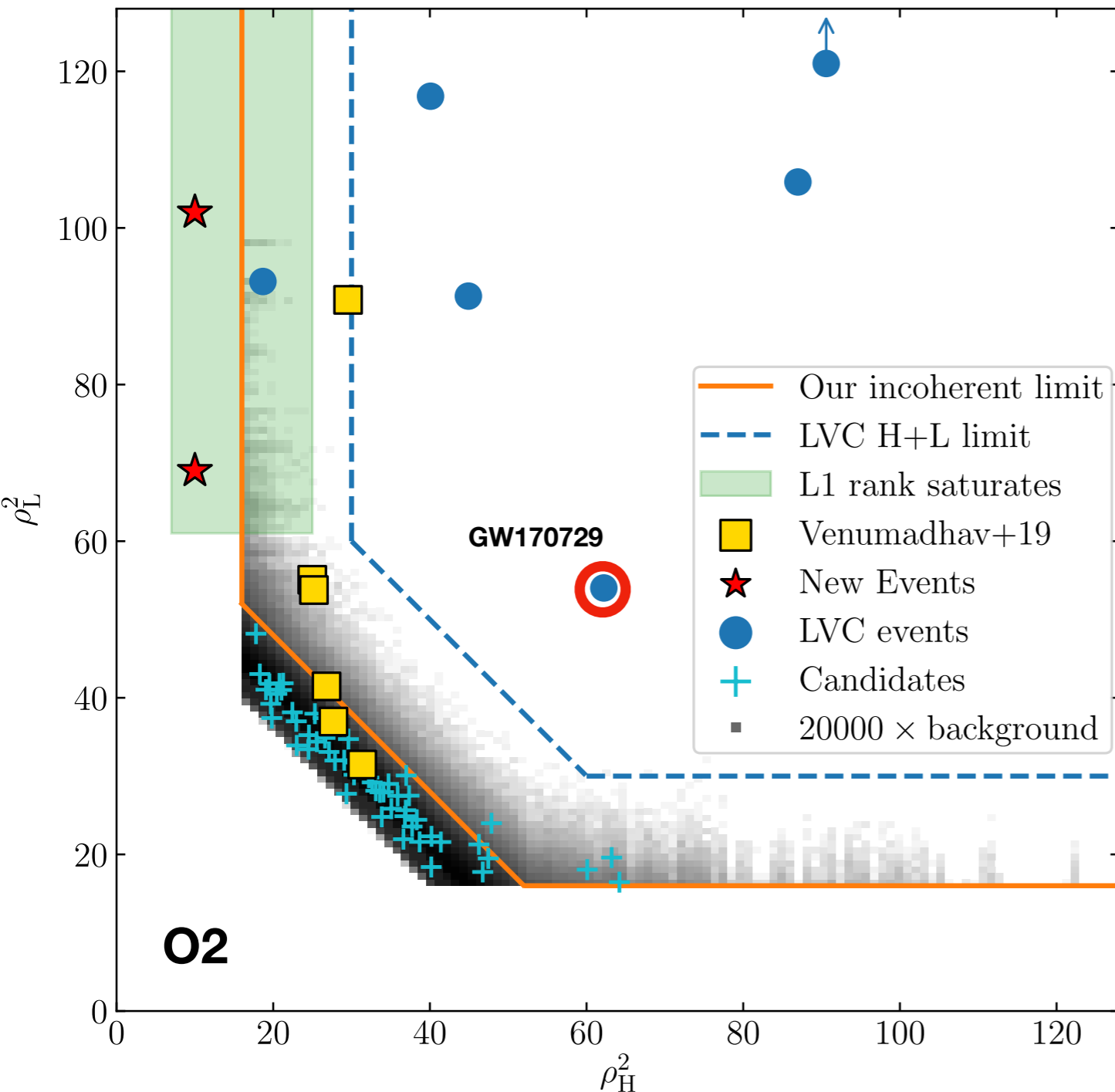


signal/noise \rightarrow

$$\frac{Z}{\sigma_Z} = \frac{\sum_f \frac{h^*(f)d(f)}{S_n(f)}}{\sqrt{\sum_f \frac{|h(f)|^2}{S_n(f)}}}$$

Sensitivity Comparison

Prior to demanding consistency between detectors



GW170729

LIGO FAR = 1 in 5 yrs

IAS FAR < 1 in 20000 O2 = 1 in 6500 yrs
(saturated by the amount of background we collected)

Additional suppression approximately $\Delta \text{snr}^2 = 20$. In trigger distributions going from 40 to 60 is approximately 3 orders of magnitude in the rate.

$$(90/64)^{1/2} = 1.2 \quad \text{and} \quad (90/64)^{3/2} = 1.7$$

Equivalent to reducing the strain noise amplitude by $\sim 20\%$

Equivalent to increasing the volume by $\sim 70\%$

You can reach the same conclusion about LVT during O1. The plot looks very similar.

Steps in a search pipeline

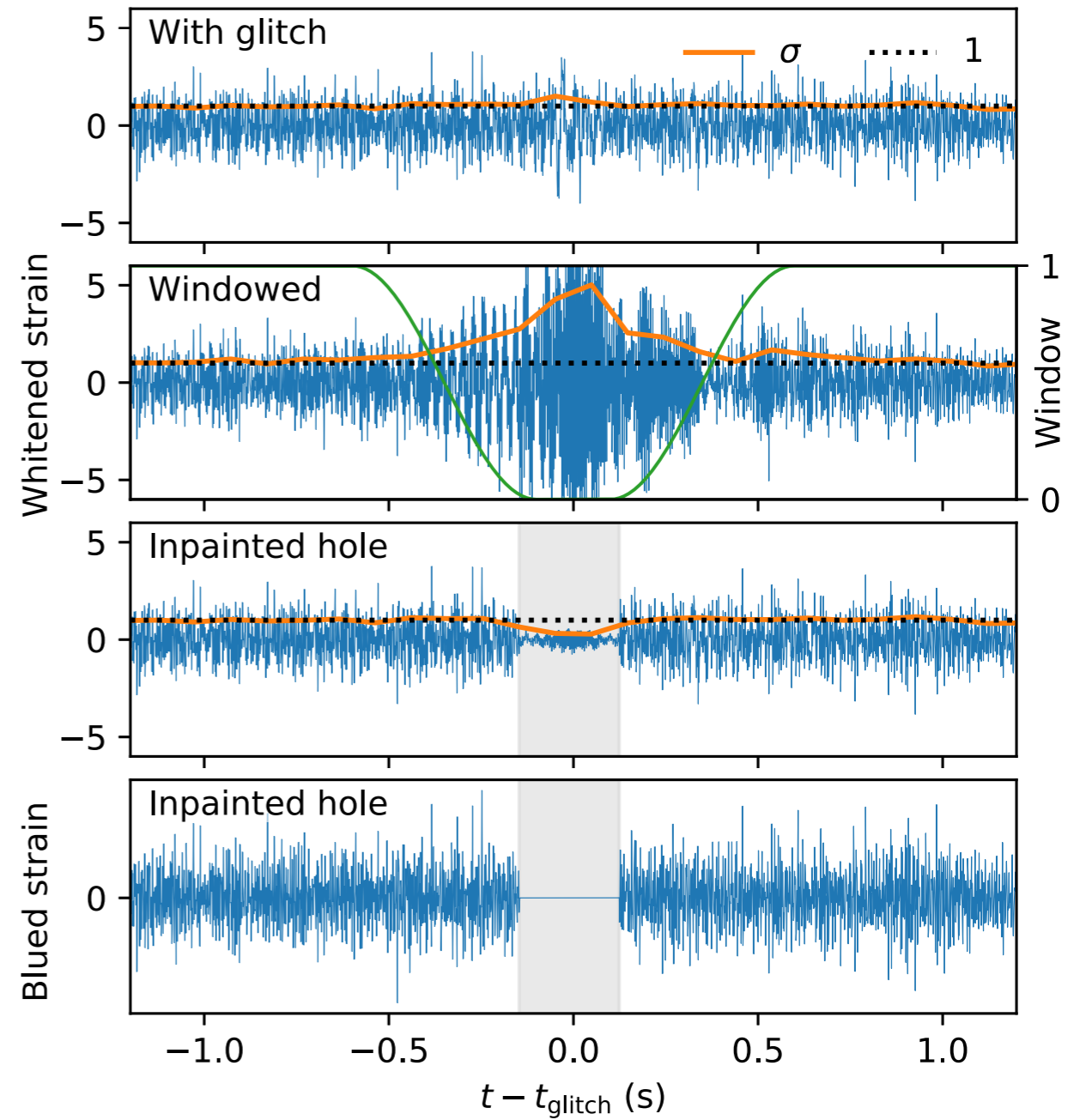
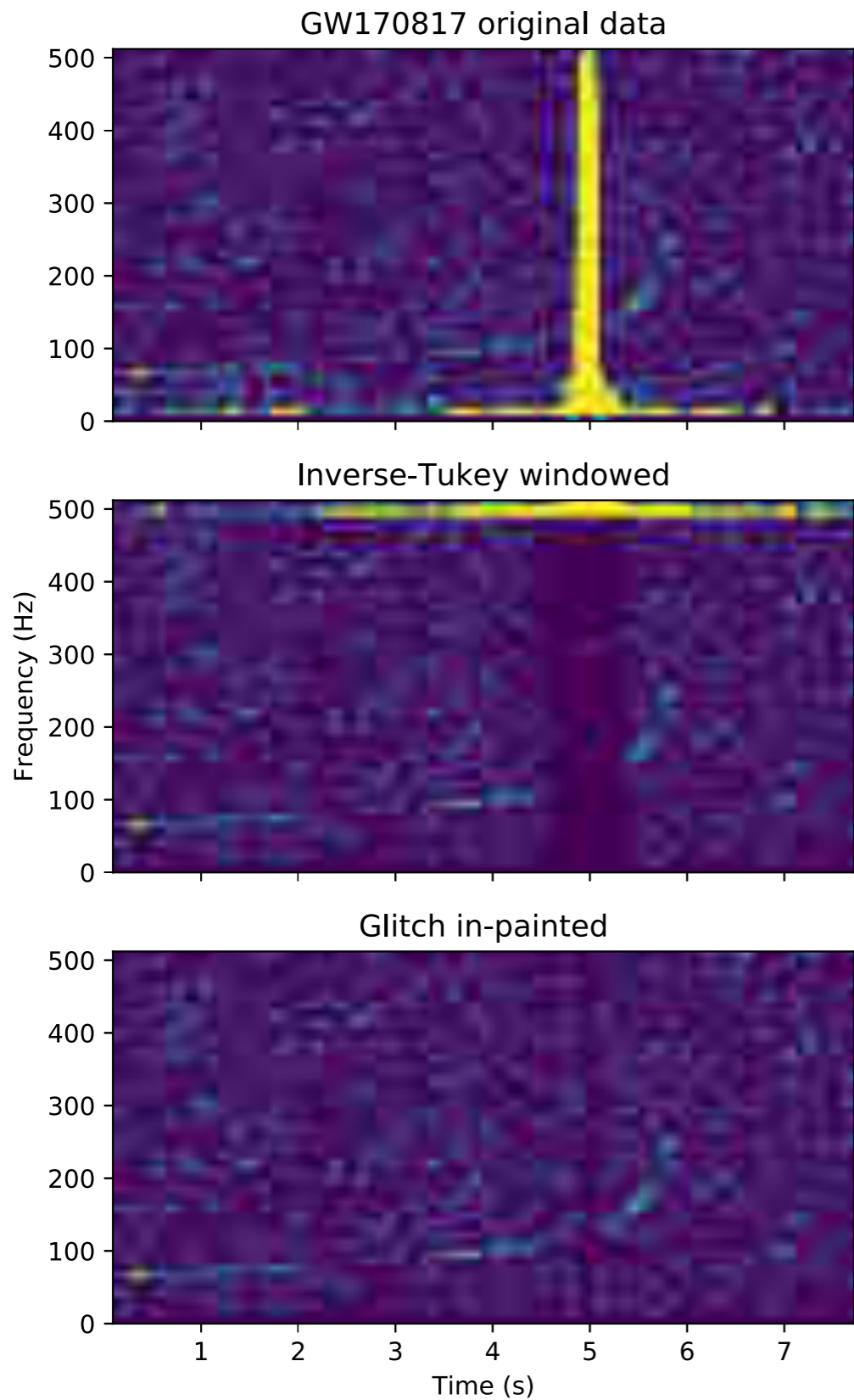
- Compute waveforms.
- Define a search strategy and construct a template bank.
- Estimate detector noise and account for its non-stationary nature.
- Detect bad data segments ("glitches") and insulate good data from them.
- Compute triggers and find coincident ones.
- Assess if triggers look like GW and veto those that don't.
- Assess if triggers are consistent between detectors.
- Estimate the background.

Philosophy

If a piece of data cannot be explained by either Gaussian noise or a gravitational wave signal of the type we are looking at it is discarded.

The residuals in the remaining should follow Gaussian statistics

Holes



$$z_w = \sum_f \frac{h^*(f) d(f)}{S_w(f)}$$

$$z_w = C_{ij}^{-1} h_i^* d_j = h^\dagger C^{-1} d,$$

$$\tilde{z}_w = h^\dagger C^{-1} F d.$$

GWTC-1: A Gravitational-Wave Transient Catalog of Compact Binary Mergers Observed by LIGO and Virgo during the First and Second Observing Runs

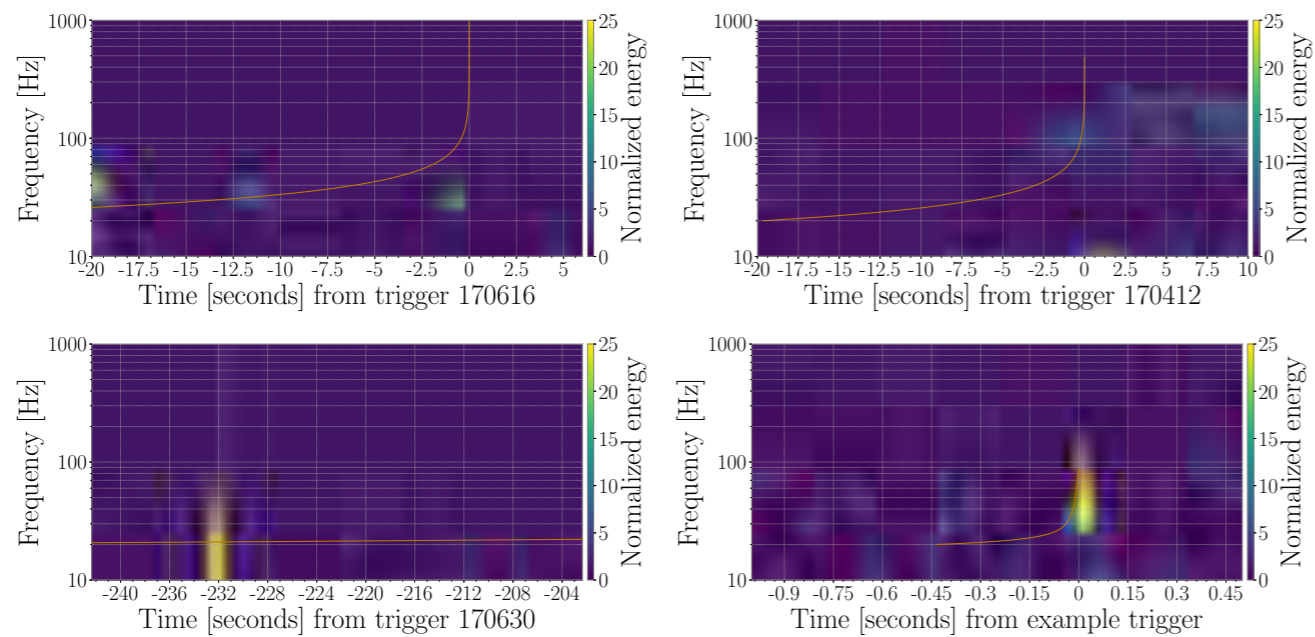


FIG. 15. Normalized spectrograms of the time around common noise artifacts with a time-frequency evolution of a related trigger template overlaid. Top Left: Scattered light artifacts at Hanford with the template of trigger 170616 overlaid. Top Right: A 60-200 Hz nonstationarity at Livingston with the template of trigger 170412 overlaid. Bottom Left: A short duration transient at Livingston with the template of trigger 170630 overlaid. Bottom Right: A blip at Hanford with the template of a sub-threshold high mass trigger overlaid.

Masking + Vetoing

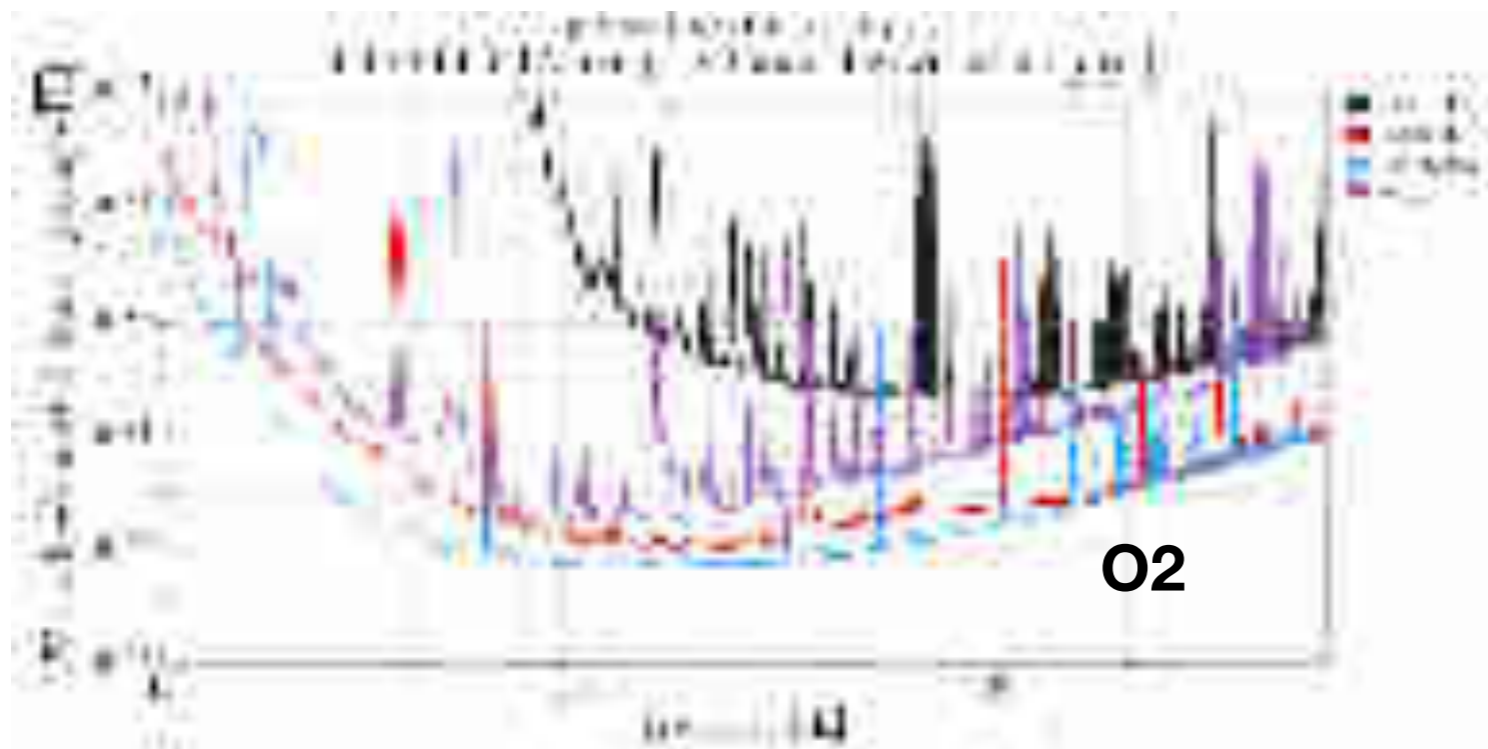
$$\frac{Z}{\sigma_Z} = \frac{\sum_f \frac{h^*(f)d(f)}{S_n(f)}}{\sqrt{\sum_f \frac{|h(f)|^2}{S_n(f)}}}$$

Replace: Use inverse covariance with infinite noise inside mask.

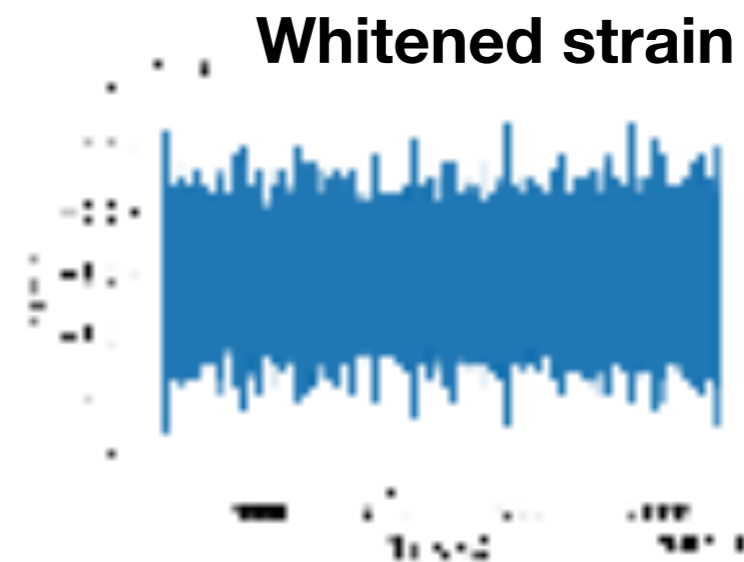
PSD drift

τ_{NL} non – Gaussianity

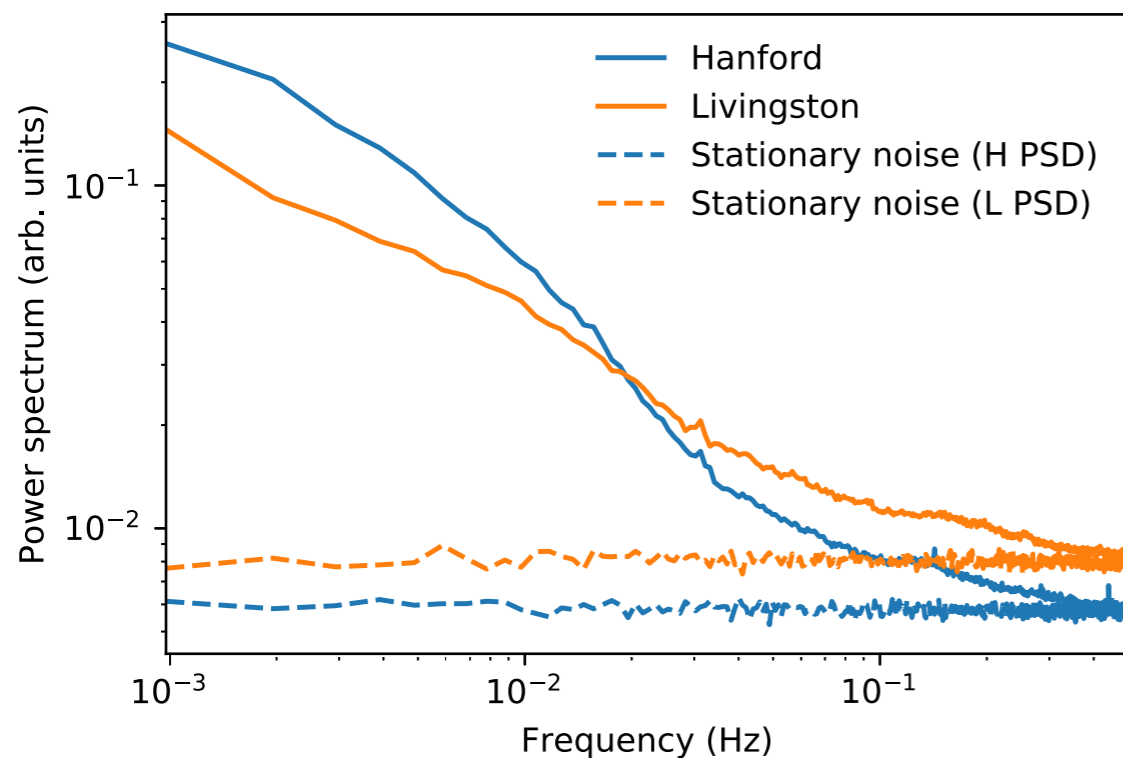
Waveform



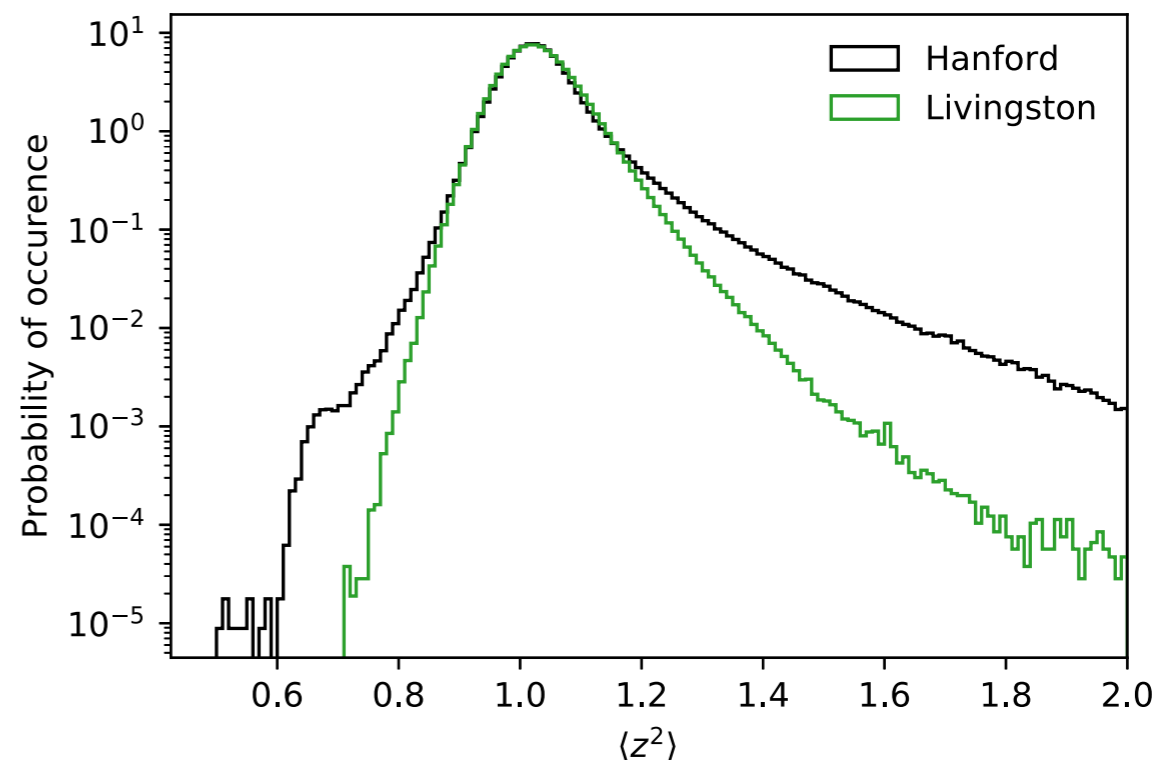
Whitened strain



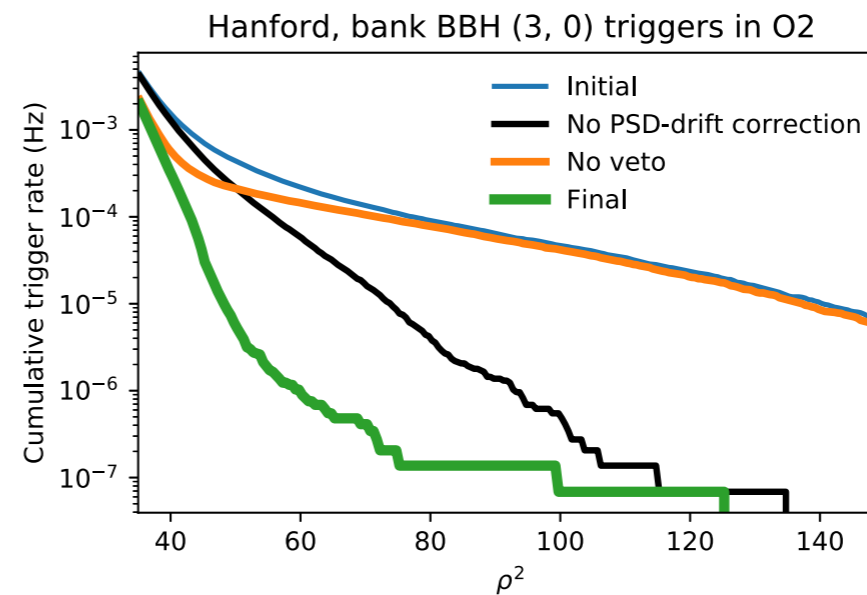
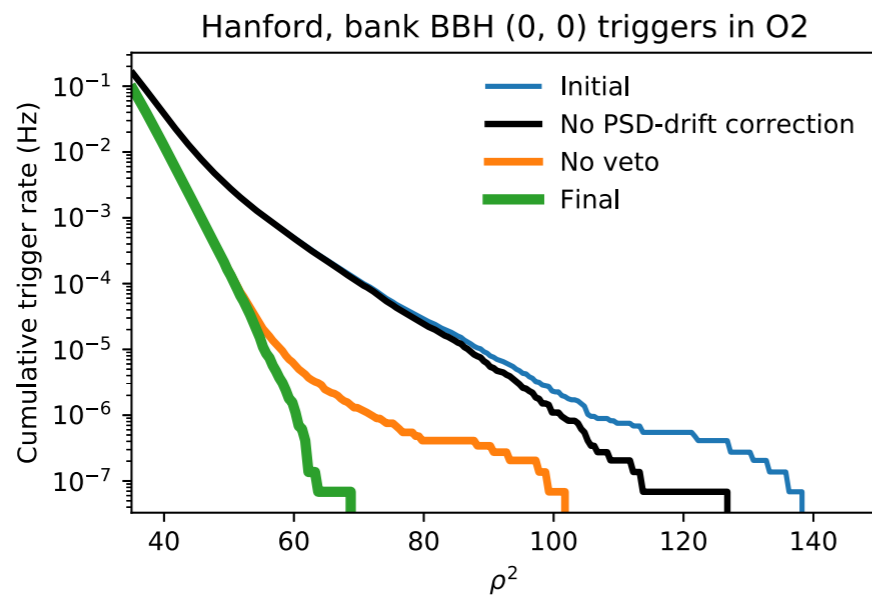
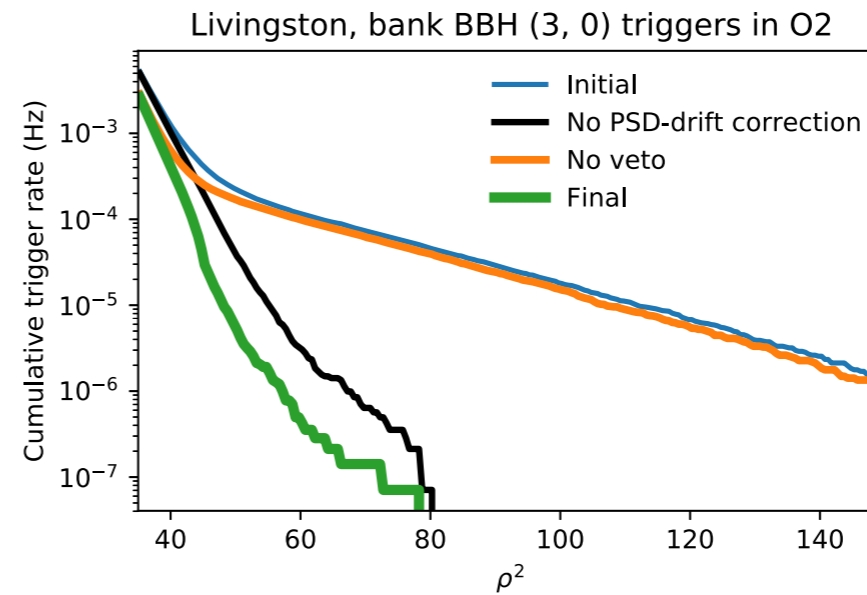
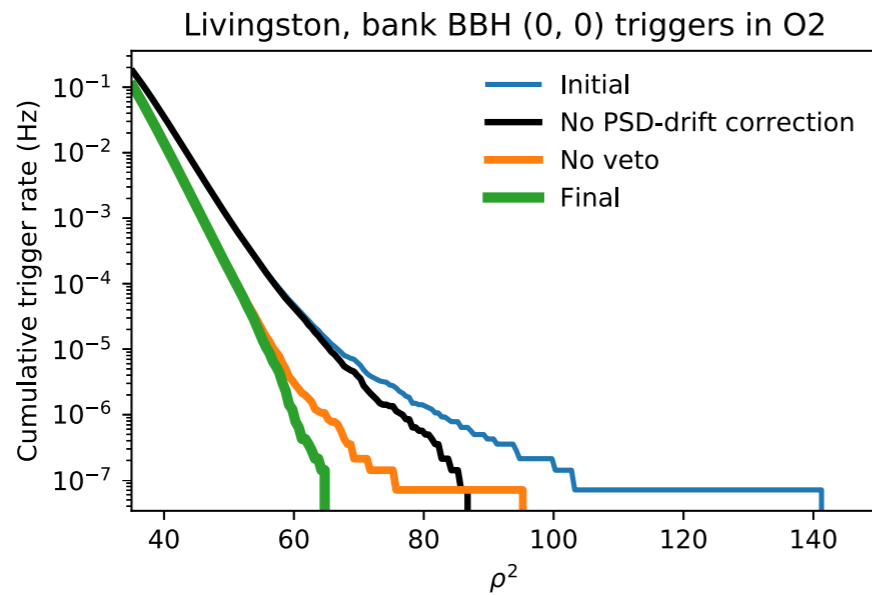
Power spectrum of the variance of the overlaps



Distribution of the variance of the overlaps



Effect of PSD drift and vetoes



Note that these plots are produced with data after masking (holes + in-painting).

Non-G of the data results in orders of magnitude increase in the rate of triggers.

Even in this heavy BBH bank all the outliers in a single detector are real events. Light BBHs and BNS have basically no glitches after masking all the non-G is PSD drift.

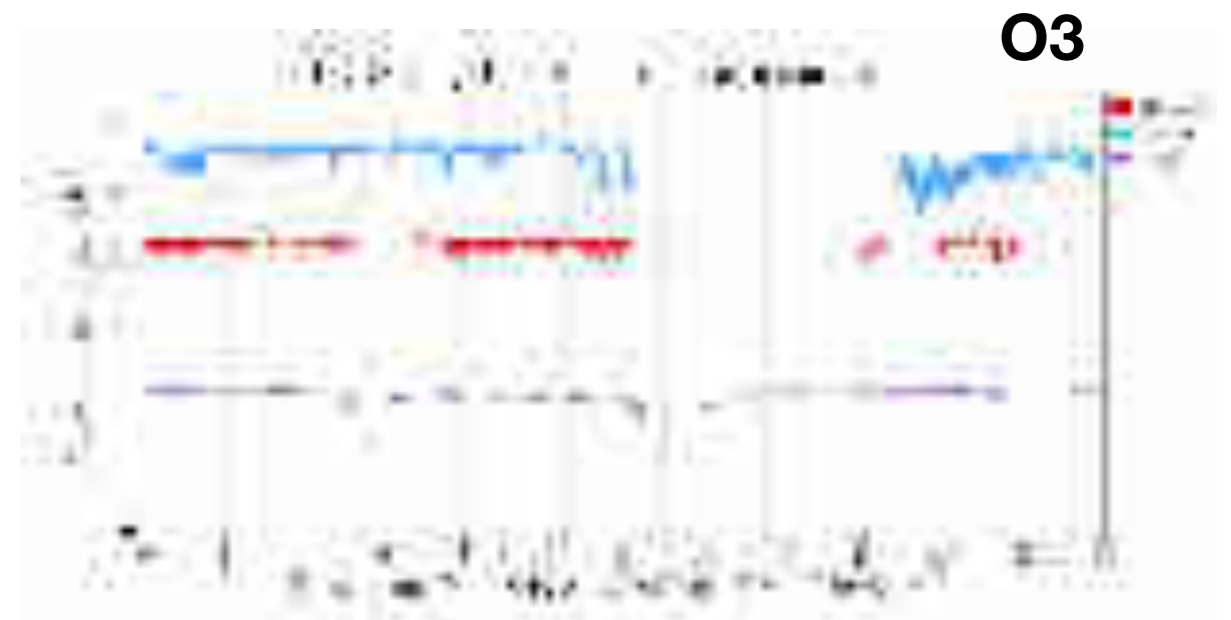
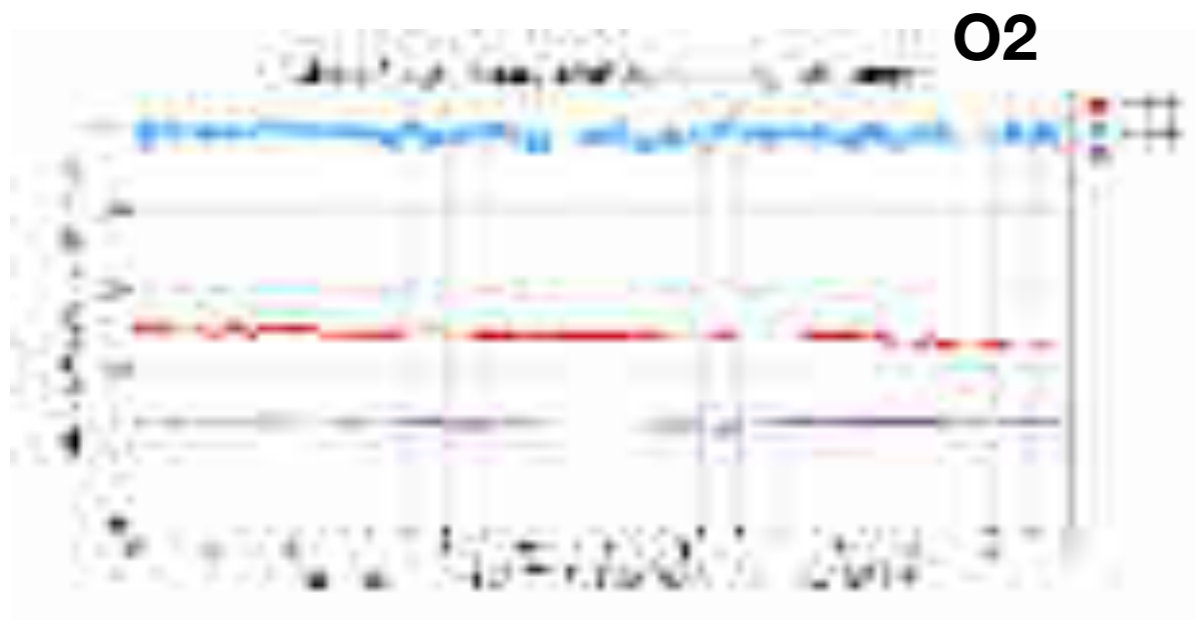
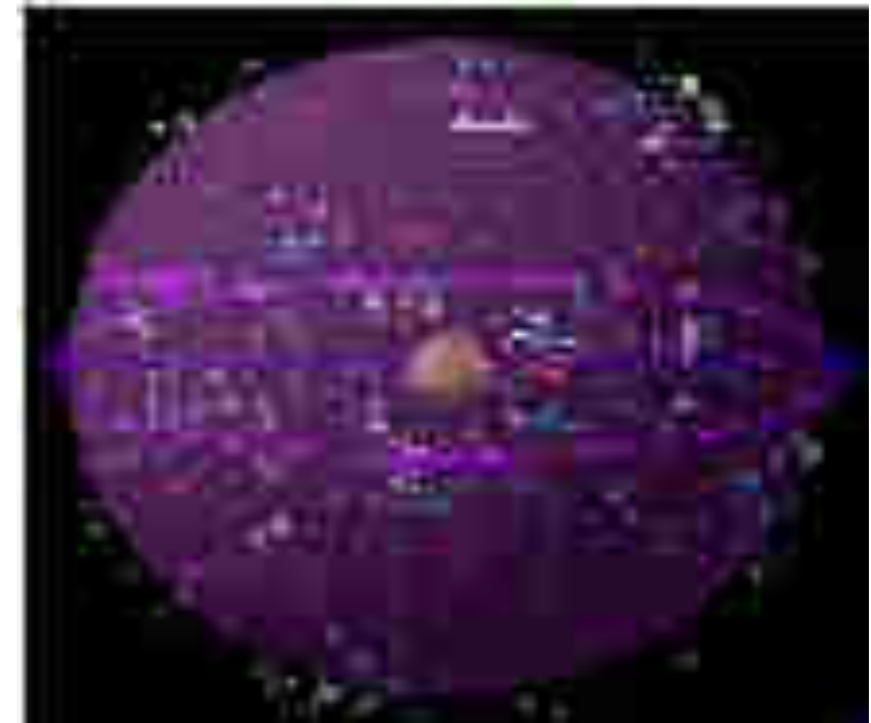
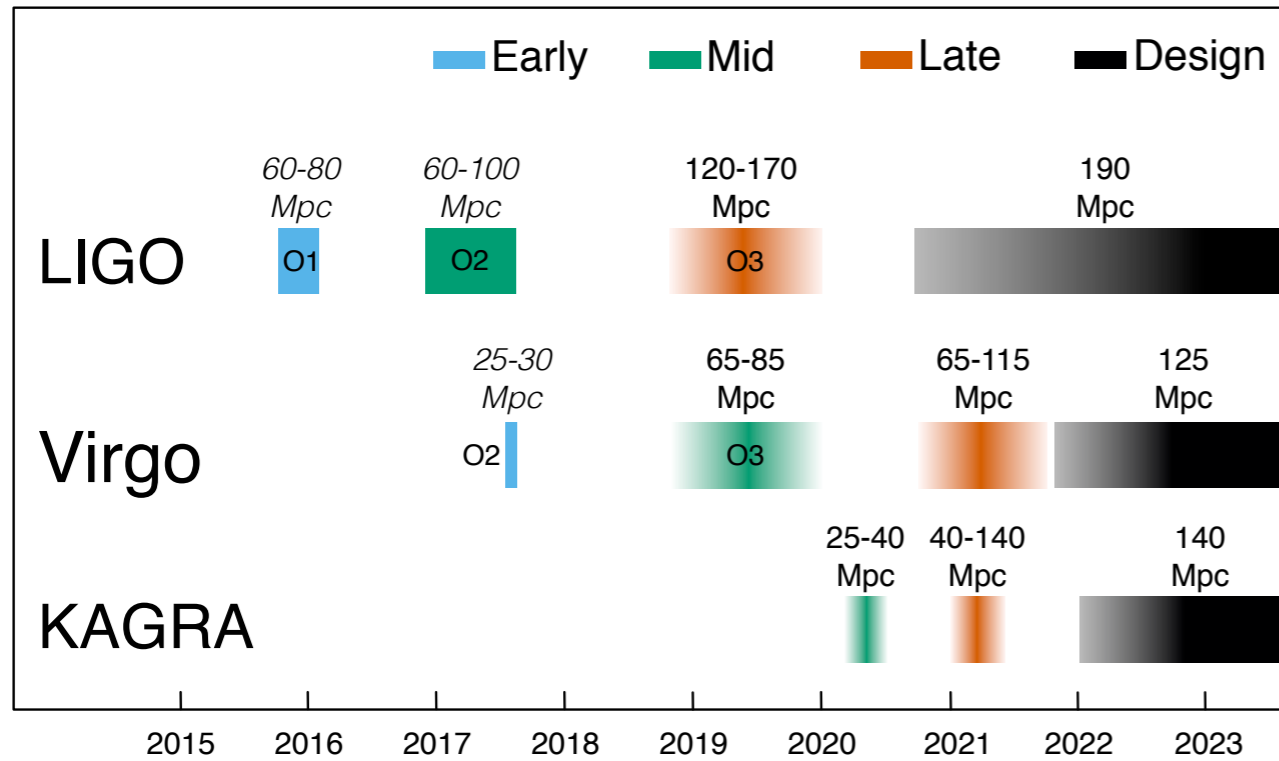
Trigger rate for PyCBC above 64 approx 10^{-4} Hz.

Summary

- The origin of BH binaries is an astrophysical puzzle. We might be able to solve it in the near future by studying the properties of individual systems.
- Puzzling results in the heavy and light ends of the BH mass function. Spin distribution begins to be informative.
- The availability of the LIGO data gives the community an opportunity to try new ideas and propose new methods. We are very grateful to the LVC.
- We have developed a new pipeline and tried to incorporate several new elements, a new geometric template bank algorithm, PSD drift correction, aggressive data masking and hole filling, objective vetoing of triggers, coherent combination of detectors, etc.
- We estimate that our pipeline is sensitive to twice the volume. We have found one new event in O1 and six new events in O2 and produced a new list of sub-threshold candidates. The properties of some of these new events are quite interesting.
- We think that our improvements carry over to the O3 data. Unfortunately that data is not public but will be soon.

Extra:

Advanced Ligo Observing Runs



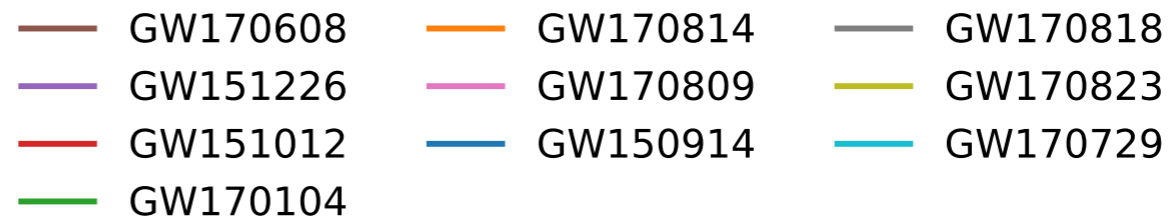
Neutron star mergers

- What happens when two neutron stars merge? What should one see at different wavelengths and in different directions?
- Sizes of neutron stars (high frequencies in the GW signal)
- What is left after the merger?
- Origin of heavy elements (r-process elements)
- Speed of propagation of gravitational waves (part in 10^{15})
- Distance scale (Hubble constant; error 10 km/s/Mpc per event)

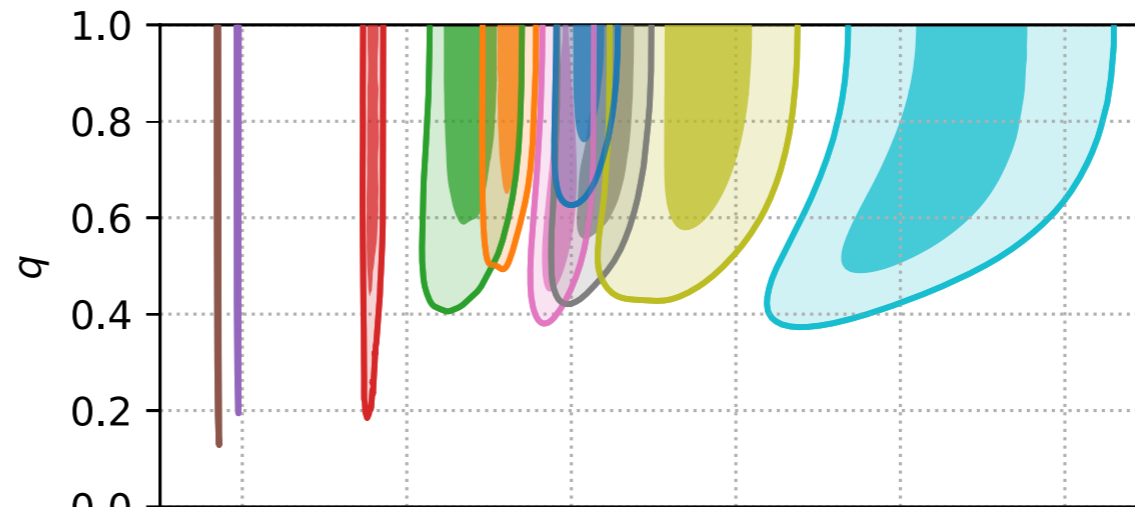
Binary Black Holes (stellar)

- Do BH behave as GR predicts?
- Distance scale (Hubble constant; no counter-part so only statistical through clustering)
- Properties of the evolution of massive stars (BH mass vs initial mass)
- What is the origin of the black hole binaries?

LIGO Events O1 + O2

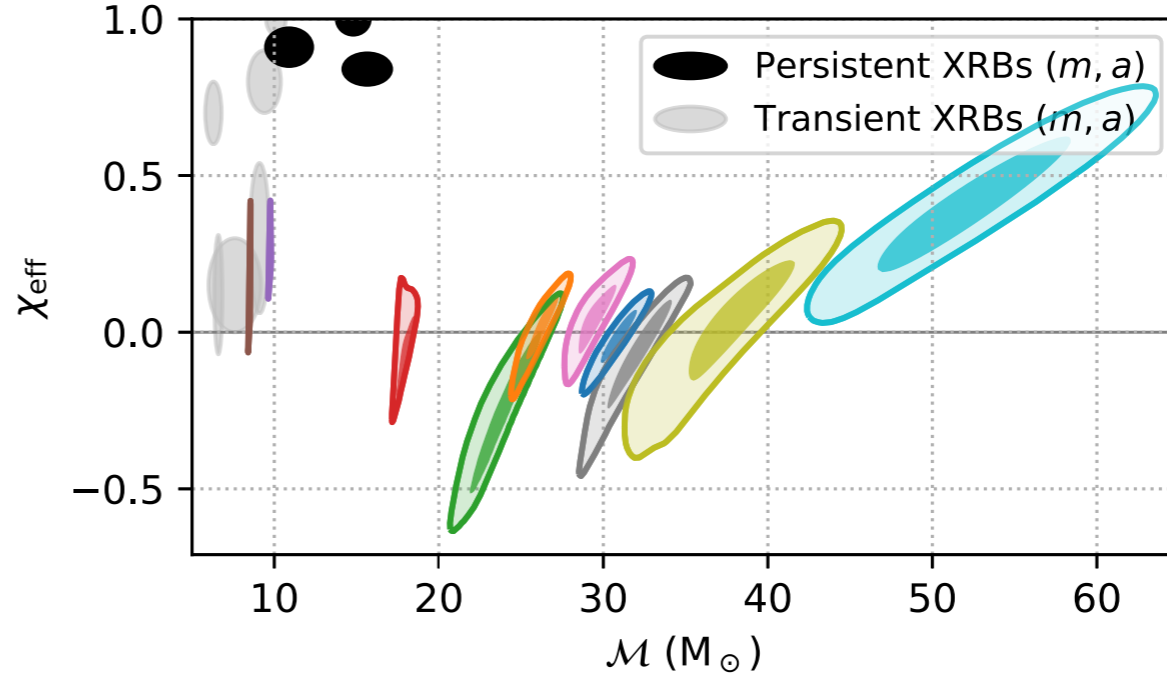


Mass ratio



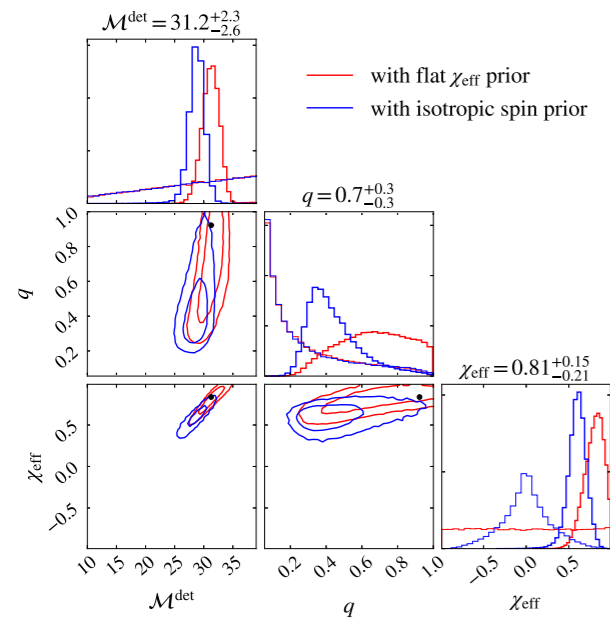
Combined spin in the
direction of the angular
momentum

$$\chi_{\text{eff}} = (m_1 \chi_{1z} + m_2 \chi_{2z})/M$$

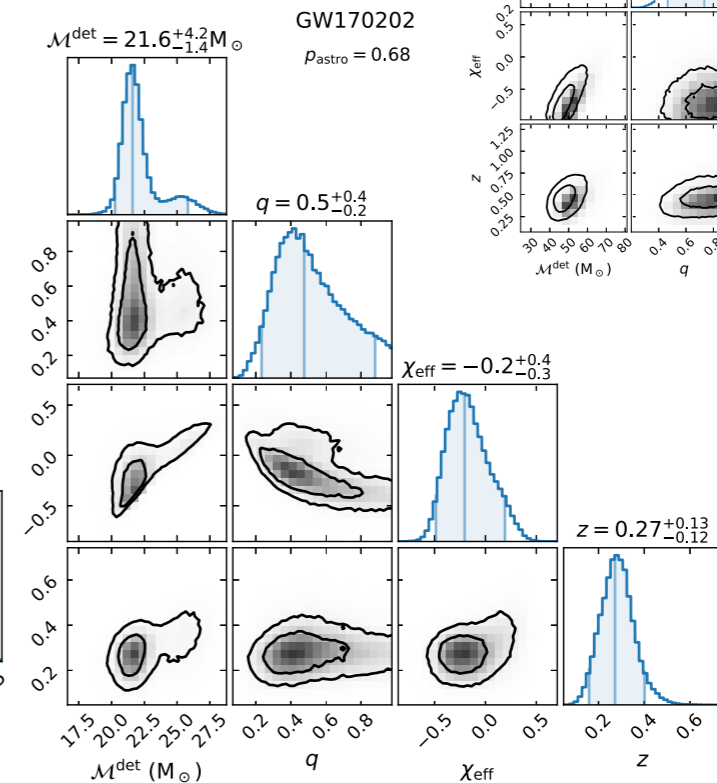
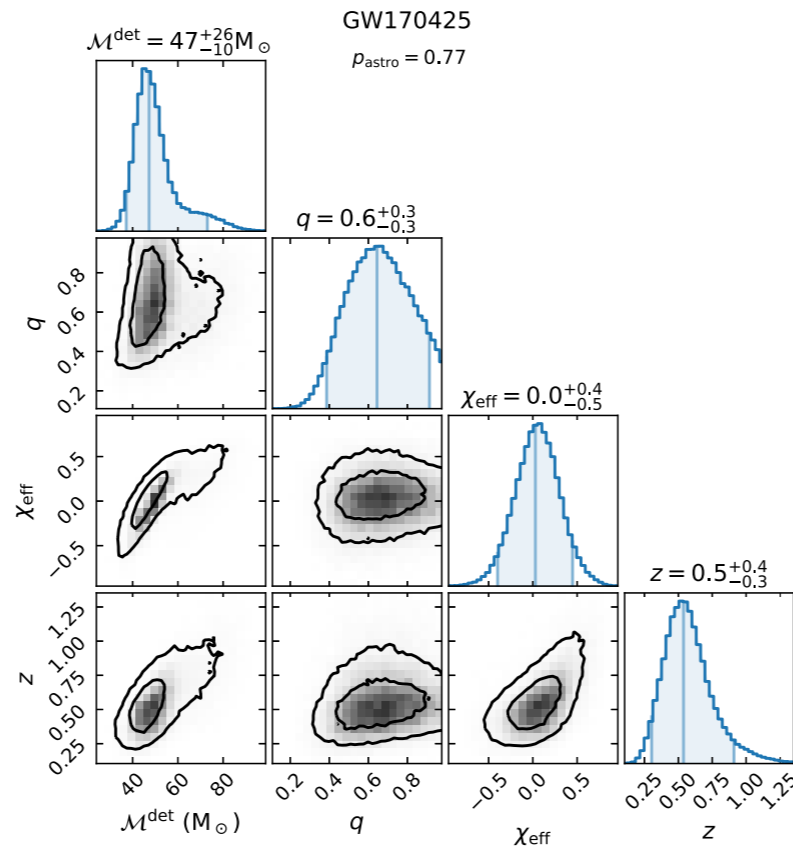
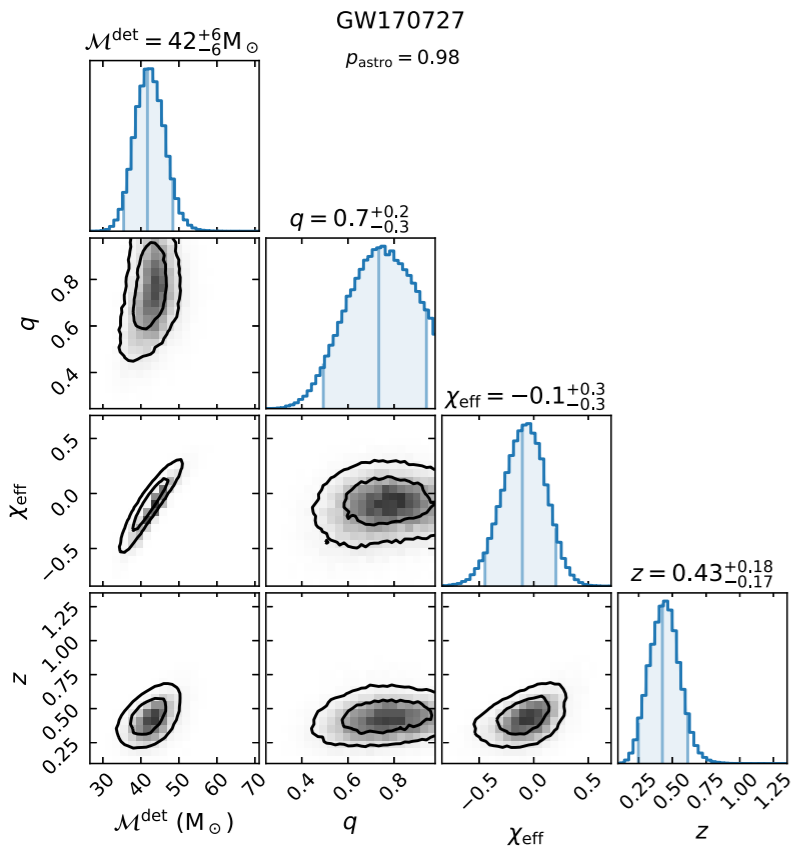
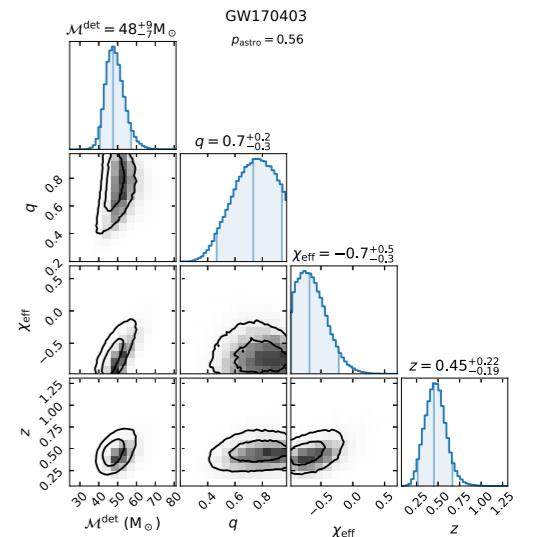
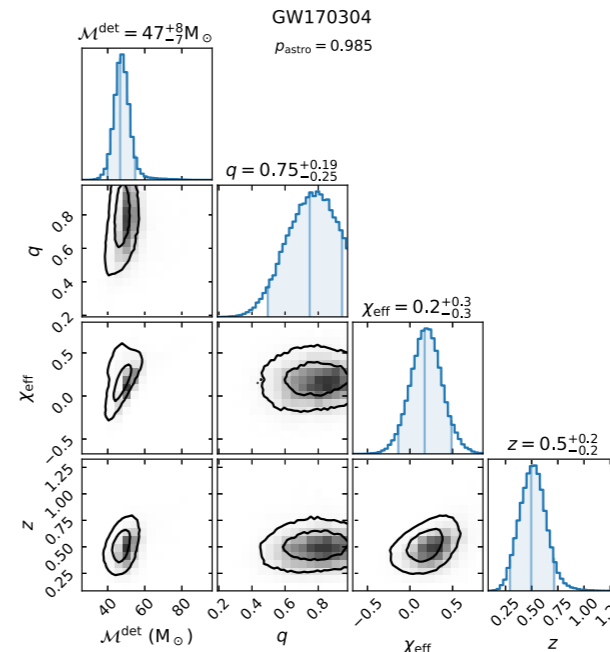
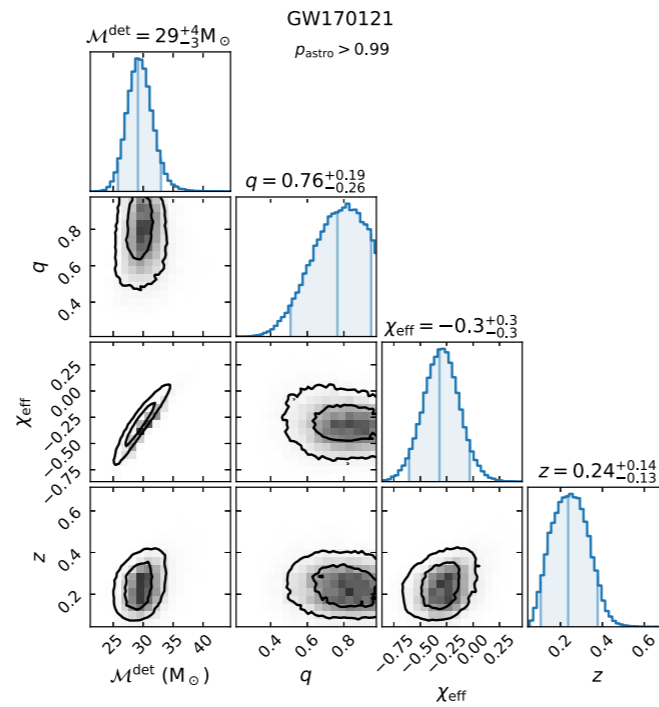


Chirp mass

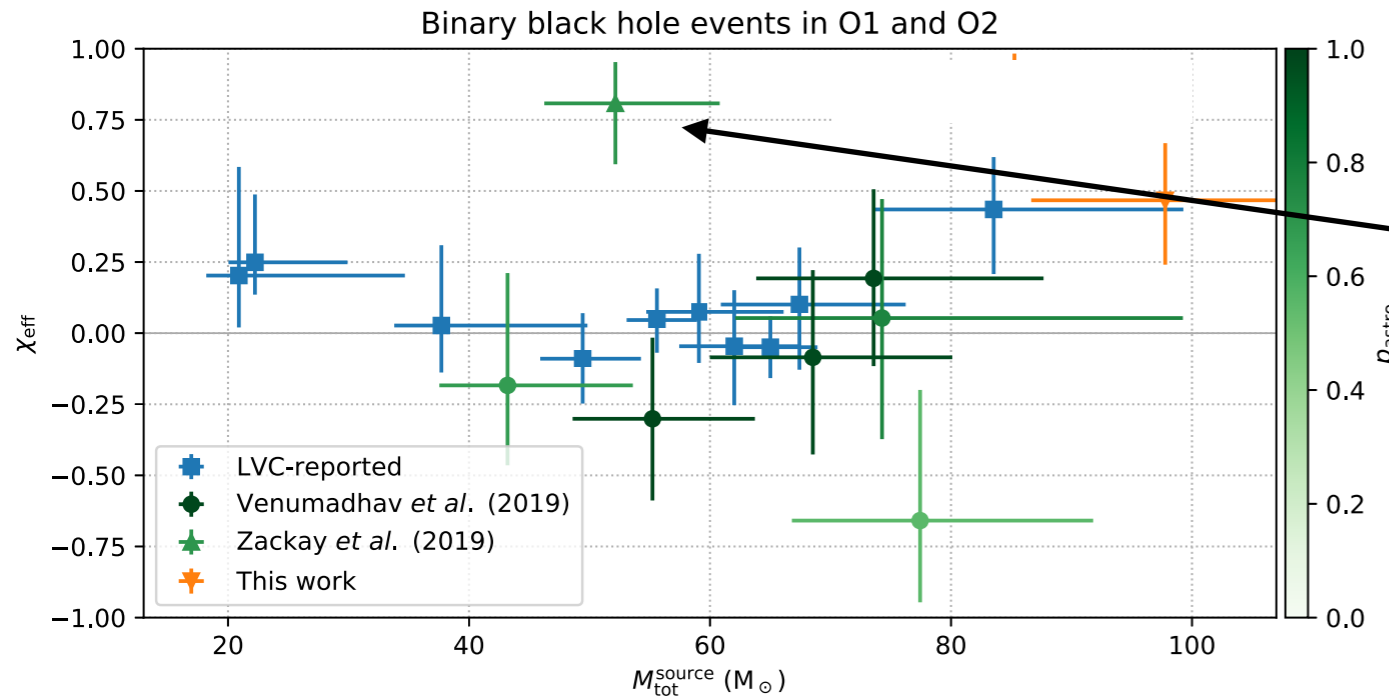
Parameters of new detections



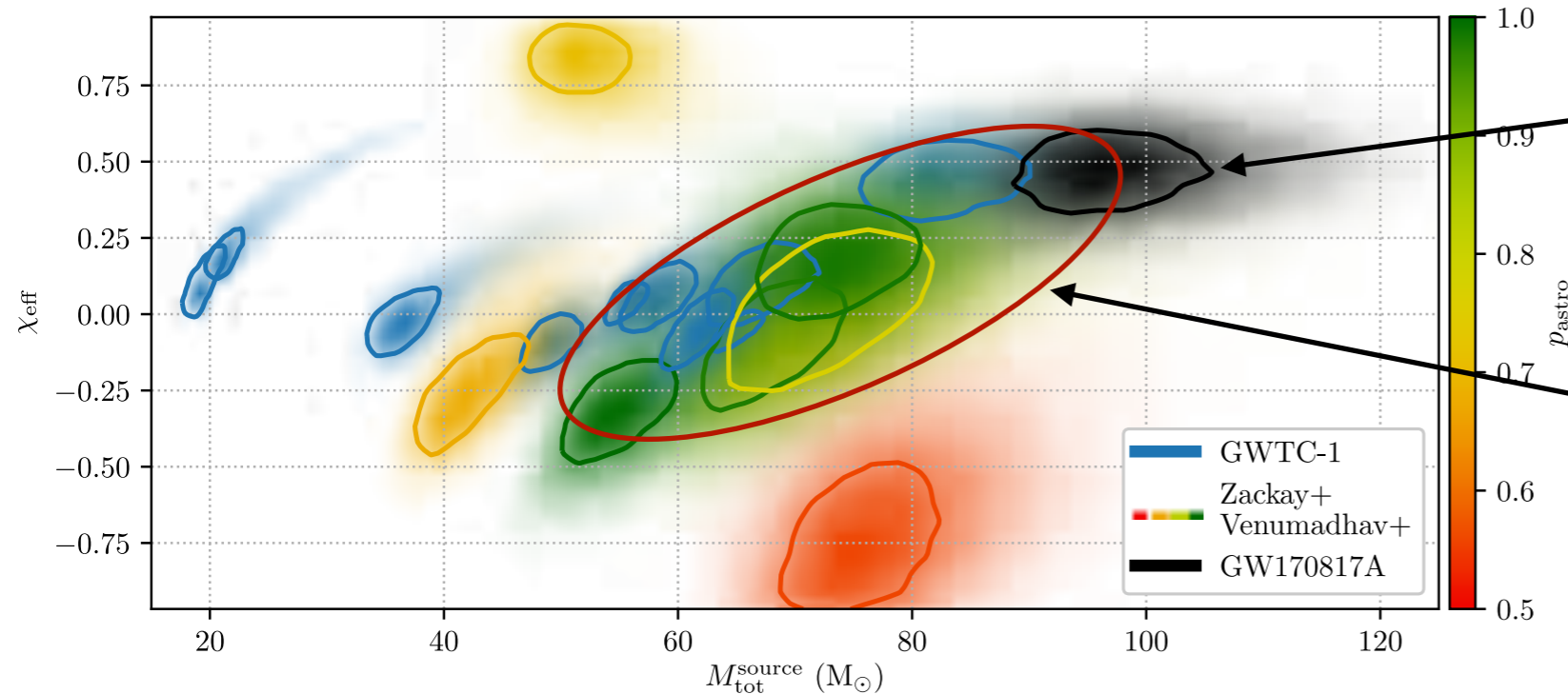
GW151216



Events in O1 & O2



High spin points to this system being formed through binary evolution. Inconsistent with the isotropic prior, meaning it is inconsistent with scenarios that produce this prior. Obviously outlier with respect to spin. Similar mass and both spinning or differ by factor of 2 in mass and heavy is highly spinning. High redshift, suggestive?

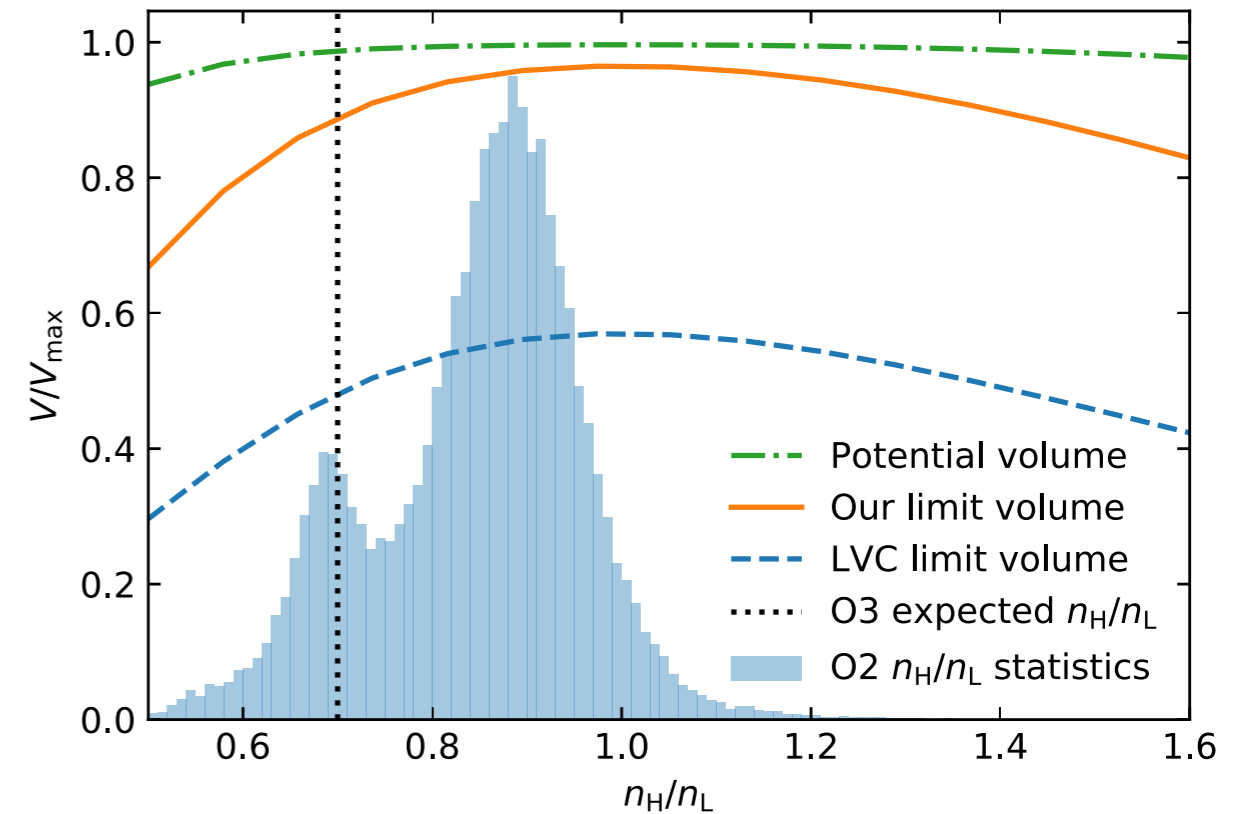
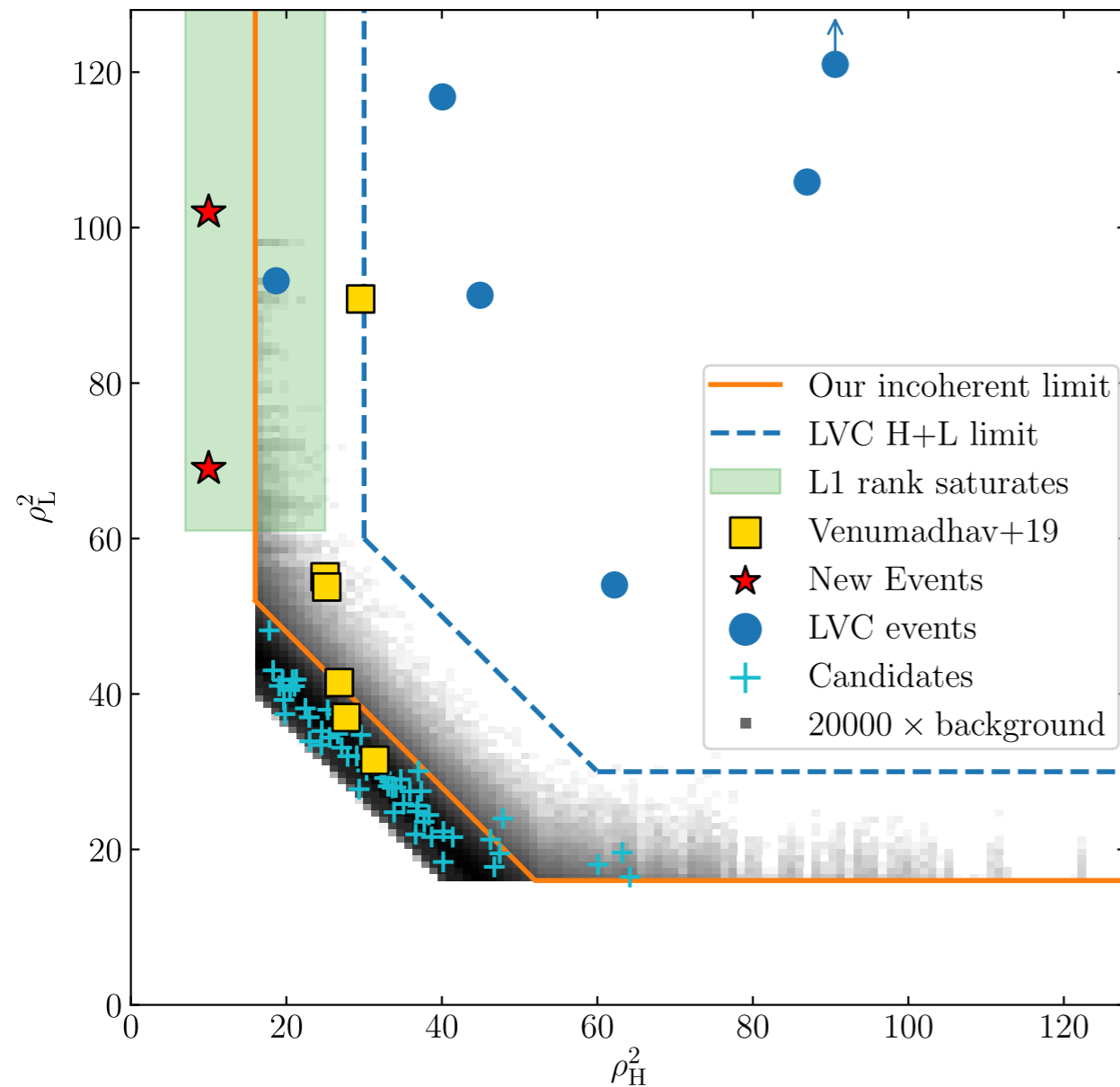


Heaviest so far. Implications for mass gap? Note this is a detector and a half event.

Suggestive trend?

FIG. 7: Binary black holes events reported from O1 and O2, in the plane of source-frame total mass vs. effective spin. In blue are shown the 10 BBH events reported in GWTC-1 [1], all of them are certainly astrophysical in origin ($p_{\text{astro}} = 1$). Color coded by p_{astro} are shown 7 additional events with $p_{\text{astro}} > 0.5$ that our previous searches found [2, 4]. In black we show GW170817A. Displayed are 1σ probability contours, i.e. enclosing $1 - e^{-1/2} \approx 0.39$ of the probability distribution.

Single detector search



Asymmetric detectors is difficult:

1. Empirical probability in L difficult to measure
2. Signal in H can be below collection limit

Single detector search

Bank ID	# $\rho_L^2 > 45$	# $\rho_L^2 > 55$	# $\rho_L^2 > 65$
(2,0)	10178	172	1
(2,1)	1558	50	7
(2,2)	734	226	102
(3,0)	337	18	7 ^a
(3,1)	157	11	3
(3,2)	41	8	4
(4,0)	37	3	1 ^b
(4,1)	14	1	0
(4,2)	9	3	2
(4,3)	32	11	4
(4,4)	215	77	31

^a Six of the seven triggers in bank (3,0) are previously declared gravitational wave signals. The seventh is declared in this paper

^b This trigger is GW170823

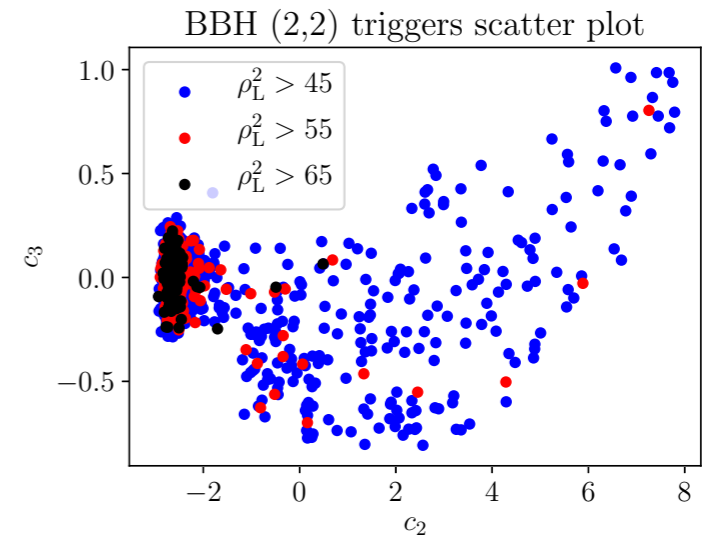


FIG. 8: The table in the left-hand panel shows the number of veto-passing L1 triggers in each sub-bank above a few threshold values of the SNR. The non-uniform numbers of triggers with $\rho_L^2 > 65$ shows that glitches are localized within certain sub-banks. The plot in the right-hand panel shows the coefficients labeling the templates for triggers above the thresholds for bank BBH (2, 2). Note that glitches are localized within a small region of parameter space.

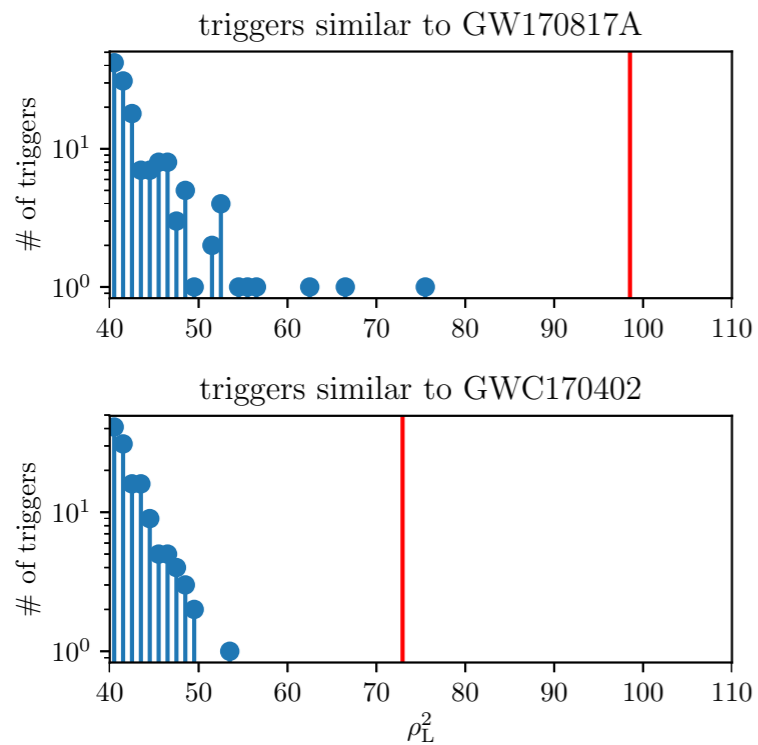
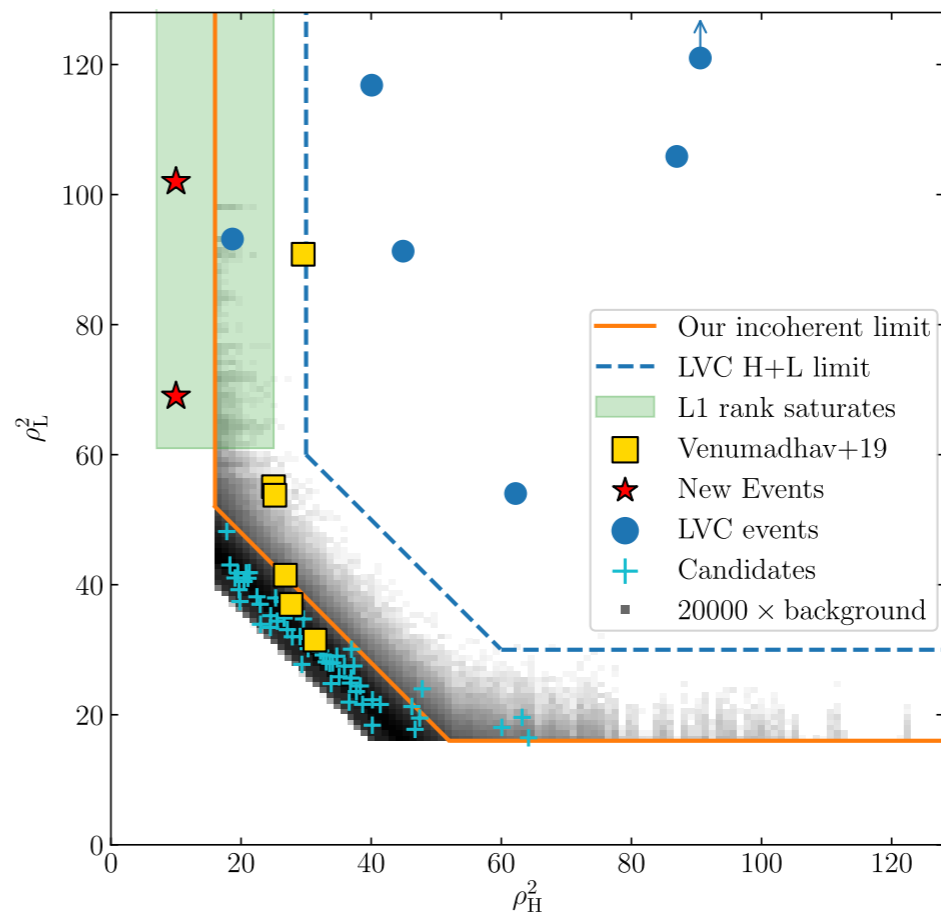
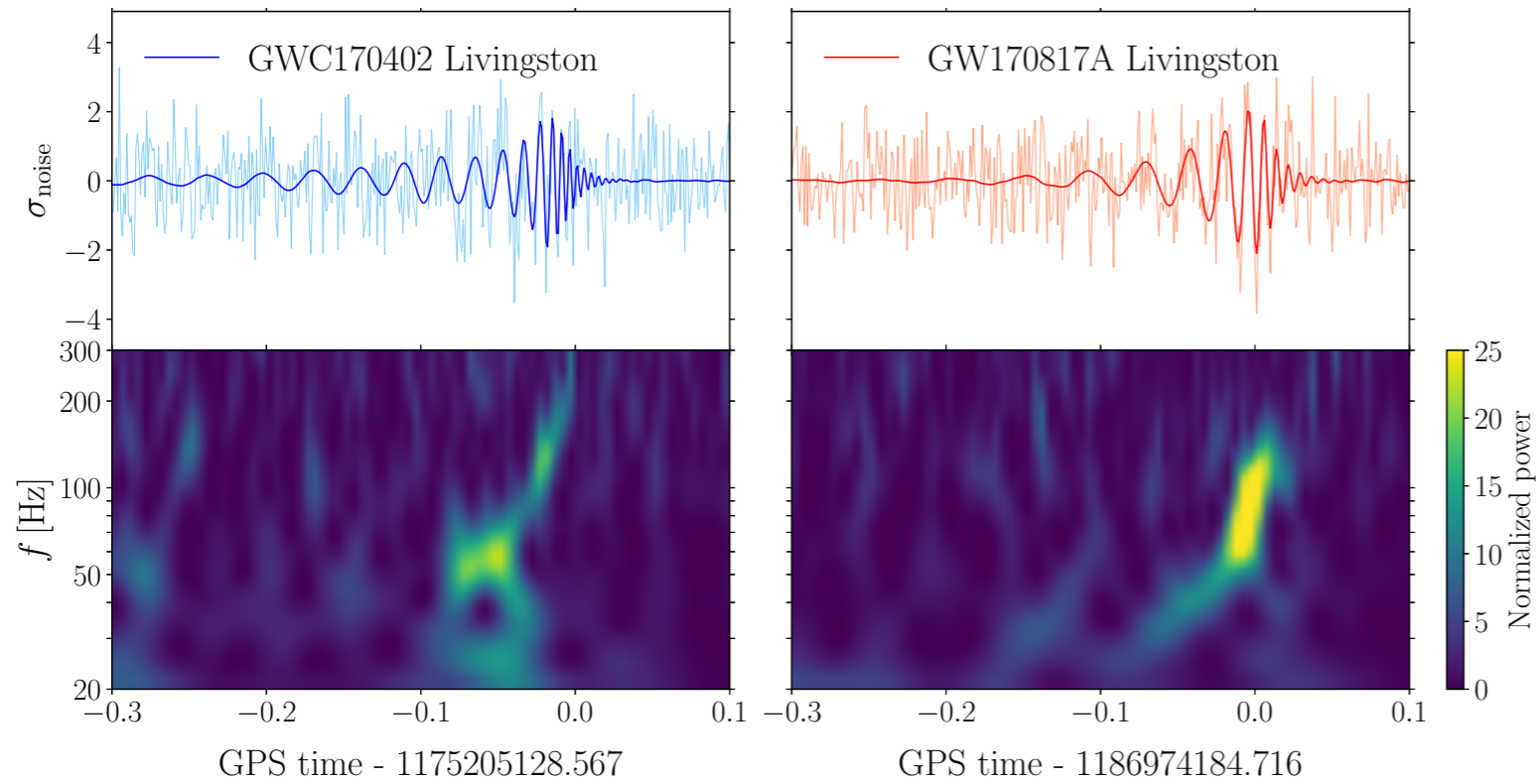


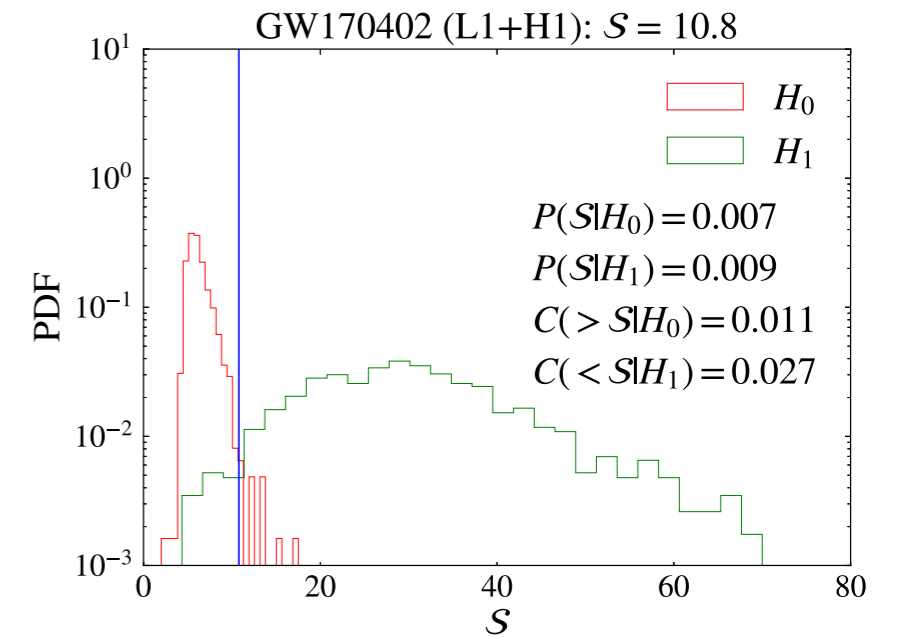
FIG. 3: Distributions of L1 SNR² for triggers for templates that are similar (match > 0.9) to the best-fit templates for the two newly found events, that occur at times when the H1 detector is operative. Vertical red lines mark the values of ρ_L^2 for the two events. To give context to the amount of phase space that is included in this plot, the upper (lower) panel includes triggers from 28% (0%) of bank BBH 4, and 1.8% (3.6%) of bank BBH 3.



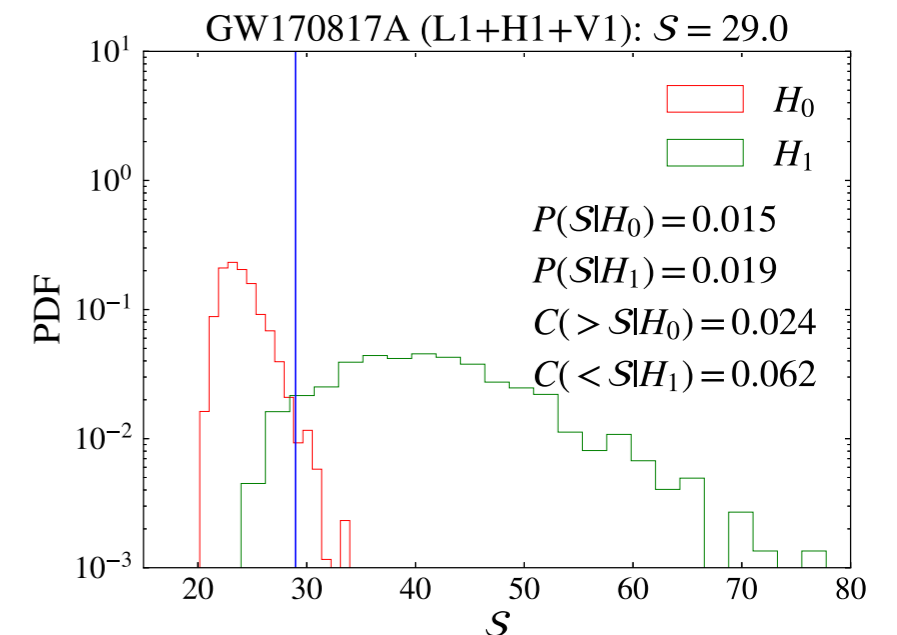
Single detector search



$$e^{\mathcal{S}} := \int \mathcal{D}\Theta_{\text{ext}} \Pi(\Theta_{\text{ext}}) \mathcal{L}(d|\Theta_{\text{intr}}, \Theta_{\text{ext}}).$$

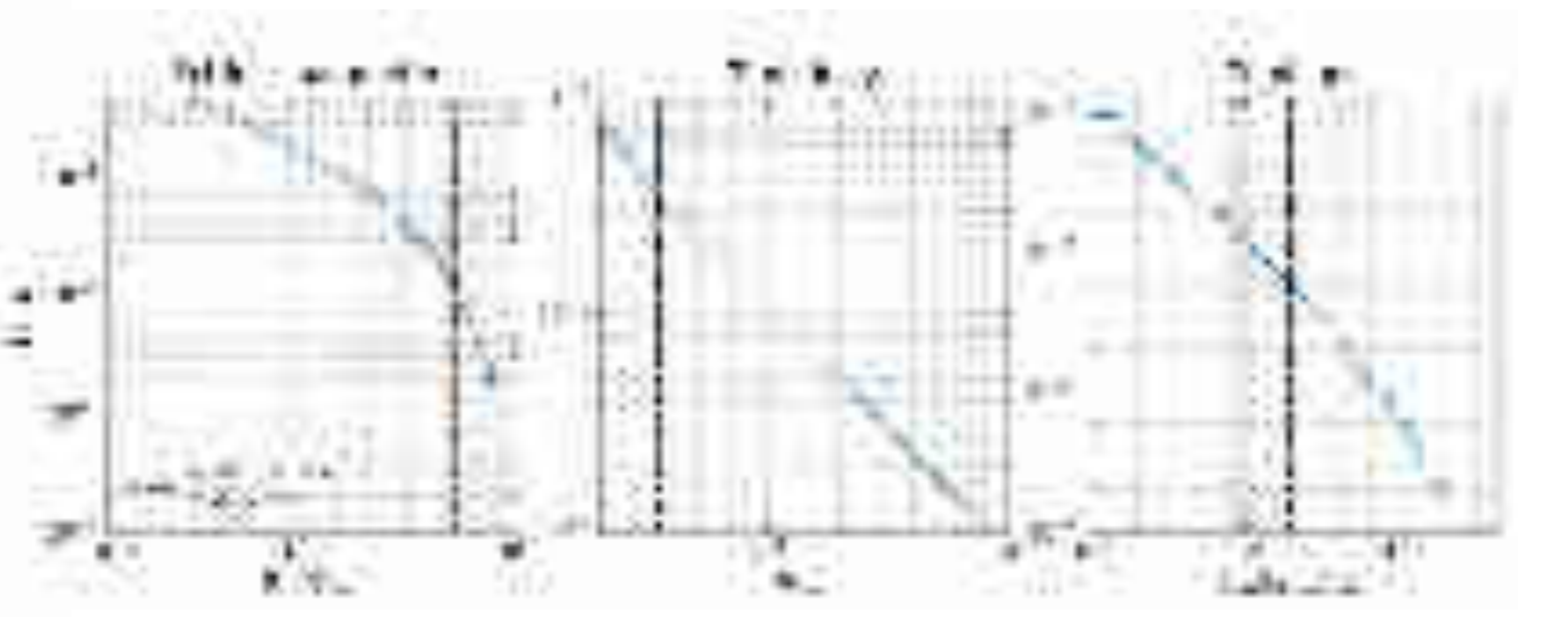
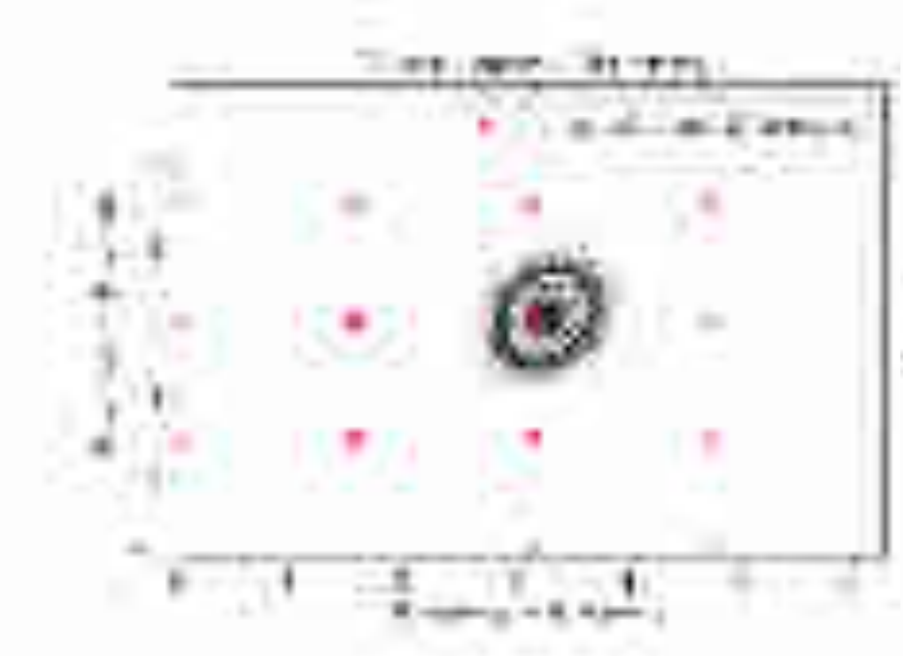
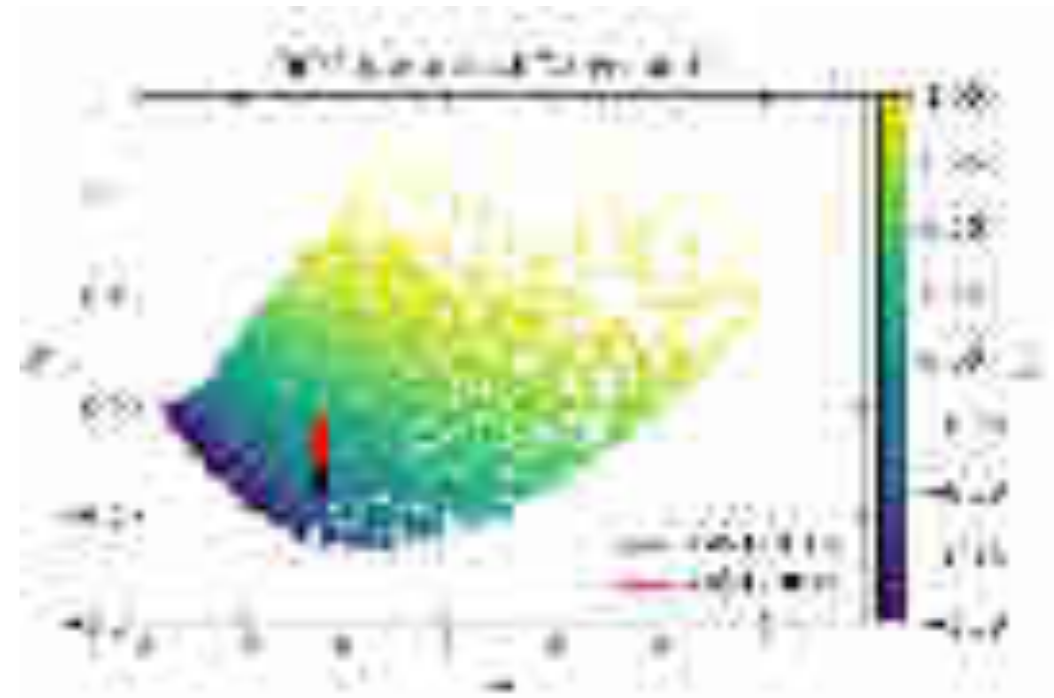


L1 rank	GPS time	ρ_L^2	# similar triggers	$C(S H_0)$	$C(S H_1)$	$\frac{P(S H_1)}{P(S H_0)}$	Comment
1	1187058327.068	93.1	0	$< 10^{-3}$	0.16	37	GW170818 ^a
2	1187529256.504	92.1	0	-	-	-	GW170823
3	1169069154.564	90.8	0	-	-	-	GW170121
4	1175205128.565	72.9	0	0.015	0.022	0.547	GWC170402
5	1186741861.51	174.6	1	-	-	-	GW170814
6	1167559936.584	107.3	1	-	-	-	GW170104
7	1186302519.731	118.6	2	-	-	-	GW170809
8	1186974184.716	98.5	5	0.028	0.055	0.98	GW170817A
9	1174043898.842	75.7	9	0.36	0.001	0.008	Background
10	1170885005.109	66.4	16	0.49	0.003	0.013	Background
11	1178083239.592	74.4	22	0.34	0.003	0.016	Background
Removed ^b	1173477193.704	69.2	1	0.38	0.014	0.011	Artifacts present

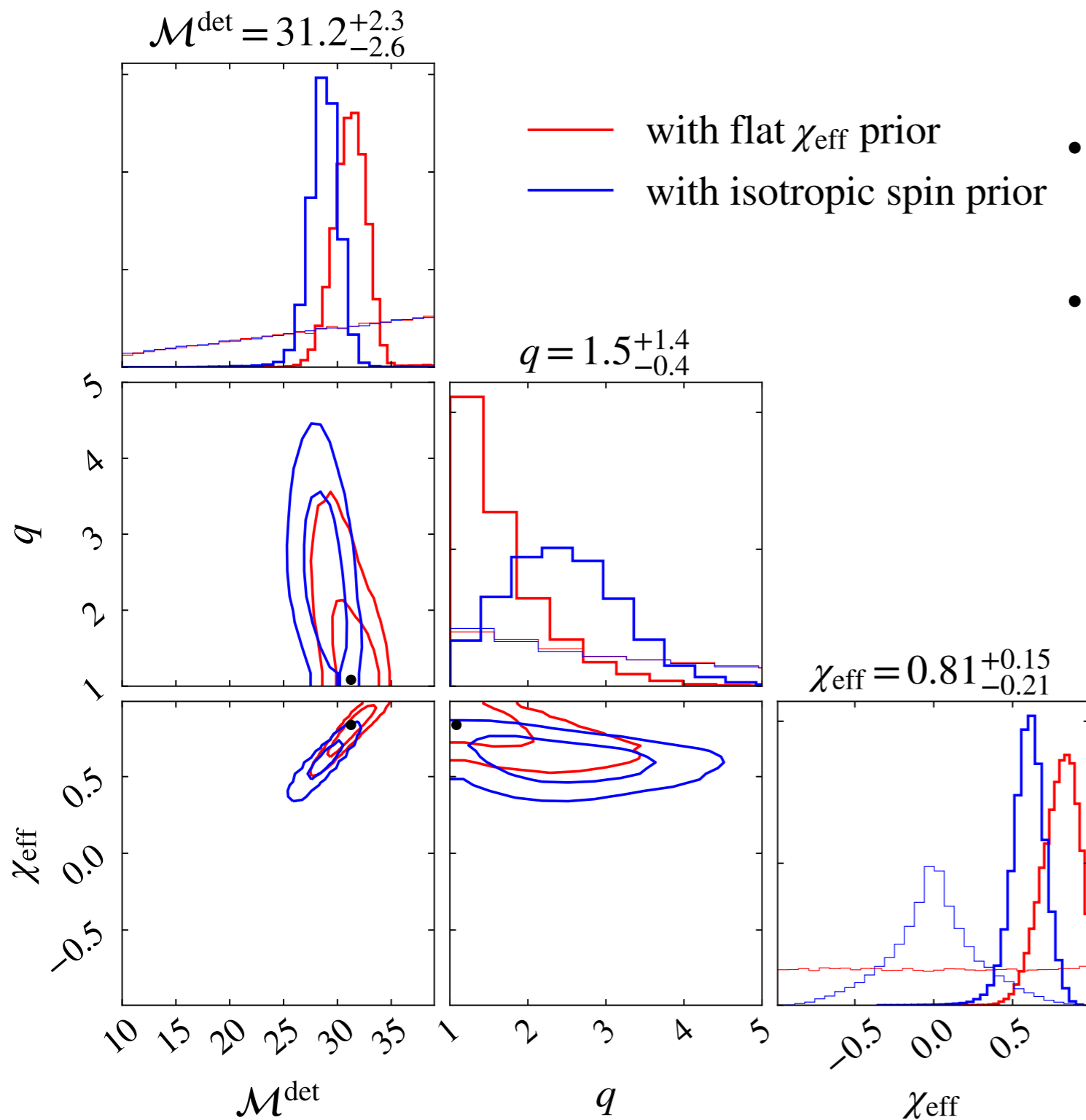


Potential Lensing Event

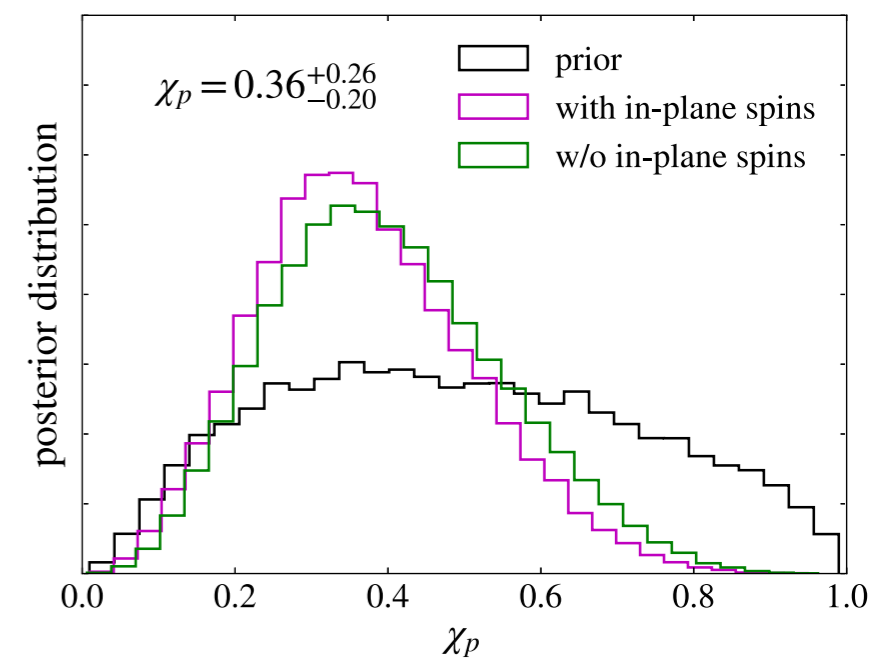
Table with 3 columns and multiple rows of data, likely a list of parameters or observations related to the lensing event.



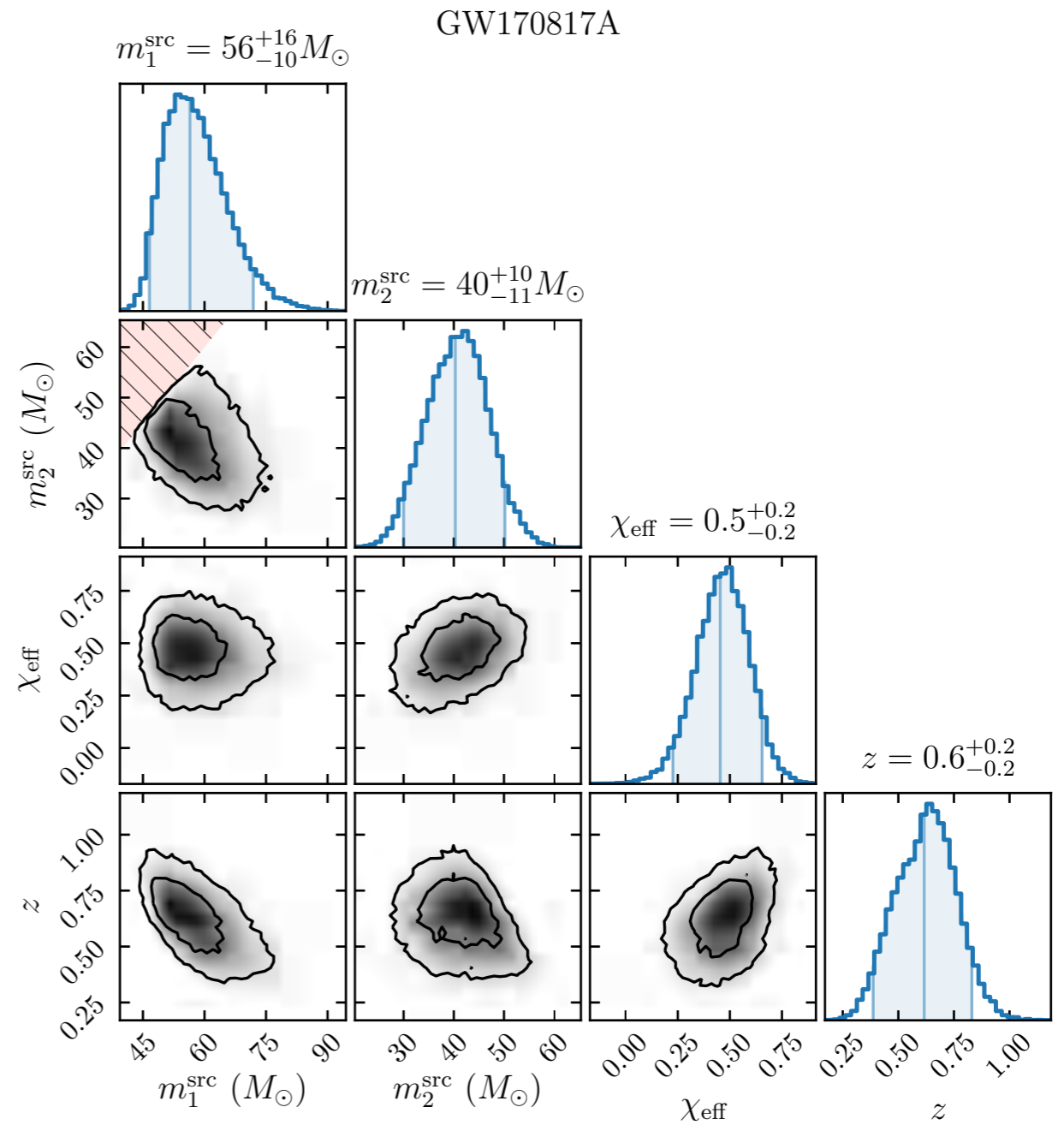
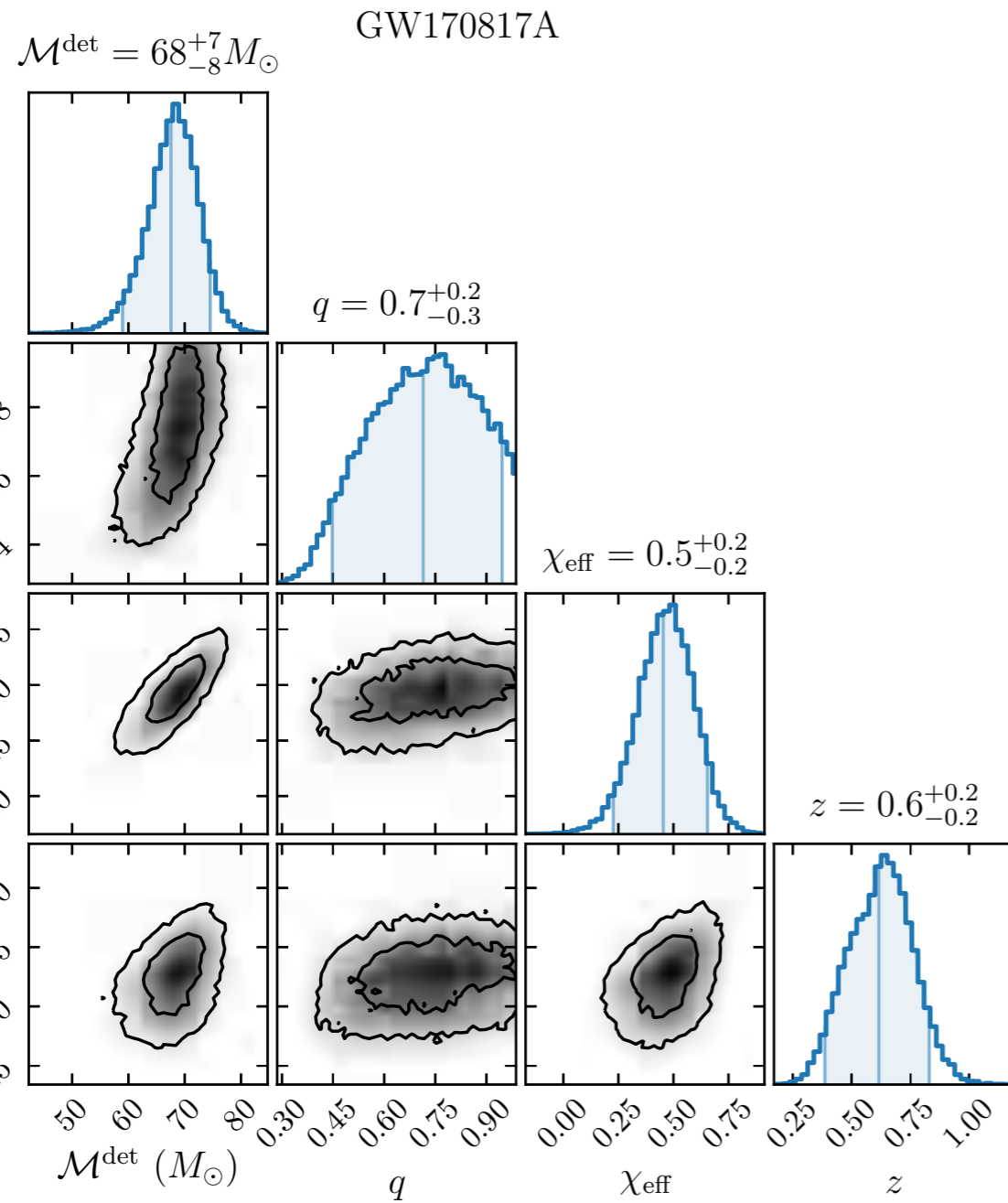
Posteriors



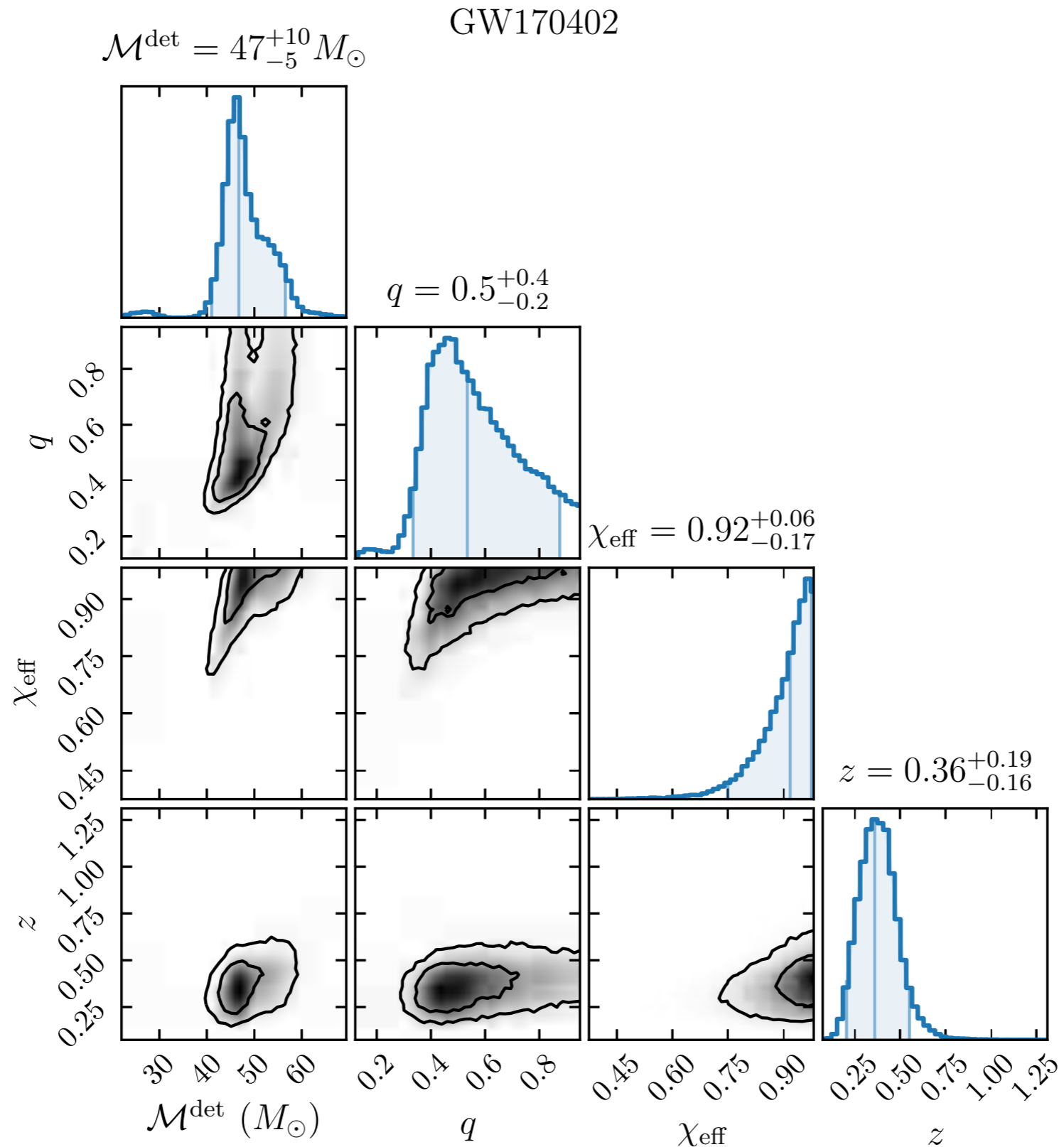
- The isotropic spin prior penalizes high aligned spins. The maximum likelihood point is penalized severely.
- Adopting a flat prior in χ_{eff} leads to significant shifts in parameters
- The data has no information about the perpendicular spin component.



“Very massive single detector event”

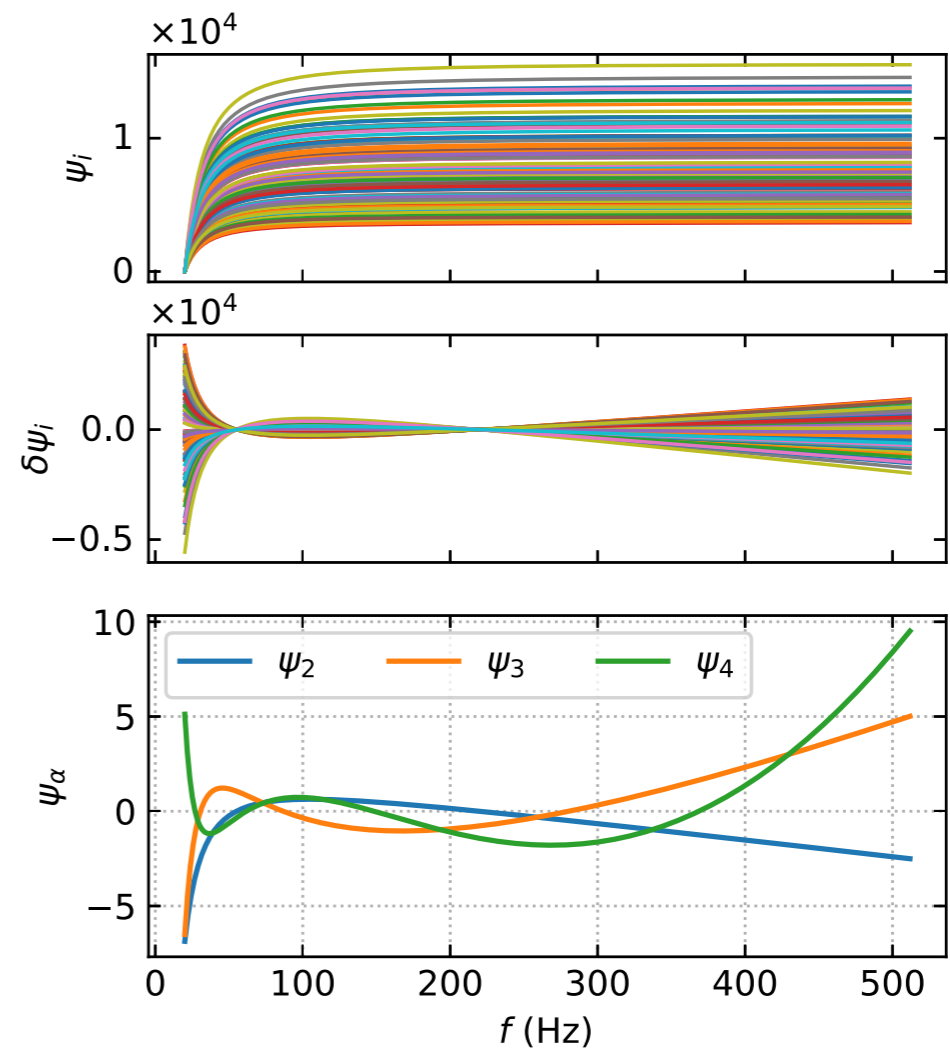
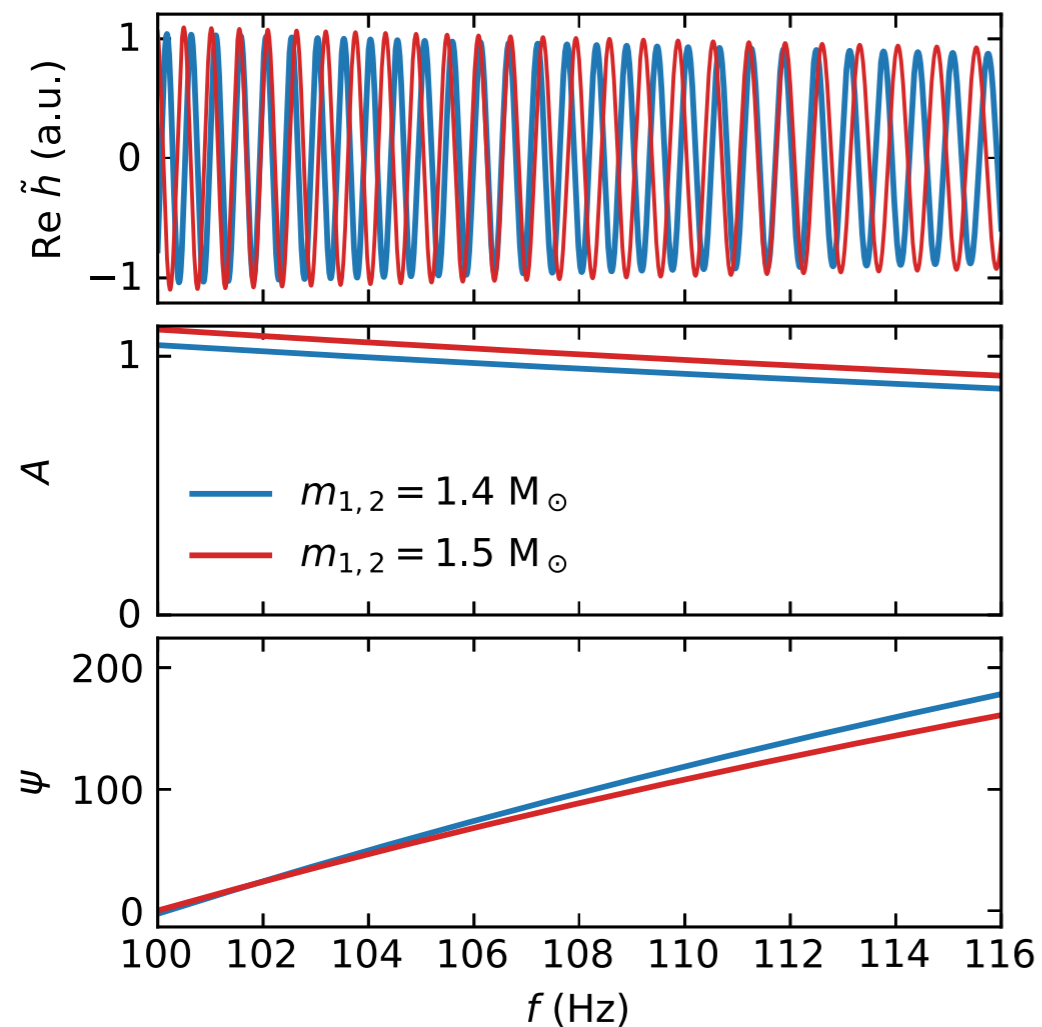


“Highly spinning single detector event”



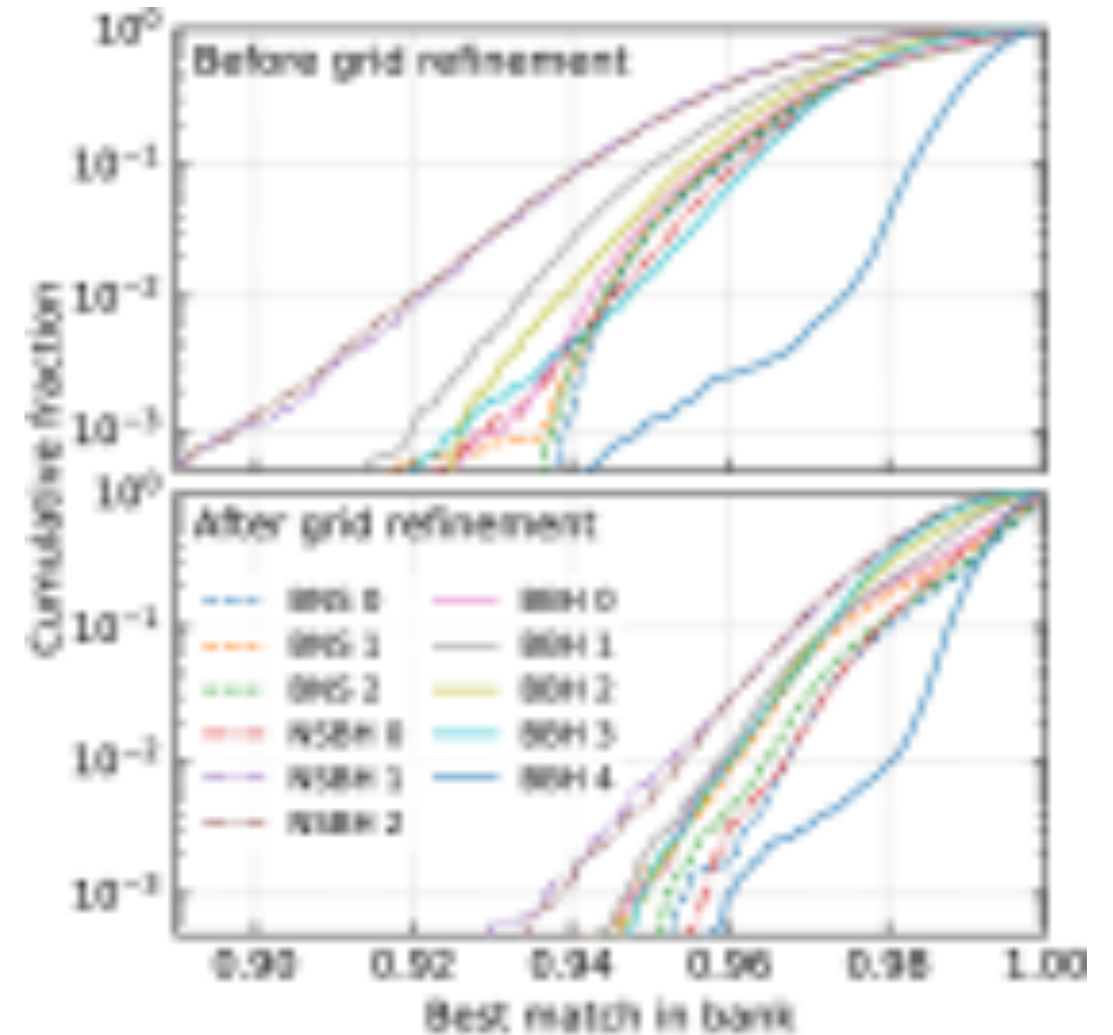
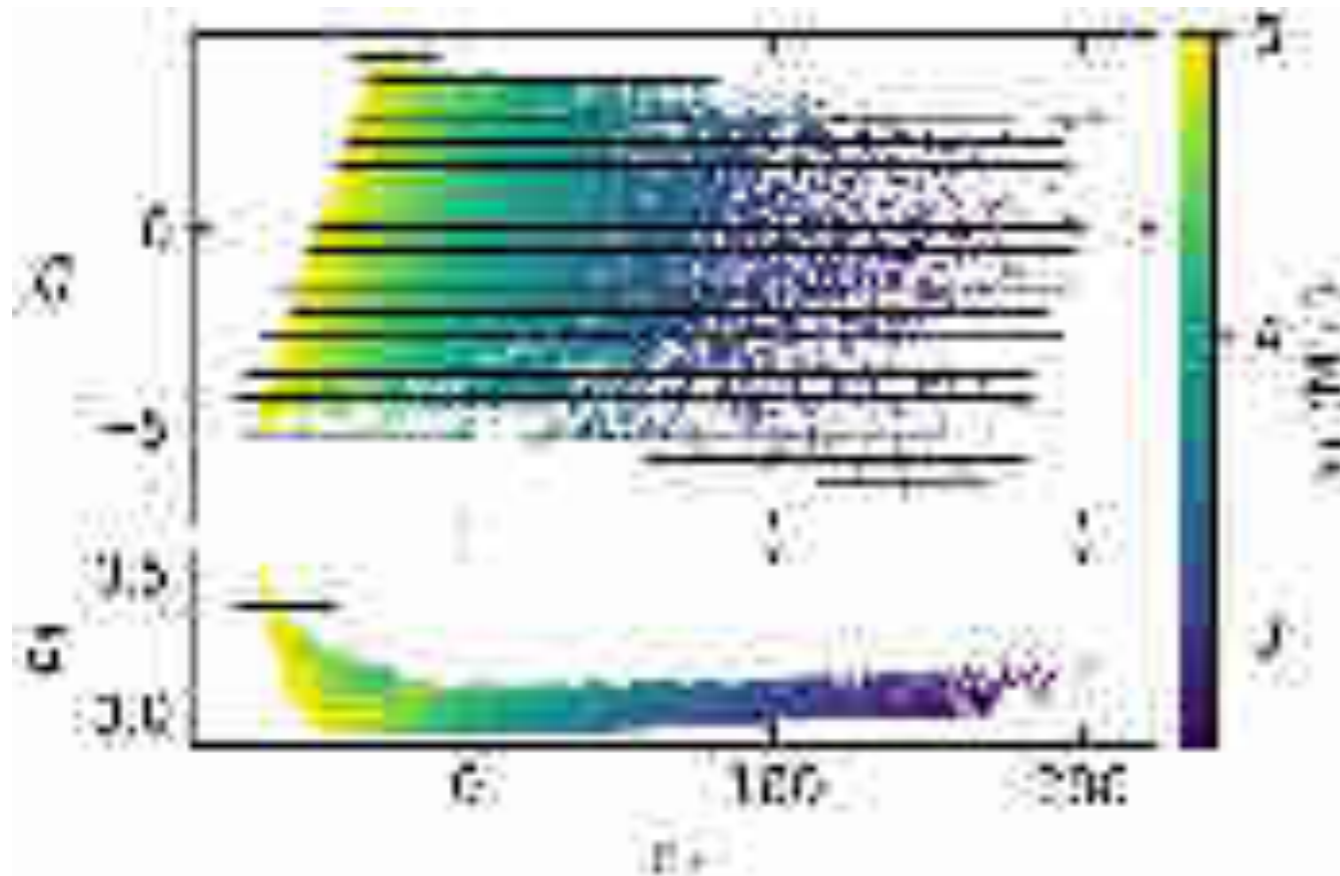
New template bank construction

$$\tilde{h}(f; \mathbf{p}) = A(f; \mathbf{p}) e^{i\psi(f; \mathbf{p})}$$



$$h(f; \mathbf{c}) = \bar{A}(f) \exp \left[i \left(\bar{\psi}(f) + \sum_{\alpha} c_{\alpha} \psi_{\alpha}(f) \right) \right]$$

New template bank construction



$$(h_i | h_j) := 4 \int_0^\infty df \frac{\tilde{h}_i(f) \tilde{h}_j^*(f)}{S_n(f)}, \quad m_{ij} = \max_\tau |(h_i | h_j e^{i2\pi f \tau})|;$$

$$\begin{aligned} d_{\mathbf{c}, \mathbf{c} + \delta \mathbf{c}}^2 &:= 1 - m(h(\mathbf{c}), h(\mathbf{c} + \delta \mathbf{c})) \\ &= \frac{1}{2} \sum_\alpha \delta c_\alpha^2 + \mathcal{O}(\delta c^3). \end{aligned}$$

Basic estimate of the efficiency

Elbert et al. 1703.02551

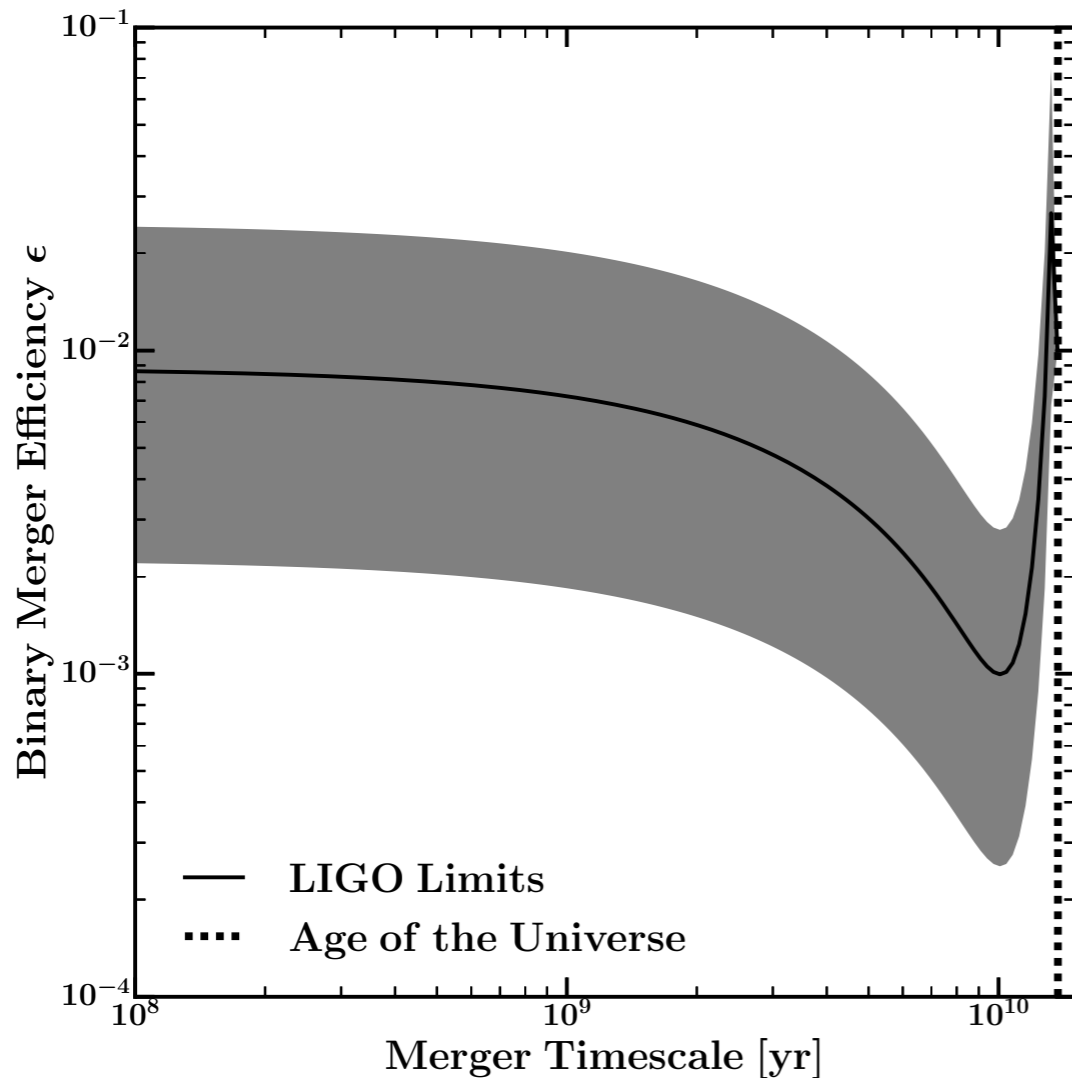


Figure 6. The shaded band shows the joint region of parameter space in binary efficiency ϵ and merger timescale τ that reproduces the merger rate density of black holes reported by Abbott et al. (2016b) for all black hole pairs more massive than $5M_{\odot}$.

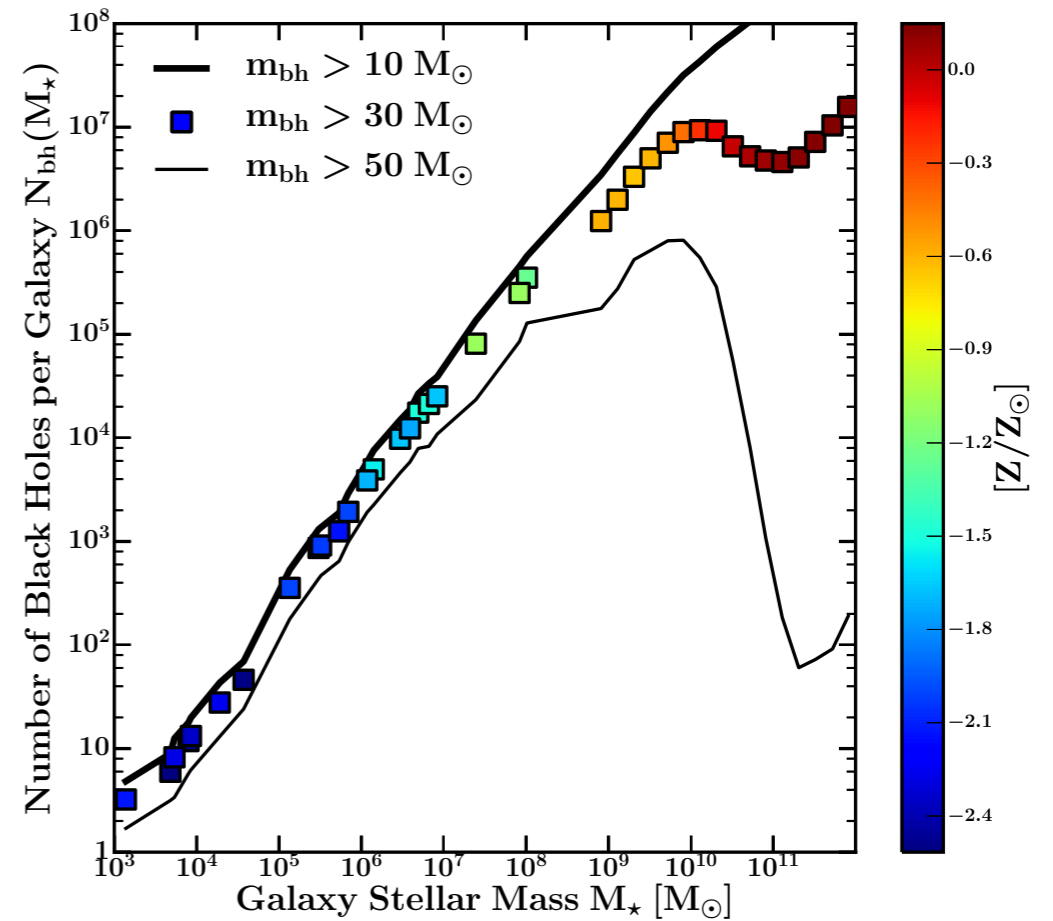


Figure 2. The number of remnant black holes per galaxy as a function of galaxy stellar mass, $N_{\text{bh}}(M_{\star})$, for black holes of mass $m_{\text{bh}} > 10, 30, \text{ or } 50 M_{\odot}$. The squares (corresponding to $30 M_{\odot}$ black holes) are color coded by the median galaxy metallicity. We see that for low metallicities, $N_{\text{bh}} \propto M_{\star}$ in all cases. For the most massive black holes ($30, 50 M_{\odot}$), the relation breaks when galaxies become too metal rich to produce remnants in proportion to their total stellar mass – these black holes form only in the low- Z tail of the distribution. At the highest stellar masses, the relations begin to rise again, when the relation between M_{\star} and Z becomes flat.

The “classic” scenario



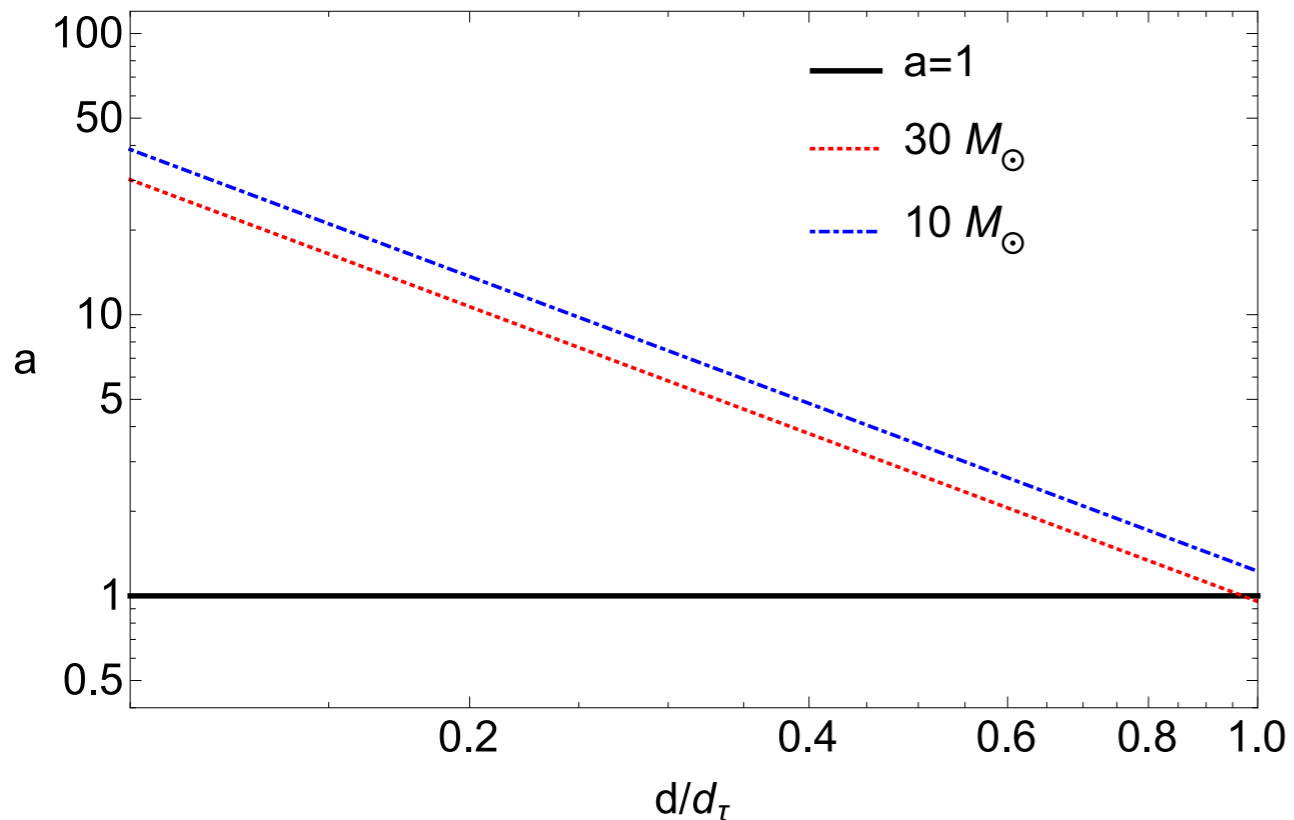
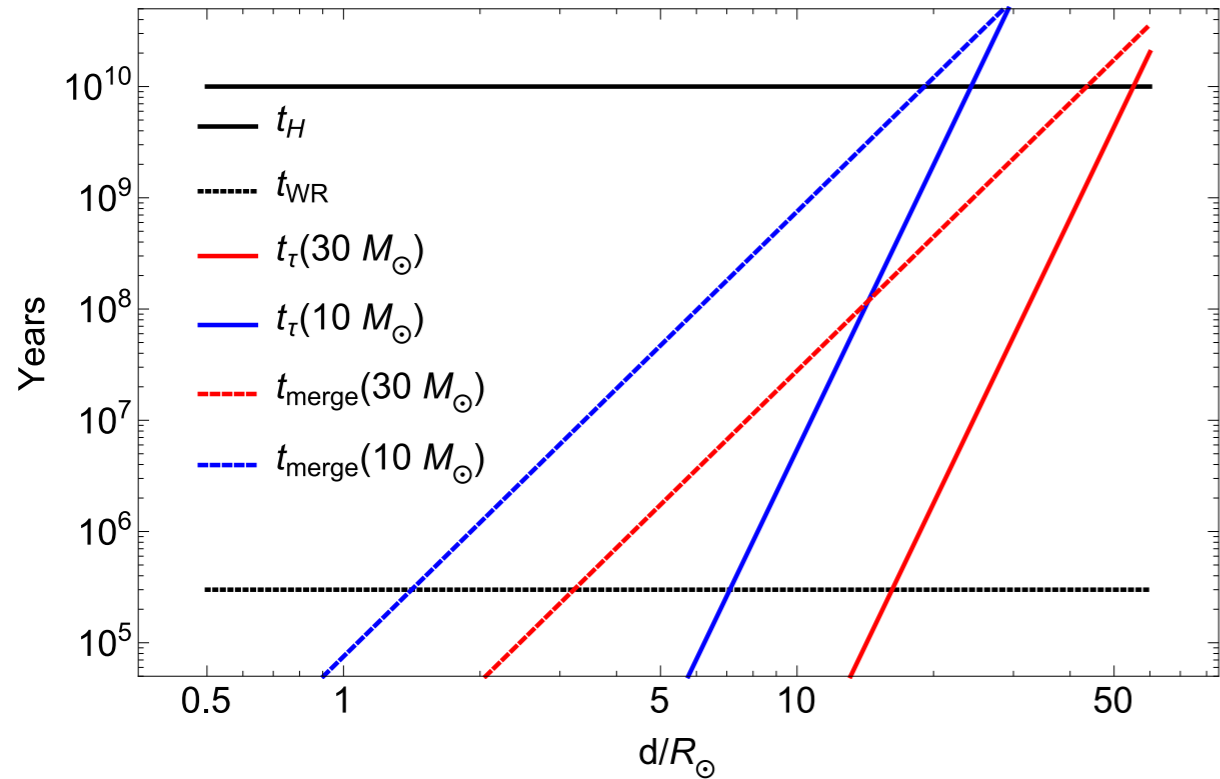
Within the large errors the estimate based on these two systems matches the LIGO rate

Bulik et al. ApJ 730:140 (2011)

	BH	WR Star	Period	D	t_{merge}	Chirp Mass
IC 10 X1	23 M_{\odot}	32 M_{\odot}	1.4 days	20 R_{\odot}	3 Gyrs	15-26 M_{\odot}
NGC 300 X1	20 M_{\odot}	26 M_{\odot}	1.4 days	22 R_{\odot}	3 Gyrs	11-15 M_{\odot}

LIGO Chirp masses from 9 M_{\odot} (GW151226) to 28 M_{\odot} (GW150914)

Tides on the WR star



$$t_{\text{merge}} = \frac{5}{512} \frac{c^5}{G^3 M^3} \frac{2q^2}{1+q} d^4.$$

$$a = \frac{cJ}{GM^2} = \frac{cr_g^2 R^2}{GM} \left(\frac{1+q}{2q}\right)^{1/2} \left(\frac{2GM}{d^3}\right)^{1/2} \frac{\Omega}{\omega}$$

$$\equiv a_{\text{sync}} \frac{\Omega}{\omega},$$

$$\dot{a} = \frac{a_{\text{sync}}}{t_{\tau}} \left(1 - \frac{a}{a_{\text{sync}}}\right)^{8/3} - \frac{a}{t_{\text{wind}}},$$

$$t_{\tau} \approx 10^7 q^{-1/8} \left(\frac{1+q}{2q}\right)^{31/24} \left(\frac{t_{\text{merge}}}{1 \text{ Gyr}}\right)^{17/8} \text{ yr.}$$

$t_{\text{merge}} \lesssim 10^8$ years (for $t_{\tau} < \text{lifetime}$)

M	d_{τ}	d_{merge}
$10 M_{\odot}$	$7 R_{\odot}$	$19 R_{\odot}$
$20 M_{\odot}$	$12 R_{\odot}$	$32 R_{\odot}$
$30 M_{\odot}$	$16 R_{\odot}$	$44 R_{\odot}$

Table 1. Separations corresponding to $t_{\tau} = 3 \times 10^5$ yrs (d_{τ}) and $t_{\text{merge}} = 10^{10}$ yrs (d_{merge}) for binaries composed of a WR and a BH of equal mass (M).

